New constraints on deep earth heterogeneity and anisotropy

by

Ludovic Ladislas Bréger

Grad University Paris VI 1993

A dissertation submitted in partial satisfaction of the requirements for

the degree of

Doctor of Philosophy

in

Geophysics

in the

GRADUATE DIVISION

of the

UNIVERSITY of CALIFORNIA at BERKELEY

Commitee in charge:

Professor Barbara Romanowicz, Chair

Professor Hans-Rudolf Wenk

Professor Ronald Gronsky

May 1999

The dissertation of Ludovic Ladislas Bréger is approved:

Chair	Date
	Date
	Date

University of California at Berkeley

May 1999

New constraints on deep earth heterogeneity and anisotropy

by

Ludovic Ladislas Bréger

To my family

Acknowledgements

I would have never had the opportunity to study seismology at Berkeley without Prof. Barbara Romanowicz. She has been an incredibly insightful adviser who has also been very supportive. I will always remember the stimulative and warm environment that she created at the Berkeley Seismological Laboratory. I thank Dr Henri-Claude Nataf for giving me the opportunity to study seismology a few years ago at the Ecole Normale Supérieure, and Dr Claude Froidevaux who initiated this whole adventure. Working with Dr Lev Vinnik was what I would call an extraordinary experience. I will not forget what I learned from him.

I am very grateful to Profs. Rudy Wenk and Ron Gronsky for having accepted to be on my dissertation commitee, and earlier on my orals commitee.

I wish to thank Profs. Raymond Jeanloz and Mark Richards for having been part of my orals commitee. I also benefited from their scientific expertise, and discussions with them.

Everybody at the Seismo Lab has always been particularly nice. Thank you to Bob, Chaincy, Charles, Charley, Eleanor, John, Joe, Lind, Rick, Roland, Uli, Hrvoje, Gung, Ruben, Mike A., Mike P., Doug D., Doug N., Bill, Bari, Christina, and Steve.

The whole Geology and Geophysics faculty make of this department one of the best of its kind. It is a very stimulating place to be in. I believe that I would have never been able to do the same research anywhere else.

I especially would like to thank Doug Neuhauser, Charley, Eleanor, Bari, Christine, and Maria for keeping the computing facilities and laboratory running perfectly, and for often having to bear with our impatient requests. Without them the Lab would certainly be bery different.

I am not too happy with Charles. For having seen a lot of him for the last 4 years, I still carry a heavy French accent. But in the process, he became one of my best friends. He has always been very supportive. I have also benefited a lot from his scientific expertise in tomography (brought to its paroxism with the birth of the "twins").

I met Dominique shortly after I arrived in Berkeley, and he too became one a wonderful friend. Sailing with him on the Bay has also been one of the most incredible outdoor

experience.

I would like to thanks Profs Edward James Garnero and Doug Dreger for helpful discussions. They have always been available when I had a question or a problem.

Thanks to Hrvoje too, for replacing Mike Antolik at the lab.

Many thanks to Chaincy. It has been a pleasure to have her as a friend and colleague for all those years.

I am particularly grateful to Elizabeth, Richards, and Myriam for being the nicest 'in laws' one could possibly have.

Finally, I would like to thank Simone and Mateo for their love and support for the last three years. I have not been as available as I would have liked, but they have always been patient.

Table of Contents

Abstract

New constraints on deep earth heterogeneity and anisotropy

by

Ludovic Ladislas Bréger

Doctor of Philosophy in Geophysics

University of California at Berkeley

Professor Barbara Romanowicz, Chair

The research that is presented in this dissertation is devoted to the study of the heterogeneity of the deep mantle and its potential implications for studies of the inner core. A new approach is developed that allows to gather informations on the very narrow regions of D". Using this method, it is qualitatively shown that the deep mantle beneath the Central Pacific is strongly heterogeneous and anisotropic (Chapters 2). The signal due to the anisotropy of D" can be contaminated by upper mantle effects. In order to separate those two signals, a new method had to be devised (Chapter 3). Chapter 4 describes an extension of the experiment presented Chapter 2, and a comparison between the results that we obtained and tomographic images of the deep mantle. It is showed that seismic tomography underpredicts the effects of D" heterogeneity by a factor of 2 to 3. Information contained in tomographic studies are then used to produce improved local models of the deep mantle. Those models strongly suggest that a large part of D" heterogeneity has a chemical origin (Chapter 5).

Most studies of the structure of the inner core are based on waves that propagate through the heterogeneous D". An analysis of the potential effect of the complex structure of the deep mantle demonstrates that most of the signal observed on PKP(AB-DF) travel times and usually attributed to inner core anisotropy can also be explained by D" heterogeneity (Chapter 6). In Chapter 7 are finally analysed the most robust evidence for inner core anisotropy, PKP(BC-DF) differential travel time residuals. Those residuals are shown to vary very rapidly, which implies a complex inner core anisotropy or deep mantle structure. The latter is proposed as the most plausible explanation since D" heterogeneity

is already well documented.

Approved:

Barbara Romanowicz, Chair Date

List of Figures

Chapter 1

General introduction

Since the discovery of the inner core by Inge Lehman (1936), we have had a fairly good idea of the one-dimensional structure of the earth (Figure 1). The next surprise came three decades later, when it was realized that the whole planet Earth has a life of its own, with the discovery of plate tectonics. From then, geophysicists have tried to understand not just how our planet looks like and what it is made of, but also importantly what its whole dynamics was. Improvements in our understanding of the earth as a whole come from concerted efforts. Geochemists tell what the earth is made of, and geodynamicists how it is moving, while seismologists are left with the delicate responsibility of giving their best guess of what the deep earth looks like.

Seismology sounds very much like the study of earthquakes, and there is indeed a whole branch of this discipline that is devoted to their study. But seismology is also the only domain of the Earth sciences that gives quasi-direct pictures of the interior of our planet by taking advantage of the earthquakes that occur regularly at its surface. The study of waves that propagate through the earth after those shocks (Figure 2) allow seismologists to map what is inaccessible to the eye, very much like medical imaging can map the human body through sonography, CAT scan, or Magnetic Resonance Imagery.

Over the past two decades, the fast deployment of high quality digital seismographs has given seismology a new dimension. Those very accurate instruments are able to records earth motion that have an amplitude as low as $10 - 9$m, and can also transmit their measurements in real time. These data are available through several storage centers around

the world and are very easy to access. This profusion of high quality digital data, along with the development of powerful computing resources, and analysis and modeling tools, is undoubtly at the origin of most of the recent exciting findings in seismology.

The earth is formed of four major units (Figure 1): the crust which has an average thickness of tens of kilometers, and is made of basalt or granite; the mantle, which is about 2900km thick, and is made of olivine; an outer core mostly composed of liquid iron, that has a radius of 3482km; and finally, an inner core, made out of solid iron, the radius of which is 1221km. Seismologists are primarily interested in the speed at which seismic waves (Figure 2-3) propagate through the earth, which, for example is directly related to the time it takes them to propagate from the earthquake to the seismograph, and is relatively easy to measure. Seismology can also provide informations on two other important characteristics of the deep earth: its density, and how anelastic mechanisms attenuate seismic waves. The seismological observation can then be used as constraints on how the temperature, pressure and composition of the earth change with the location.

We now have a fairly reasonable idea of how the average seismic velocity and density vary with depth (Figure 3). It was realized long ago that the earth was not perfectly spherically symmetric and that the high heterogeneity that one could observe at its surface was likely to also exist deeper. A large part of the contemporary seismological effort has been dedicated to the imaging of this lateral heterogeneity, which has lead to very interesting results, two of which are particularly relevant to the research work presented in this dissertation, and are presented hereafter. A complete and accurate understanding of the dynamics and chemistry of the deep mantle is obviously intimately linked to its imaging.

1.1 Deep mantle structure and heterogeneity

The Core Mantle Boundary (CMB) is the most important discontinuity in the earth. It represents a transition between two radically different media, with on one side a vigorously convecting liquid iron core, and on the other a silicate solid mantle. Bullen (1950) realized early that the last few hundreds kilometers of the mantle were probably associated with large heterogeneity. He called this region D". D" is a 'multi-disciplinary region'. It is

of interest to geochemists, since some small domains of D" may have a composition that is very much like that of the Earth when it formed, about 4.5 billions years ago. D" is believed to be the ultimate graveyard for slabs sinking into the mantle, and may also play an important role in the formation of plumes. It is therefore important to geodynamicists. The CMB and D" are responsible for the magnetic, chemical, thermal, and dynamical coupling between the outer core and the mantle. They may also play a critical role at the early stages of the earth formation, while the core and mantle were differentiating. For additional details, the interested reader is invited to consult some of the general review papers which have been written on D" (Young and Lay, 1987, Loper and Lay, 1995, Lay et al., 1998).

Over the past thirty years or so, several recent studies have contributed to making the seismic picture of D" considerably clearer (Figure 4). In 1972, Cleary and Haddon showed that seismic waves were scattered while propagating through the deep mantle, and proposed the existence of small-scale heterogeneities in this region. Ten years later, Lay and Helmberger (1983) showed the existence of a sharp seismic reflector about 300km above the CMB, corresponding to a velocity increase of about 1 to 3%. In 1989, Vinnik et al. (1989) added anisotropy [1] to this already complex structure. And more recently, the work of Garnero and Helmberger (1995) and Williams and Garnero (1996) lead to the hypothesis that some pockets of melted material were lying at the CMB, in some regions of D". Meanwhile, seismic tomography [2] had started in 1984 (Woodhouse and Dziewonski, 1984) to produce the first reliable long wavelengths picture of whole mantle heterogeneity. Tomographic studies showed the presence of very large slow and fast domains in the deep mantle (Figure 4), which were generally interpreted in terms of hot and light material rising towards the upper mantle, and cold and dense rock sitting at the CMB.

[1] A medium is seismically anisotropic when the wave speed depends on the direction of propagation. Anisotropy provides additional critical informations on the composition, structure and possibly dynamics of the medium.

[2] Seismic tomography is the art of extracting pictures of the inside of the earth using a large volume of data recorded at its surface (the records of waves that have propagated through the Earth), and inverse methods. Although conceptually very similar to its medical cousin, it relies on the earthquakes that occur at the surface of the earth as wave sources. Those earthquakes provide unfortunately a sporadic coverage of the Earth volume, and the resolution of seismic images is therefore much lower that any available sonogram, cat-scan, or magnetic resonance cross-sections.

1.2 Inner core structure and heterogeneity

Two recent discoveries drew the attention of the scientific community towards the inner core, the deepest and less accessible region of our planet. In 1983, Poupinet et al. showed that waves traveling through the inner core along the earth's spin axis were on average faster than those propagating parallel to the equatorial plane, which was interpreted three years later by Morelli et al. (1986) as an effect of anisotropy. Particularly excited by those results, mineral physicists and geodynamicists started investigating some possible mechanism that would explain the texturing of the inner core: convection (Jeanloz and Wenk, 1988)? crystal growth in a magnetic field (Karato, 1993)? solidification texturing (Bergman, 1997)? And in 1996, Song and Richards published some results that showed that the inner core was rotating slightly faster than the rest of the earth (super-rotation). Despite an important amount of work over the last few years, the problem of the origin of the inner core anisotropy and super-rotation have not been convincingly solved.

1.3 Towards an improved image of the strong heterogeneity of D"...

Most of the research effort that is presented in this dissertation is devoted to the study of the heterogeneity of the deep mantle. Many studies have shown that this region of the earth was particularly heterogeneous, but they have failed to give an accurate 3-dimensional picture of its structure.

We started by developing a new but simple approach that allowed us to gather informations on the very narrow regions of D". The deep mantle beneath the Central Pacific was probed using this method. We were interested not only by the isotropic structure of D", but also by its anisotropy, which carries critical dynamical and petrological informations. Those results were published in Vinnik et al. (1998a), and are presented in Chapter 2. The signal due to the anisotropy of D" can be contaminated by upper mantle effects. In order to separate those two signals, we devised a new method that is presented in Chapter 3, and was published in Vinnik et al. (1998b). Chapter 4 describes an extension of the experiment presented Chapter 2, and a comparison between the results that we obtained and tomographic images of the deep mantle. This study, published in Bréger et al. (1998a),

showed that semi-quantitative high resolution studies and seismic tomography gave very different estimates of deep mantle anomalies. In other words, tomographic models of the earth mantle could not fully explain our observations. At this point, we had also never tried to model our observations, and had just obtained an estimate of the degree of heterogeneity of D" beneath the Pacific. We then showed that the information contained in tomographic studies could be used to produce improved local models of the deep mantle, and managed to forward model our previous observations. This modeling is described in Chapter 5, and was published in Bréger et al. (1998b).

1.4 Consequences for studies of the inner core

Most studies of the structure of the inner core are based on waves that propagate through the heterogeneous D". The results presented in Chapters 2 to 5 lead us to believe that the complex structure of the deep mantle could have seriously biased studies of the inner core, which commonly assumed that the signal due to D" was a second order effect. We used a technique similar to that presented in Chapter 5 and showed that most of the signal usually attributed to inner core anisotropy could also be explained by D" heterogeneity, which lead us to question the existence of any texture of the inner core. This study is described in Chapter 6, and has been revised for *Science*.

In order to confirm or infirm our hypothesis that inner core anisotropy was an artifact, we finally analysed in Chapter 7 the most robust evidence for it, PKP(BC-DF) differential travel time residuals. We showed that those observations could be explained by either a very complex inner core anisotropy or deep mantle structure, and argued that the latter was the most plausible since D" heterogeneity was already well documented. This work has been submitted for publication in *Nature*.

1.5 References

Bergman, M.I. Measurements of elastic anisotropy due to solidification texturing and the implications for the Earth's inner core. *Nature* **389**, 60-63 (1997).

Bréger, L. Romanowicz, B., & Vinnik, L. Test of tomographic models of D" using differential travel time data. *Geophys. Res. Lett.* **25**, 5-8 (1998a).

Bréger, L. & Romanowicz, B. Three-Dimensional structure at the base of the mantle beneath the Central Pacific. *Science* **382**, 718-720 (1998b).

Bréger, L., Romanowicz, B. & Tkalcic, H. PKP travel times: Inner core anisotropy or complex structure in the deep mantle? Revised for *Science*, (1999a).

Bréger, L., Romanowicz, B. & Tkalcic, H. PKP(BC-DF) travel times residuals: New constraints on short scale heterogeneity in the deep earth. Submitted to *Nature*, (1999b).

Bullen, K. E., An earth model based on compressibility–pressure hypothesis, *Month. Not. R. Astr. Soc., Geophys. Suppl.* **6**, 50-59 (1950).

Cleary, J.R., & Haddon, R.A.W. Seismic wave scattering near the CMB: a new interpretation of precursors to PKP. *Nature* **240**, 549-551 (1972).

Garnero, E.J., Revenaugh, J., Williams, Q., Lay, T., Kellogg, L.H. A very slow basal layer underlying large-scale low-velocity anomalies in the lower mantle beneath the Pacific: evidence from core phases. *Phys. Earth Planet. Inter.* **91**, 161-176 (1995).

Jeanloz, R. & Wenk, H.R., Convection and anisotropy of the inner core, *Geophys. Res. Lett.* **15**, 72-75 (1988).

Karato, S.-I. Inner core anisotropy due to the magnetic field-induced preferred orientation of iron. *Science* **262**, 1708-1711 (1993).

Lay, T., & Helmberger, D.V. A lower-mantle S-wave triplication and the shear velocity structure of D".*Geophys. J. R. Astron. Soc.* **75**, 799-837 (1983).

Lay, T., Williams, Q., & Garnero, E.J. The core-mantle boundary layer and deep Earth dynamics. *Nature* **392**, 461-468 (1998).

Lehman, I. P'. *Bur. Cent. Seismol. Int.* **14**, 3 (1936).

Li, X.D. & Romanowicz, B. Global mantle shear velocity model developed using nonlinear asymptotic coupling theory. *J. Geophys Res.* **101**, 22245-22272 (1996).

Loper, D.E, & lay, T. The core-mantle boundary region. *J. Geophys. Res.* **100**, 6397-6420 (1995).

Morelli, A., & Dziewonski, A.M. Anisotropy of the core inferred from PKIKP travel times. *Geophys. Res. Lett.* **13**, 1545-1548 (1986).

Poupinet, G., Pillet, R. & Souriau, A. Possible heterogeneity of the Earth's core deduced from PKIKP travel times. *Nature* **305**, 204-206 (1983).

Song, X.-D. & Richards, P.G. Seismological evidence for differential rotation of the Earth's inner core. *Nature* **382**, 221-224 (1996).

Vinnik, L., Farra, V. & Romanowicz, B. Observational evidence for diffracted SV in the shadow of the Earth's core. *Geophys. Res. Lett.* **16**, 519-522 (1989).

Vinnik, L., Bréger, L. & Romanowicz, B. Anisotropic structures at the base of the Earth's mantle. *Nature* **393**, 564-567 (1998a).

Vinnik, L., Bréger, L. & Romanowicz, B. On the inversion of Sd particle motion for seismic anisotropy in D". *Geophys. Res. Lett.* **25**, 679-682 (1998b).

Williams, Q. & and Garnero, E.J. Seismic evidence for partial melt at the base of the Earth's mantle. *Science* **273**, 1528-1530 (1996).

Woodhouse, J.H., & Dziewonski, A.M. Mapping the upper mantle: three dimensional modeling of earth structure by inversion of seismic waveforms. *J. Geophys. Res.* **89**, 5953-5986 (1984).

Young, C.J. & lay, T. The core-mantle boundary. *Ann. Rev. Earth Planet. Sci.* **15**, 25-46 (1987).

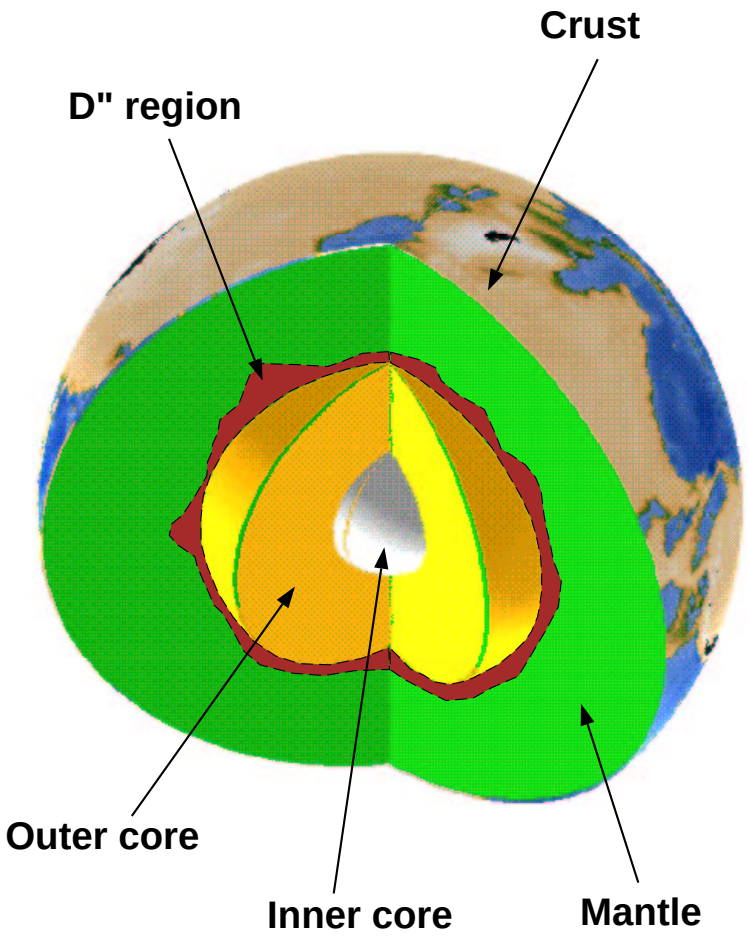

Figure 1.1. The one-dimensionnal earth structure (simplified).

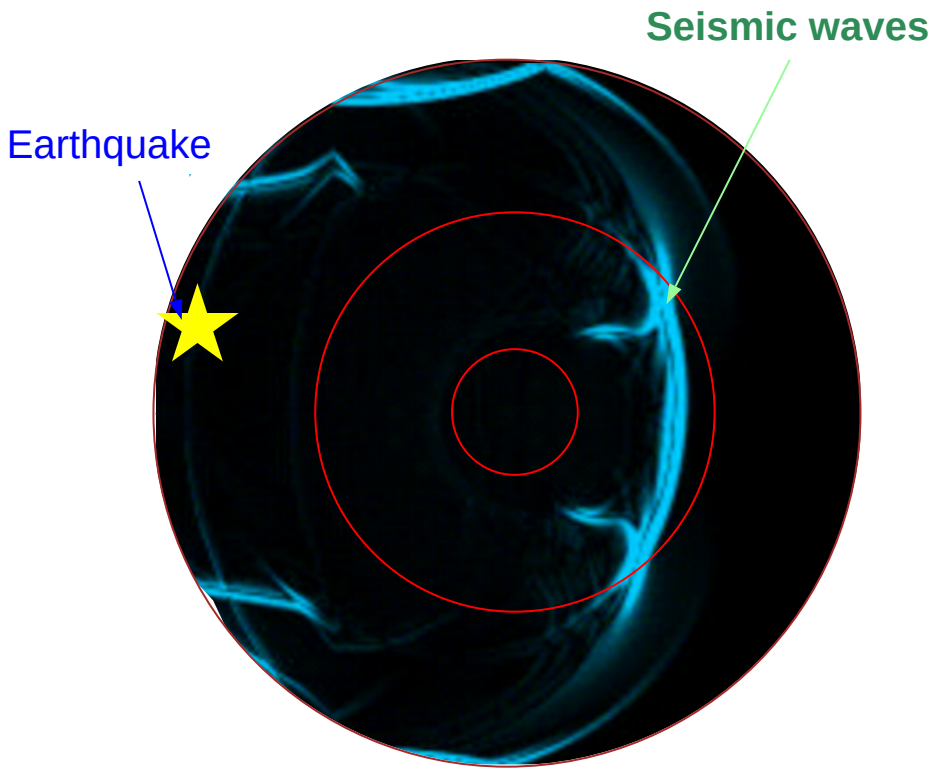

Figure 1.2. Regions of the earth where there is a significant amount of acoustic wave energy (light blue), about fifteen minutes after an earthquake (yellow star).

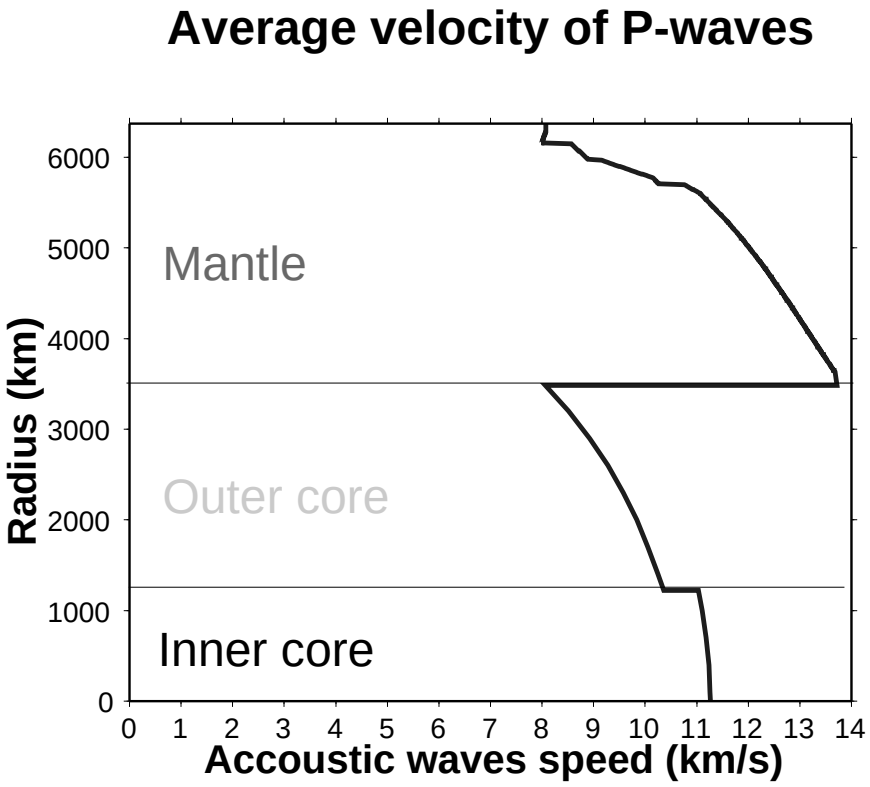

Figure 1.3. An example of one-dimensionnal earth model: PREM ().

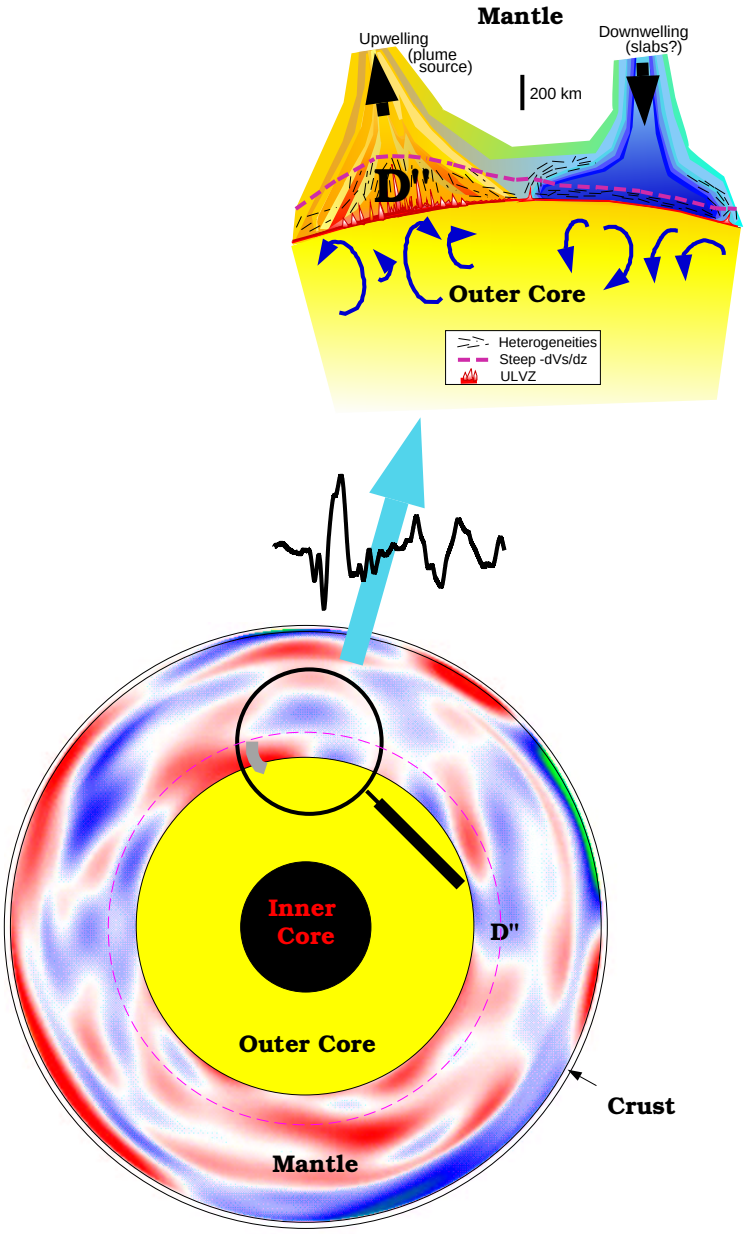
Mantle
Upwelling
(plume
source)
Downwelling
(slabs?)
200 km
D"
Outer Core
Heterogeneities
Steep -dVs/dz
ULVZ
Inner
Core
D"
Outer Core
Crust
Mantle

Figure 1.4. Tomographic studies give global maps of the heterogeneity of the earth, but those pictures are unfortunetaly smoothed and dominated by long wavelengths features (bottom; the tomographic picture presented here is from Li and Romanowicz (1996)). It is fortunately possible to investigate the fine scale structure of specific regions of the earth through high-resolution body wave studies (top, courtesy of Ed Garnero).

Chapter 2

Anisotropic Structures at the Base of the Earth's Mantle

2.1 Summary

The D" shell at the base of the mantle is a thermal and compositional boundary layer, where vigorous dynamic processes may be taking place[1-4]. An important property of D" is its seismic anisotropy, expressed in different velocities for horizontally and vertically polarized S waves, diffracted ($SHdiff$ and $SVdiff$) or reflected at the core-mantle boundary[5,6]. The nature of this anisotropy has been the subject of debate[7-11]. Our analysis of various seismic phases generated in the Kermadec-Fiji-Tonga zone and recorded at stations in North America (Fig. 1) reveals a region at the base of the mantle beneath the southwest Pacific, where horizontally propagating SV is slower than SH by at least 10%. The observed anisotropy is by an order of magnitude larger than previously thought to exist in the lower mantle, and corresponds to lateral variations of SH velocity of about the same magnitude. This anisotropy might be generated by mixing and shearing of a strongly heterogeneous material in the boundary layer.

2.2 SH-SKS differential travel time residuals

The first part of our analysis is based on the residuals of differential travel times between seismic phases $SHdiff$ and $SKS/SKKS$ relative to those for standard model

$PREM$[12]. Differential travel times are helpful because they are not sensitive to errors in focal parameters of seismic events and structural complexities in the source region. Contrary to earlier studies[13,14], we consider (1) not the absolute values of the residuals, but the slopes of the resulting time-epicentral distance plots, (2) not the average residuals for many stations, but the individual slope for every station, and (3) not only the residuals for deep events, but also for intermediate and shallow events. For the given source-receiver geometry (Fig. 1) and a fixed station, changes of the wavepath occur practically only at the source side of the wavepath.

The residuals as a function of epicentral distance show a remarkable trend, consistent from station to station, for shallow and deep events and whether SKS or $SKKS$ is used as reference phase. Fig. 2 shows examples for three best stations. Each panel can be divided into two parts, with rapidly increasing residuals at shorter distances, and slowly rising or decreasing residuals at larger distances. To make this trend better visible, we divide each set of measurements into two subsets corresponding to epicentral distances smaller or equal and greater or equal than a variable cutoff distance. When the best fitting position of the cutoff and linear fits on both sides of it are obtained by regression, the average variance reduction is twofold with respect to a single regression line. Note that the epicentral distance of the kink varies (e.g. $116 - 117°$ at HRV; $103 - 104°$ at RSON), depending on the epicentral distance range of the Kermadec-Fiji-Tonga seismic zone to the given station. Comparable results are obtained for the other stations where a similar analysis was performed: RSCP, LMQ, RSNY and GAC (Fig. 1).

The features in Fig. 2 cannot be explained by mantle complexity immediately beneath the seismic foci, because the change of slope is present in the data for both deep and shallow events. Therefore, our preferred explanation for the kink is a first-order change in the properties of the lowermost mantle at the source side of the wavepath. Moreover, SKS and $SKKS$ raypaths are separated in D" by a distance exceeding 10°, and a similar trend in the residuals in Fig. 2 with respect to SKS and $SKKS$ implies that the effect is mainly in the travel times of $SHdiff$. If the position of the kink for every station is inverted for the position of the corresponding border in the D" layer, assuming that SH enters D" at a height of 300 km above the CMB, the estimates for different stations are

mutually consistent and correspond to the white bar in Fig. 1b. In experiments with synthetic seismograms, the anomaly of slowness of $1.1 s/^\circ$ corresponds to S velocity in D" reduced approximately by 10% with respect to $PREM$. The region of anomalously low SH velocity is located to the northeast of the bar (Fig. 1b), whereas SH velocity to the southwest of the bar is either slightly elevated or normal. Qualitatively, this division is confirmed by two recent tomographic models[15,16] (Fig. 1b), but the magnitude of the low-velocity anomaly in both models is about 3 times smaller than in our data. Robustness of our technique is confirmed by other data[17].

2.3 SKKS-SKS differential travel time residuals

The residuals of $SKKS - SKS$ differential travel times relative to $PREM$, derived from our data (Fig. 3) are positive, with an average value around 2-3 s. As argued by [18], these positive residuals can only be explained by anomalously low S velocity in the lowermost mantle on the source side, due to the longer paths of $SKKS$ relative to SKS. Our data, however, indicate that, on the source side, SKS and $SKKS$ propagate in a region of D" with normal SH velocity (Fig. 1b). Since SKS and $SKKS$ are SV polarized, to explain the discrepancy at least partly, we suggest that, while SH velocity is normal, SV velocity in the lowermost mantle on the source side is anomalously low.

2.4 SVdiff-SHdiff differential travel time residuals

To obtain quantitative estimates of this anisotropy, we assume that the lowermost mantle is intrinsically isotropic, finely layered, and horizontally stratified. For long waves, it behaves like a homogeneous transversely isotropic medium with a vertical axis of symmetry[19,20,21]. In this medium, $SHdiff$ and $SVdiff$ propagate independently, with $SHdiff$ faster than $SVdiff$, which is consistent with the seismic observations[5]. To explain residuals of around 2 s, SKS and $SKKS$ velocities in a layer 300 km thick should be about 10% lower than standard velocity. For the angles of incidence characteristic of SKS and $SKKS$, the SV velocities are higher than for horizontal propagation. Then the difference between SH and SV velocities for horizontal propagation can be even higher than 10%. This prediction can be tested by observing propagation of $SHdiff$ and $SVdiff$.

The seismic phase $SVdiff$ is usually weak, and can be easily distorted by effects of azimuthal anisotropy in the mantle outside D" and side refraction of $SHdiff$. To eliminate these effects and to pick arrivals of $SVdiff$ accurately, a special technique[22] is devised, which is illustrated in[22] for the records of HRV/WFM and RSON. For the present study, a search for $SVdiff$ has been conducted in the records of the deep Fiji-Tonga events at seismograph stations shown in Fig. 1b. The best data set has been obtained at HRV/WFM, RSON and CCM. Remarkable features of the detected $SVdiff$ signals are their distance-dependent delays relative to $SHdiff$ (Fig. 4). At shorter distances the slopes of the plots are close to 0 $s/^\circ$, whereas at larger distances they are in the range of 1.0-1.6 $s/^\circ$. Then anisotropy is weak (not more than a few percent) in the region of very low SH velocity (NE of the white bar in Fig. 1b), and around 15% in the region of normal SH velocity, southwest of the bar. Anisotropy of around 15% is stronger by about an order of magnitude than reported elsewhere.

2.5 Discussion and conclusions

Additional data on the properties of D" beneath the southwest Pacific are provided by the the observations of $SPdKS$ (Fig. 1a). This phase propagates as $Pdiff$ in D" and as SKS elsewhere[23]. $Pdiff$ beneath the southwest Pacific is anomalously slow[18,24], with a remarkable correlation between the anomalous delays of $SPdKS$ relative to SKS and positive $SKKS - SKS$ residuals, similar to those shown in Fig. 3. An explanation for this phenomenon is partial melting[25]. The anomalously slow $Pdiff$, however, propagates on the source side in a medium with normal SH velocity (Fig. 1b), which is hard to reconcile with a strong reduction of S velocity, expected in the case of partial melting. Since, as we have demonstrated, the $SKKS - SKS$ residuals can be related to anisotropy, the correlation between them and $SPdKS$ delays suggests that the delays are affected by anisotropy, as well. Moreover, east of the white bar in Fig. 1b, where, according to our data, anisotropy is weak, the low P velocity layer, if present, is very thin[26]. Assuming that the $SPdKS$ delays are related to anisotropy, we note that the low horizontal P velocity in a fine-layered horizontally stratified medium is possible, if the variations of S velocity between the layers are much stronger than those of P velocity[20]. Another possibility to be

considered is lattice preferred orientation[27].

For normal distribution of random variations of S velocity in the stack of thin horizontal layers with m mean and σ standard deviation, the SH/SV velocity ratio for horizontal propagation is expressed[20] as $SH/SV \approx \sqrt{1+4(\sigma/m)^2}$. For S anisotropy of 15%, σ thus evaluated is 28% of m. It is not possible to explain the variations exceeding a few per cent solely by temperature variations[28]. S velocity can be significantly lowered by partial melting or/and by accumulation of crystalline Fe-alloy products of chemical reactions between iron of the outer core and mantle perovskite[29]. Among these possibilities, relatively weak variations of P velocity favour partial melting. The layered structure in D" could be generated by convective mixing and shearing. Then, strong anisotropy in D" should be accompanied by strong wave scattering. The anomalous region of D", if projected on the surface of the earth, is close to Polynesia, a region of unusual thermal agitation, where a large-scale thermo-chemical plume may be present at the top of the lower mantle[30]. The anisotropic region in D" could somehow be related to the same plume.

Finally, comparable magnitudes of lateral heterogeneity and anisotropy suggest that lateral variations of anisotropy can be mistaken for lateral velocity variations, when the models are derived under the assumption of isotropy. Whatever its origin, the observations of strong and laterally variable anisotropy add a new dimension to the question of properties and processes in D".

2.6 Acknowledgements

We thank M. Wysession and two anonymous reviewers for constructive reviews. This work was partially supported by NSF. It is Seismological Laboratory contribution #9801. Reprinted by permission from Nature, Vinnik, L., Bréger, L., & Romanowicz, B. Anisotropic structures at the base of the Earth's mantle. *Nature* **393**, 564-567 (1998).)

2.7 References

1. Doornbos, D.J., Spiliopoulos, S. & Stacey, F.D. Seismological properties of D" and the structure of a thermal boundary layer. *Phys. Earth Planet. Int.* **41**, 225-239 (1986).

2. Knittle, E. & Jeanloz, R. Earth's core-mantle boundary: results of experiment at high pressures and temperatures. *Science* **251**, 1438-1443 (1991).

3. Kellogg, L.H. & King, S.D. Effect of mantle plumes on the growth of D" by reaction between the core and mantle. *Geoph. Res. Lett.* **20**, 379-382 (1993).

4. Loper, D.E., & Lay, T. The core-mantle boundary region. *J. Geophys. Res.* **100**, 6397-6420 (1995).

5. Vinnik, L., Farra, V. & Romanowicz, B. Observational evidence for diffracted SV in the shadow of the Earth's core. *Geophys. Res. Lett.* **16**, 519-522 (1989).

6. Lay, T. & Young, C.J. Analysis of seimsic SV waves in the core's penumbra. *Geophys. Res. Lett.* **18**, 1373-1376 (1991).

7. Maupin, V. On the possibility of anisotropy in the D" layer as inferred from the polarization of diffracted S-waves. *Phys. Earth Planet. Int.* **87**, 1-32 (1994).

8. Vinnik, L., Romanowicz, B., Le Stunff, Y. & Makeyeva, L. Seismic anisotropy in the D" layer. *Geophys. Res. Lett.* **22**, 1657-1660 (1995).

9. Kendall, J. M. & Silver, P.G. Constraints from seismic anisotropy on the nature of the lowermost mantle. *Nature* **381**, 409-412 (1996).

10. Matzel, E., Sen, S.E. & Grand, S.P. Evidence for anisotropy in the deep mantle beneath Alaska. *Geophys. Res. Lett.* **23**, 2416-2420 (1996).

11. Garnero, E. & Lay, T. Lateral variations in lowermost mantle shear wave anisotropy beneath the north Pacific and Alaska. *J. Geophys Res.* **102**, 8121-8135 (1996)

12. Dziewonski, A.M. & Anderson, D.L. Preliminary Reference Earth Model. *Phys. Earth Planet. Int.* **25**, 297-356 (1981).

13. Schweitzer, J. & Mueller, G. Anomalous difference traveltimes and amplitude ratios of SKS and SKKS from Fiji-Tonga events. *Geophys. Res. Lett.* **13**, 1529-1532 (1986).

14. Garnero, E. & Helmberger, D.V. Travel times of S and SKS: implication for three-dimensional lower mantle structure beneath the central Pacific. *J. Geophys. Res.* **98**, 8225-8241 (1993).

15. Li, X.D. & Romanowicz, B. Global mantle shear velocity model developed using nonlinear asymptotic coupling theory. *J. Geophys Res.* **101**, 22245-22272 (1996).

16. Grand, S., van der Hilst, R. & Widiyantoro, S. Global seismic tomography: a snapshot of convection in the Earth. *G.S.A. Today* **7**, 1-7 (1997).

17. Breger, L., Romanowicz, B. & Vinnik, L. Test of tomographic model of D" using differential travel time data. *Geophys. Res. Lett.* **25**, 5-8 (1998).

18. Garnero, E. & Helmberger, D.V. Seismic detection of a thin laterally varying boundary layer at the base of the mantle beneath the central-Pacific, *Geophys. Res. Lett.* **23**, 977-980 (1996).

19. Backus, G. E. Long-wave elastic anisotropy produced by horizontal layering, *J. Geophys. Res.* **67**, 4427-4440 (1962).

20. Nevsky, M. V. *Quasianisotropy of velocities of seismic waves* (Nauka, Moscow 1974) (in Russian).

21. Levin, F. K. Seismic velocities in transversely isotropic media. *Geophysics* **44**, 918-936 (1979).

22. Vinnik, L., Breger, L., & Romanowicz, B. On the inversion of Sd particle motion for anisotropy in D". *Geophys. Res. Lett.*, in press (1998).

23. Kind, R. & Mueller, G. Computations of SV waves in realistic Earth models. *J. Geophys.* **41**, 142-162 (1975).

24. Garnero, E. & Helmberger, D.V. A very slow basal layer underlying large-scale low-velocity anomalies in the lower mantle beneath the Pacific; evidence from core phases. *Phys. Earth Planet. Int.* **91**, 161-176, (1995).

25. Williams, Q. & Garnero, E. Seismic evidence for partial melt at the base of Earth's mantle. *Science* **273**, 1528-1530 (1996).

26. Mori, J. & Helmberger, D.V. Localized boundary layer below the mid-Pacific velocity anomaly identified from a PcP precursor. *J. Geophys. Res.* **100**, 20359-20365 (1995).

27. Karato, S. I.. Seismic anisotropy in the deep mantle, boundary layers and the geometry of mantle convection. In *Geodynamics of the lithosphere and the earth's mantle* (ed. Plomerova, J., Babuska, V.N. & Liebermann, R.C.), *Pageoph.*, in press (1998).

28. Wysession, M. E., Okal, E.A. & Bina, C.R. The structure of the core-mantle boundary from diffracted waves. *J. Geophys. Res.* **97**, 8749-8764 (1992).

29. Jeanloz, R. Chemical reactions at the Earth's core-mantle boundary: Summary of evidence and geomagnetic implications. in *Relating Geophysical Structures and Processes, The Jeffreys Volume, Am. Geophys. Union Geophysical Monogr.* **76**, 121-127 (1993).

30. Vinnik, L., Chevrot S. & Montagner, J.P. Evidence for a stagnant plume in the transition zone? *Geophys. Res. Lett.* **24**, 1007-1011 (1997).

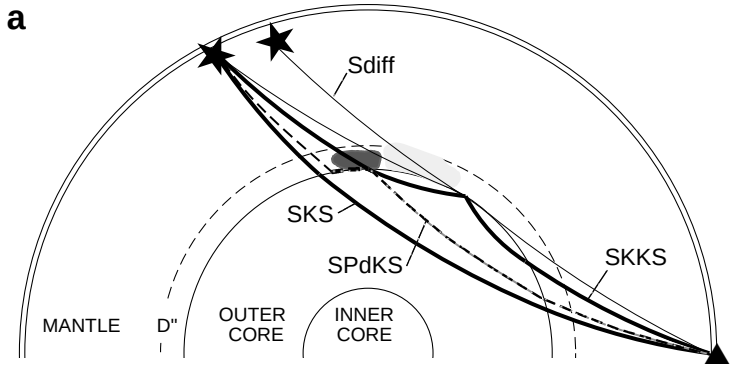

Figure 2.1. (a) Schematic representation of the wavepaths of SKS, $SKKS$, $Sdiff$ and $SPdKS$. The wavepaths of $Sdiff$ for two different positions of the source (stars) differ only at the source side. The lightly hatched area indicates the region where SH is slow, as discussed in the text. The darker hatched area is the region where SH velocity is elevated or normal, but SV is much slower than SH.

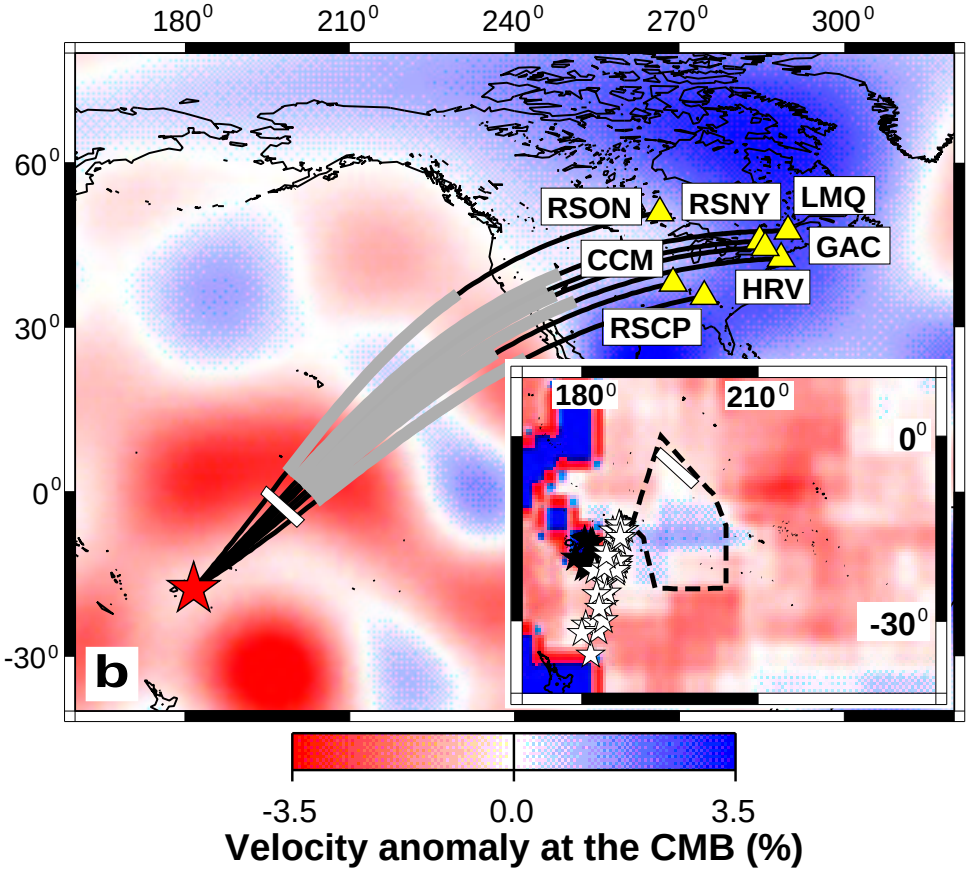

Figure 2.1. (b) Surface projections of wavepaths superimposed on a tomographic model of SH velocity in D"[15]. The light gray zone of the wavepath indicates approximately the D" leg of $Sdiff$ for the shortest distances considered. The white bar corrresponds to the kink for $SHdiff - SKS$ residuals, discussed in text. Insert: close-up look at the source side of the wavepaths. Epicenters of deep Fiji-Tonga events and of shallow Kermadec-Fiji-Tonga events are shown by filled and open stars, respectively. The background tomographic model of S velocity in D" is[16]. The polygon indicates the zone of ultra-low P velocity in D", as found by[18].

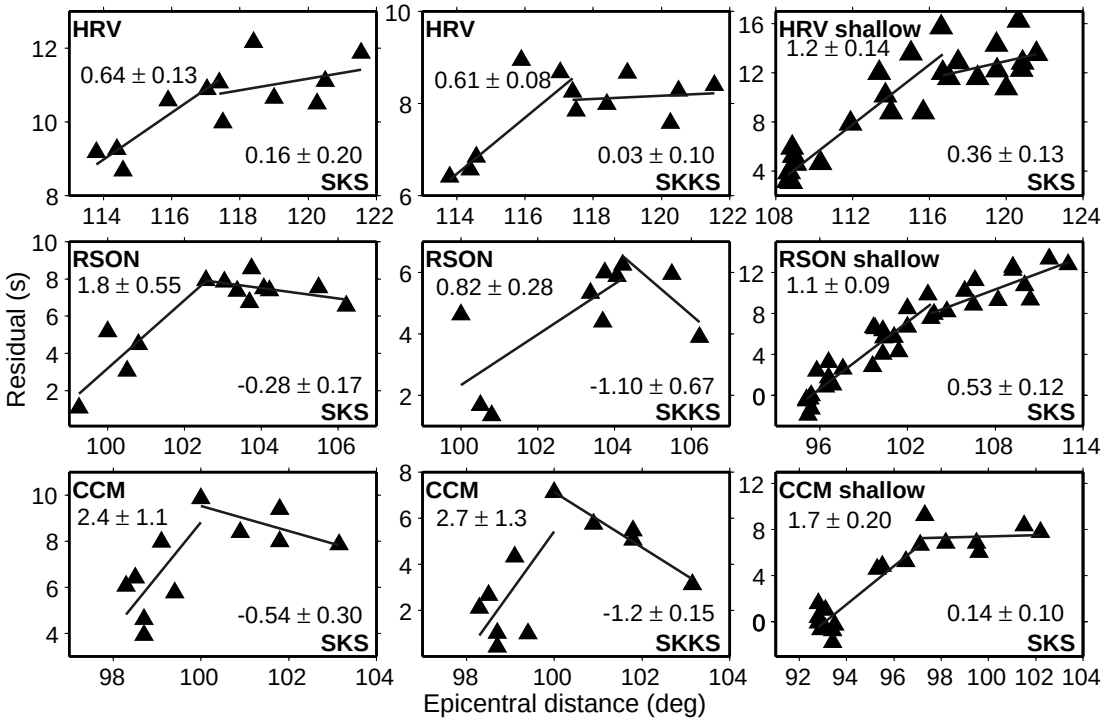

Figure 2.2. Residuals of $SHdiff - SKS$ and $SHdiff - SKKS$ differential travel times with respect to those for $PREM$[12], for HRV/WFM, RSON and CCM, and corresponding regression lines. The data labeled shallow are for shallow and intermediate events; all others are for deep events. Shallow events broaden the distance interval available for SKS. The slopes of the plots are controlled mainly by the slowness of $SHdiff$ and, consequently, by SH velocity at the source side of D". The slope is negative, positive or equal to 0, if SH velocity is higher, lower or similar to that in $PREM$. Numerical values of the slopes of the regression lines with their respective confidence intervals are shown in the upper left and lower right corners of each panel. Confidence intervals are usually around $\pm 0.1 - 0.3 s/^\circ$, but they exceed $\pm 1.0 s/^\circ$ for deep events at CCM, left of the kink. If the latter data are excluded, the average values of the slopes are $1.12 \pm 0.2 s/^\circ$ and $-0.21 \pm 0.2 s/^\circ$, left and right of the kink, respectively.

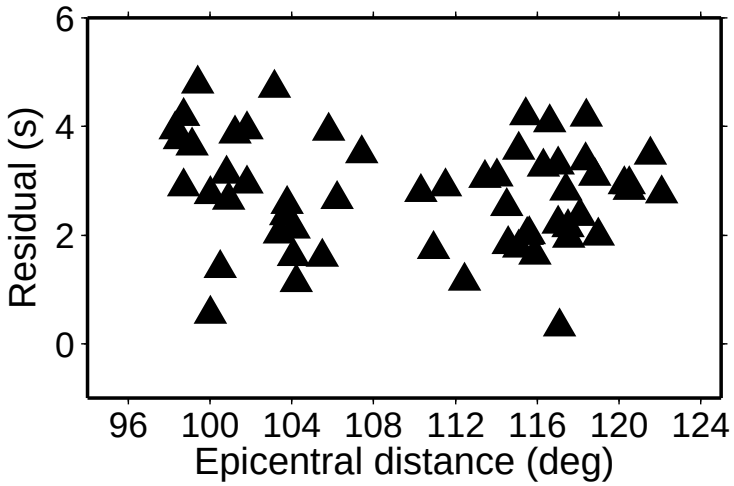

Figure 2.3. $SKKS - SKS$ residuals for all paths in Fig. 1b. Comparable residuals were reported for similar wavepaths in earlier studies[13,18,24]. For other paths beneath the Pacific and America, the residuals are close to 0[18,24].

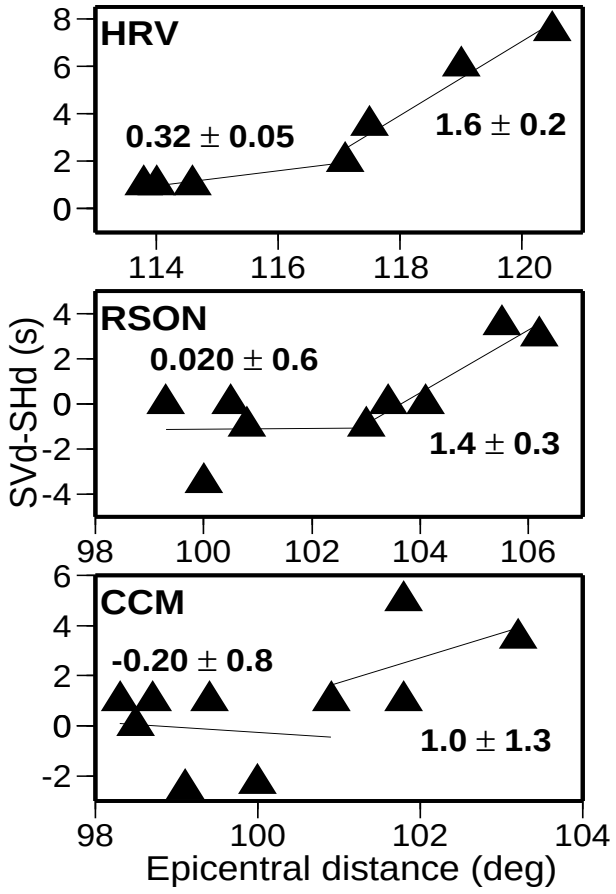

Figure 2.4. Delays of $SVdiff$ with respect to $SHdiff$ as a function of epicentral distance for stations HRV/WFM, RSON and CCM. The slope of any of the plots is the difference in slowness between $SVdiff$ and $SHdiff$ at the source side of the wavepath. Magnitude of anisotropy can be determined as the ratio between these slopes, and the standard slowness of 8.4 $s/°$. Each data set is approximated by two regression lines. The boundaries between the corresponding distance intervals are taken from Fig. 2. Numerical values of the slopes of the regression lines with their respective confidence intervals are shown adjacent to the corresponding portions of the plots.

Chapter 3

On the inversion of Sd particle motion for seismic anisotropy in D"

3.1 Summary

In order to make accurate estimates of anisotropy in D", as measured from observations of $Sdiff$ (Sd) it is necessary to correct the observed waveforms for anisotropy outside of the deepest mantle as well as side refraction along the path, and to pick arrivals of SVd and SHd as accurately as possible. We show that corrections based on estimates of upper mantle anisotropy inferred from $SKS/SKKS$ splitting measurements are sometimes insufficient and propose a master event method to directly obtain more accurate corrections on specific source-station paths. Our study illustrates the complexity of structure that needs to be taken into account when addressing issues of D" properties using seismic body wave methods. We also describe a method to accurately measure the arrival time of the corrected SVd wave.

3.2 Introduction

In the past few years, evidence for the existence of anisotropy in the D" region of the mantle has been accumulating, based on observations of travel time discrepancies between SV and SH components of waves sampling the deepest part of the mantle, such as S diffracted (Sd) (Vinnik et al., 1989a;1995;1997; Lay and Young, 1991; Garnero and Lay, 1997) or ScS (Kendall and Silver, 1996; Matzel et al., 1996). As such studies become more quantitative, it is critical to accurately correct the records of Sd (or ScS) for unwanted perturbing effects, and to pick the SV and SH arrivals as accurately as possible. Indeed, in the presence of strong SHd, SVd can be easily distorted by coupling between SV and SH, due to propagation of Sd in the azimuthally anisotropic mantle outside D" or by side refraction of SHd. We here describe improved Sd processing techniques, and demonstrate that the results thus obtained may depart significantly from those based on the standard approach. This is illustrated with examples for the paths between the Fiji-Tonga region and stations in North America (Fig. 1).

3.3 Master event technique

In the presence of azimuthal anisotropy outside D" (receiver anisotropy), the spectra of the observed S components of motion at the earth's surface, $SV(\omega)$ and $SH(\omega)$ respectively are related to the unperturbed spectra, $SV_0(\omega)$ and $SH_0(\omega)$ through (Farra et al., 1991):

$$\begin{Bmatrix} SV_0(\omega) \\ SH_0(\omega) \end{Bmatrix} = F^{-1}(\omega) \begin{Bmatrix} SV(\omega) \\ SH(\omega) \end{Bmatrix} \tag{1}$$

where ω is angular frequency, and $F(\omega)$ is the matrix of the frequency response of the anisotropic layer. The related waveforms: $SV_0(t)$, $SH_0(t)$, $SV(t)$ and $SH(t)$ can be found from their spectra by inverse Fourier transformation. For a small incidence angle and on the assumption of hexagonal receiver anisotropy with a horizontal axis of symmetry, the elements of $F(\omega)$: $SV_{sv}(\omega)$, $SV_{sh}(\omega)$, $SH_{sv}(\omega)$, and $SH_{sh}(\omega)$ can be expressed as functions of β and δt, the angle in the horizontal plane between the fast direction of anisotropy and the radial (R) direction, and the delay of the slow split wave relative to the fast one, respectively (Vinnik et al., 1992). Assuming $SH_0(\omega) = 0$, $SH_{th}(t)$, the theoretical $SH(t)$

for arbitrary β and δt, can be obtained from the observed $SV(t)$ through

$$SH_{th}(t) = \frac{1}{2\pi} \int_{-\infty}^{\infty} \frac{SH_{sv}(\omega)}{SV_{sv}(\omega)} SV(\omega) \exp(i\omega t) d\omega \tag{2}$$

Similarly, assuming $SV_0(\omega) = 0$, the expression for $SV_{th}(t)$ to be derived from the observed $SH(t)$ is

$$SV_{th}(t) = \frac{1}{2\pi} \int_{-\infty}^{\infty} \frac{SV_{sh}(\omega)}{SH_{sh}(\omega)} SH(\omega) \exp(i\omega t) d\omega \tag{3}$$

The assumption of $SH_0(\omega) = 0$ in (2) corresponds to observations of SKS or $SKKS$. The actual values of β and δt minimize the rms difference between $SH_{th}(t)$ and $SH(t)$ (Vinnik et al. 1989b). The values of the parameters of anisotropy thus found can be used to correct the recordings of Sd, using (1). Vinnik et al. (1989a, 1995) did not correct recordings of Sd of Fiji-Tonga events at IRIS station HRV and a neighbouring Geoscope station WFM, because the analysis of SKS and $SKKS$ for this path (Fig. 1) has shown that $\beta = 0°$. In such a situation, $SV_{sh} = SH_{sv} = 0$. At some other stations, Kendall and Silver (1996) applied corrections, using the parameters of anisotropy derived from the analysis of splitting of SKS.

We here demonstrate that the corrections, if derived from observations of SKS and $SKKS$, can be misleading. Instead, we propose a more efficient technique, where the corrections are derived directly from the observations of Sd. The idea is to derive the corrections from the 'master' recordings of Sd, with extremely weak SV radiation in the source, as compared with SH. On the assumption of transverse anisotropy in D" (hexagonal anisotropy with the vertical axis of symmetry), there should be no coupling between SHd and SVd. This means that the signal, which can be present in the SV component of the master event is not SVd, but an effect of receiver anisotropy or side refraction of Sd. The critical assumption of transverse isotropy in D" is based mainly on the observation, that the amplitude of SVd is correlated with that of $SKKS$ rather than SHd (Vinnik et al., 1995). Additional arguments in favour of this assumption are provided by the results of data processing, which are obtained through this study and discussed in the last section.

Receiver anisotropy is manifested by quarter-period phase shift between the R or

SV and SH components of Sd. The parameters of this anisotropy can be evaluated by minimizing the rms difference between $SV(t)$ and $SV_{th}(t)$, as derived through (3). The correction eliminating this signal can then be applied to other records of Sd with a similar wavepath. Contrary to azimuthal anisotropy, side refraction is manifested by either 0 or π phase shift between the two components of Sd. The deviation from the theoretical back azimuth of the event can be evaluated by the analysis of the corresponding covariance matrix, and the effect can be eliminated by appropriate rotation of the R, SH coordinate frame.

In what follows, we illustrate applications of the master event technique to the records of deep events at station HRV/WFM. The list of events is modified from Vinnik et al. (1995) by including two additional Fiji-Tonga events (88070 and 86146a; the numbers here indicate year and Julian day of the event). The records were integrated to obtain displacement and low-pass filtered with a corner at around 9 s. The records of radial (R) and vertical components were rotated by 25° to obtain SV component of Sd. SV amplitudes of SKS, $SKKS$ and Sd are only slightly different from those in the R component, but the rotation sometimes improves signal/noise ratio, if the noise is formed by multiply reflected P-waves. Figure 2 shows two recordings (88070 and 93190), with very weak or missing SKS and $SKKS$, and for comparison, a record with strong $SKKS$ (93219). Take-off angles of $SKKS$ and Sd are very close, and the weakness of $SKKS$ at these epicentral distances implies that the focal mechanism is unfavourable for generating SVd. This is further confirmed by calculations of synthetic seismograms with the reflectivity technique (Kind and Mueller 1975). The SV component of Sd in the records of events 88070 and 93190 is clearly coupled with SH: the SV component of every record looks like the derivative of the SH component, which is characteristic of azimuthal anisotropy.

For the records in Figure 2a,b, and one additional similar record, we deconvolved the two components of Sd by the respective SHd. Deconvolution eliminates differences between the records depending on the differences between source functions and magnitudes of the individual events. To suppress noise, the deconvolved components are stacked (Fig. 3A). There is a quarter-period phase shift between the components of Sd, which is characteristic of azimuthal anisotropy. The parameters of anisotropy are determined for the stacked components via (3). The resulting estimates of α, azimuth of fast velocity counted clockwise

from North, and δt are 100° and 1.2s, respectively and differ from 80° and 0.8s, as found by Vinnik et al. (1989b) from the analysis of SKS. When the stacked SVd is corrected by using (1) with $\alpha = 100°$ and $\delta t = 1.2s$, the signal is reduced to the level of noise (Fig. 3B).

To verify that the particle motions of *SKS* or *SKKS*, in our records, are compatible with the direction of anisotropy determined by *Vinnik et al.* [1989b], we considered seven recordings of events with strong *SKS* or *SKKS*. The azimuth of fast axis of this receiver anisotropy (80°) is close to back azimuths of the Fiji-Tonga events at HRV/WFM (around 263° or 83°), which would imply that no correction for upper mantle anisotropy should be needed. We deconvolved both horizontal components of *SKKS* by the *SV* component of *SKKS*, and stacked the deconvolved components (Fig. 3C). The stacked *SH* component of $SKKS$ is correlated with the *SV* component, indicating that it is due to side refraction. The signal in the *SH* component is reduced to the level of ambient noise by determining the principal motion direction in $SKKS$ and rotating the coordinate frame correspondingly (Fig. 3D). The direction thus determined differs by 5° from the true back azimuth. A similar result is obtained in experiments with SKS. A signal with a quarter-period phase shift relative to *SV* is clearly missing in *SH* in Figure 3C, which suggests that the azimuth of fast axis of receiver anisotropy is indeed in agreement with that determined by *Vinnik et al.* [1989b]. This confirms that the value of α found above for Sd is distinctly different from that suitable for SKS and $SKKS$. Another example of a similar discrepancy is provided by the data of station RSON (RSTN network), where the parameters of receiver anisotropy appropriate for Sd, as determined via (3), are 115° and 0.6s, different from 80° and 1.7 s obtained from SKS splitting [*Vinnik et al.*, 1992]. Effect of this anisotropy in the records of Sd can be eliminated with the correction obtained from the master event analysis, but not using the parameters appropriate for SKS. In what follows, we illustrate the consequence of these corrections for differential travel time measurements.

3.4 Measurement of $SVd - SHd$ differential travel times

The corrected records at HRV/WFM with detected SVd are displayed in Figure 4a. The arrivals of SHd in Figure 4a are identified by comparing them with the theoretical

first motion directions for the respective focal plane solutions. In two cases (events 93080 and 86146a), when the first arrivals of SHd are too weak to be seen, their arrival times are determined by interpolating $SHd - SKKS$ differential times for the neighbouring events (94068, 89320 and 86146b). The procedure for detecting first motion in SVd and determining $SVd - SHd$ differential time, which is illustrated by Figure 4a, consists of several steps. First motion of $SKKS$ is identified by Hilbert transforming $SKKS$ and matching the first cycle of the transformed waveform of $SKKS$ to the raw SKS (Choy and Richards 1975). We verify with the help of synthetic seismograms, that this technique works well even in the distance range where the SKS waveform is distorted by $SPdKS$. To identify SVd arrivals, synthetic seismograms are calculated with the isotropic reflectivity technique for the reference model PREM (Dziewonski and Anderson 1981) with an S velocity in D" reduced by 4%. The synthetics are calculated for the source functions providing good fit between the theoretical and observed waveforms of $SKKS$ and for the focal plane solutions of the corresponding events. Differential time between $SKKS$ and SVd can be found accurately in synthetics calculated for an arbitrary source function with a sharp onset, and, using this time, the arrival of SVd is identified in the synthetic corresponding to the actual source function. The SVd arrival in the real record can be identified by comparing the real record with the theoretical waveform.

The synthetic SVd waveforms in Figure 4a are generally not much different from the real ones, in support of the transverse isotropy assumption. Some differences should not be surprising, considering extreme complexity of the lower mantle in the study region. A rule of thumb derived from our experiments is that the sign of SVd first motion should always be the same as that of $SKKS$, and at large distances there should be correlation between the waveforms of $SKKS$ and SVd. Remarkable features of the SVd signals are their distance- dependent delays relative to SHd, as indicated by the arrows in Figure 4a. A similar trend is present in the records of RSON, where a generally similar processing procedure was applied to the raw data (Fig. 4b). These measurements, as well as similar ones at other stations, have been used to infer the presence of strong anisotropy in D", locally reaching 10% or more (Vinnik et al., 1997), which is an order of magnitude stronger than previously reported.

3.5 Discussion and conclusions

The distance-dependent delays of SVd relative to SHd would hardly be detected without our technique. This is well illustrated by comparing the raw record of event 93219 (Fig. 2c) and its processed version in Figure 4a. Whereas the first visible arrival in the SV component of Sd in Figure 2c is delayed relative to SHd by about 15 s, the true SVd arrival, as shown by Figure 4a, is delayed by only 6 s. In a number of other cases considered at HRV/WFM, the signals previously interpreted as the SVd arrivals are either fully suppressed or significantly modified by the corrections. This eliminates some internal inconsistencies noted in previously published data (Maupin, 1995).

The assumption of transverse isotropy in D" is critical to the correction method proposed. It is supported by four arguments: (1) the earlier observation that the amplitude of SVd is correlated with that of $SKKS$ rathen than SHd (Vinnik et al., 1995); (2) the isotropic reflectivity synthetics computed with different models for SH and SV yield SVd waveforms in good agreement with observed ones; (3) the delays of SVd are similar in pairs of records at similar epicentral distances, one of which contains very strong SHd, and requires large correction for SV, whereas in the other, SHd is weak, and the correction is insignificant: compare 94068 with 93080 and 86146a with 86146b in Figure 4a; (4) strong discrepancies between the estimates of receiver anisotropy based on the $SKS/SKKS$ and Sd data are found at some stations, but they are missing at other stations, along practically the same wavepaths in D".

The discrepancies can be an effect of unmodelled complexity of the crust and upper mantle beneath the receiver, but another explanation cannot be excluded. The wavepaths of Sd and $SKKS$ are very similar in the upper mantle beneath the receiver, but they are strongly different in the lowermost mantle. Hence, it is conceivable that anisotropy in the lowermost mantle is azimuthal but laterally variable, and it contributes differently to $SKKS$ and Sd. Transverse isotropy in D" can be a result of averaging azimuthal anisotropies along the wavepath of Sd or ScS.

3.6 Acknowledgments

This work was partially supported by NSF, grant EAR 9417862. It is Berkeley Seismological Laboratory contribution 97-06. Reprinted by permission from American Geophysical Union, Vinnik, L., Bréger, L. & Romanowicz, B. On the inversion of Sd particle motion for seismic anisotropy in D". *Geophys. Res. Lett.* **25**, 679-682 (1998).

3.7 References

Choy, G. L. and P. G. Richards, Pulse distortion and Hilbert transformation in multiply reflected and refracted body waves, *Bull. Seismol. Soc. Am.*, **65**, 55-70, 1975.

Dziewonski, A. M. and D. L. Anderson, Preliminary Reference Earth Model, *Phys. Earth Planet. Int*, **25**, 297-356, 1981.

Farra, V., L. P. Vinnik, B. Romanowicz, G. L. Kosarev and R. Kind, Inversion of teleseismic S particle motion for azimuthal anisotropy in the upper mantle - A feasibity study, *Geoph. J. Int.*, **106**, 421-431, 1991.

Garnero, E. and T. Lay, Lateral variations in lowermost mantle shear wave anisotropy beneath the north Pacific and Alaska, *J. geophys Res.*, **102**, 8121-8135, 1997.

Kendall, J. M. and P.G. Silver, Constraints from seismic anisotropy on the nature of the lowermost mantle, *Nature* **381**, 409, 1996.

Kind, R. & G. Mueller, Computations of SV waves in realistic Earth models, *J. Geophys.*, **41**, 142-172, 1975.

Lay, T. and C.J. Young, Analysis of seimsic SV waves in the core's penumbra, *Geophys. Res. Lett.* **18**, 1373, 1991.

Matzel, E, S.W. Sen and S. P. Grand, Evidence for anisotropy in the deep mantle beneath Alaska, *Geophys. Res. Lett.*, **23**, 2417-2420, 1996.

Maupin, V., On the possibility of anisotropy in the D" layer as inferred from the polarization of diffracted S-waves, *Phys. Earth Planet. Int.* **87**, 1-32,1994.

Vinnik, L., V. Farra and B. Romanowicz, Observational evidence for diffracted SV in the shadow of the earth's core, *Geophys. Res. Lett.* **16**, 519, 519-522, 1989a.

Vinnik, L., V. Farra and B. Romanowicz, Azimuthal anisotropy in the Earth from observations of SKS at Geoscope and NARS broadband stations, *Bull. Seismol. Soc. Amer.*,

79, 1542-1558, 1989b.

Vinnik, L. P., L. I. Makeyeva, A. Milev and A. Yu. Usenko, Global patterns of azimuthal anisotropy and deformations in the continental mantle, *Geoph. J. Int.*, bf 111, 433-447, 1992.

Vinnik, L., B. Romanowicz, Y. Le Stunff and L. Makeyeva, Seismic anisotropy in the D" layer, *Geophys. Res. Lett.* **22**, 1657-1660, 1995.

Vinnik, L., L. Breger and B. Romanowicz, Anisotropic structures at the base of the mantle, submitted to *Nature*, 1997.

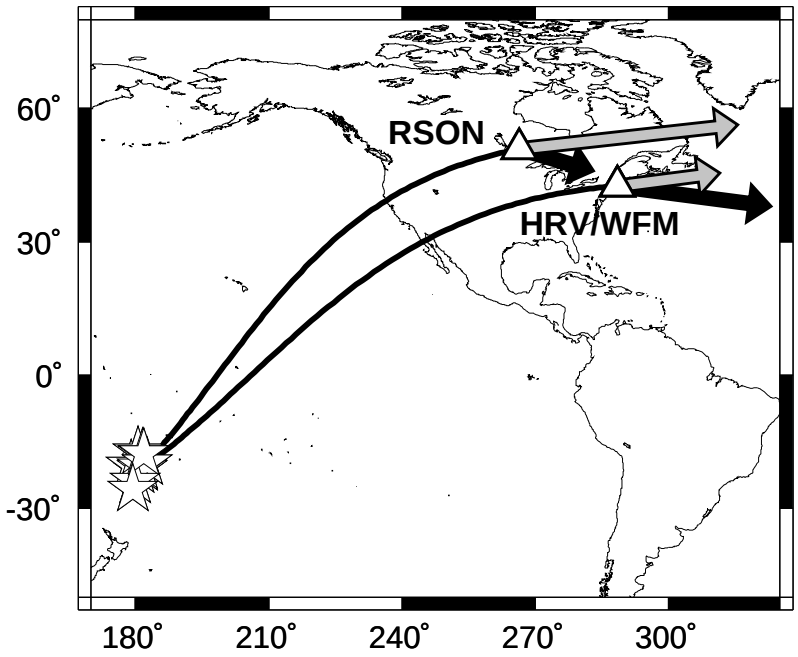

Figure 3.1. Surface projection of paths between Fiji-Tonga earthquakes and seismograph stations considered. The grey and black arrows indicate the fast direction of anisotropy, at each station, as obtained using standard SKS splitting measurements and the master event method described in the text, respectively.

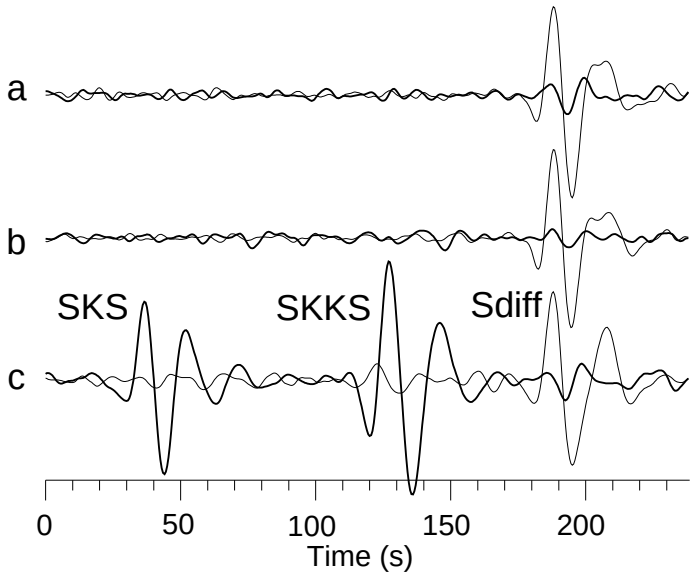

Figure 3.2. (a) and (b) Examples of records at HRV (88070 and 93190, respectively) for which no *SKS*/*SKKS* energy is present. Polarity is inverted for the record of the event 88070. (c) For comparison, a record (93219) with strong *SKS*/*SKKS* presence.

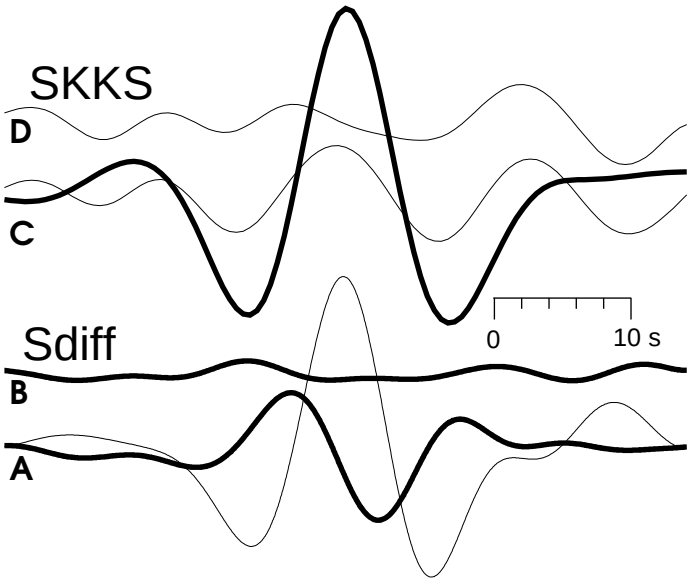

Figure 3.3. (A): SV (bold line) and SH components of Sd of the master events, deconvolved by SH and stacked. SV is amplified 3 times relative to SH. (B): The same SV component, as in (A), but corrected for receiver anisotropy inferred from (A). (C): SV and SH components of $SKKS$, deconvolved by SV and stacked. SH is amplified 3 times relative to SV. (D): The same SH component as in (C), but corrected for the side refraction of $SKKS$.

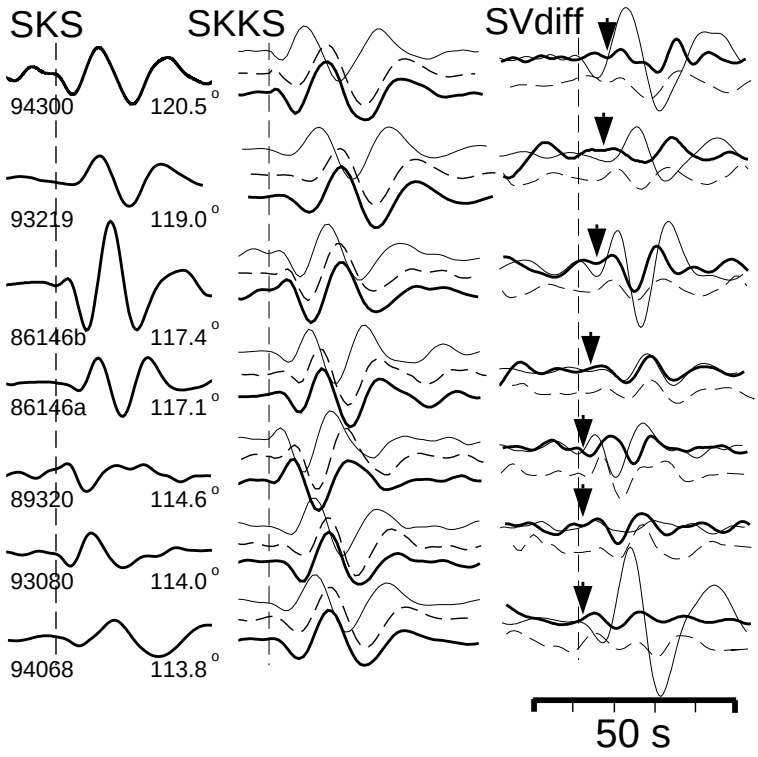

Figure 3.4. (a) SV and SH components of the records at HRV/WFM. Left column - SKS. Central column - $SKKS$ (bold line), synthetic $SKKS$ (dashed line) and Hilbert-transformed $SKKS$ (thin line). Right column - SV component of Sd (bold line), synthetic SV component of Sd (dashed line) and SH component of Sd (thin line). SV components of Sd are amplified twice relative to SH. Arrivals of SKS, $SKKS$ and SHd correspond to the vertical dashed lines. The records are corrected for receiver anisotropy.

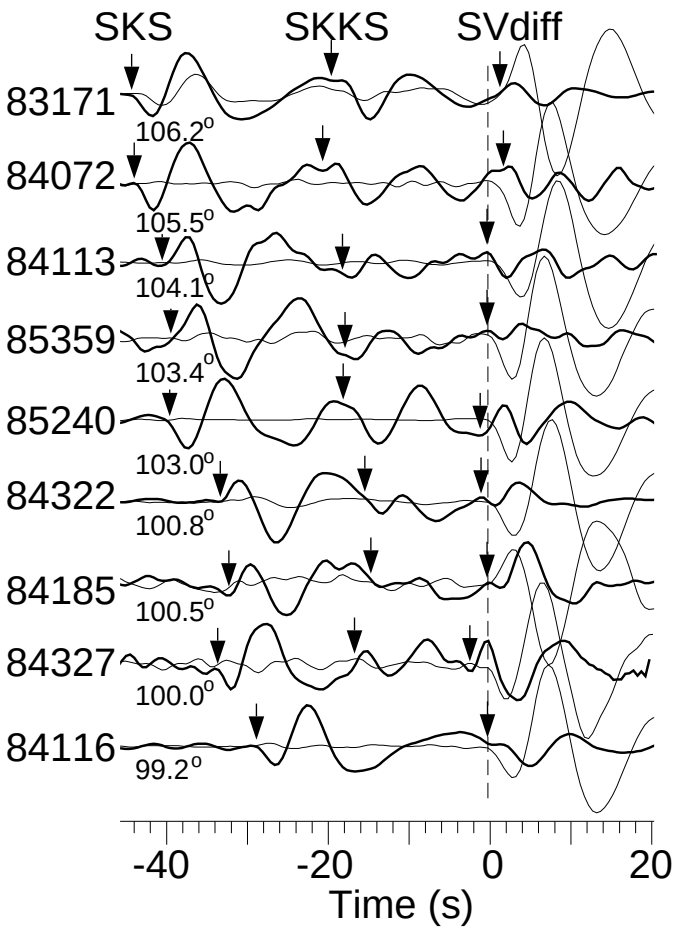

Figure 3.4. (b) R (bold line) and SH components of the records at RSON, corrected for side refraction and receiver anisotropy. Arrivals of SHd correspond to the vertical dashed line.

Chapter 4

Test of tomographic models of D" using differential travel time data

4.1 Summary

We compare local measurements of SH-velocity in D" under the Pacific Ocean with four recent S-velocity models derived with different techniques. From the local measurements, we find evidence for both strong fast and slow anomalies with an amplitude sometimes exceeding 10%, as well as strong lateral velocity gradients. The tomographic models underestimate the magnitude of the observed anomalies by roughly a factor of 3. The model that best matches both the sign and the localisation of the anomalous structures is exclusively an SH model. This indicates, in particular, that the presence of anisotropy in D" may not be ignored and that it is important to separate SH and SV contributions in tomographic studies of the lowermost mantle.

4.2 Introduction

Over the past few years, global tomographic models of mantle S-velocity have been developed with higher resolution than was previously attainable, in particular in the lowermost mantle [*Liu et al.*, 1994; *Masters et al.*, 1996; *Li and Romanowicz*, 1996; *Grand et al.*, 1997]. While there is qualitative agreement in the large scale features of these models, there are many differences in the details of the 3-D structure recovered. Such details are

of interest for geodynamics and mineral physics interpretations, it is therefore important to confirm the validity of specific models and particularly for the deepest mantle, where strong lateral variations and strong anisotropy [e.g. *Vinnik et al.*, 1997] have recently been documented. These recent findings raise issues as to whether standard wave propagation approaches used in tomography, which assume smooth structure, are appropriate, and whether, at least in D", the assumption of isotropy is justified.

The path between earthquake sources in the Fiji-Tonga Islands and North American stations provides an optimal setting for a local comparison experiment with several large earthquakes each year recorded at a large number of stations in North America. We adopt the approach of *Vinnik et al.* [1997] and consider the variation with distance of $SH - SKS$ travel time residuals for a fixed source or a fixed station along narrow azimuthal corridors. This allows us to infer variations in SH-velocity in well specified locations in D". We then compare the mapped anomalies with those of four recent tomographic S-velocity models.

4.3 Method and data

The data used are $SH - SKS$ travel time residuals with respect to the reference model PREM [*Dziewonski and Anderson*, 1981], from two data collections: one assembled from a combination of analog and digital data [*Garnero et al.*, 1988] and the other a smaller set of measurements made by us on digital records at IRIS station LON. In both cases, we considered deep, intermediate and shallow events.

Travel times were picked manually with an accuracy around 0.5-1s. No cross-correlation method was used, so the broadening of the S pulse with respect to that of SKS du to differential attenuation should not affect the residuals significantly.

For a fixed source in the Fiji-Tonga region or a fixed receiver in North America, we selected a subset of paths corresponding to a narrow azimuthal range (at most a few degrees) and, as in *Vinnik et al.* [1997], plotted the residuals as a function of epicentral distance. A similar analysis was also performed by *Garnero and Helmberger* [1993] and *Ritsema et al.* [1997], but these authors binned their data into much broader azimuth ranges and did not separate the contribution of each station or event, which resulted in estimates of velocity averaged over broader regions. We considered epicentral distances larger than

84^o where S starts diving into D". By using differential travel times, the effect of upper mantle heterogeneities and errors in focal parameters are minimized. Assuming the outer core is laterally homogeneous [*Buchbinder*, 1972], the observed travel time anomalies must originate in the deepest mantle, where the paths of SKS and S differ the most (Fig. 1).

SKS is unlikely to contribute significantly to the observed trends since the time spent by SKS in D" is no more than 1/5 of that of S. Finally, since deep and shallow events produce consistent trends, as also documented by *Vinnik et al.* [1997], and since there is a good agreement between the trends observed at different stations, upper-mantle anisotropy should not affect our results.

Under these assumptions, we will be discussing structure near the base of the mantle as seen by SH-polarized waves, which, in the presence of anisotropy [e.g. *Vinnik et al.*, 1989; 1995; 1997], could be somewhat different from the structure seen by SV-polarized waves. When the source or the receiver is fixed, and for a fixed azimuth, the S leg nearest to the fixed point remains roughly fixed whereas the other leg samples an increasingly larger portion of D" as epicentral distance increases (Fig. 1). The slope of the corresponding residual versus distance plot can be attributed to heterogeneity in that particular region of D". A positive slope will be characteristic of locally low SH-velocities in D", and a negative slope of high velocities. The magnitude of the slope allows us to give a crude estimate of the magnitude of the local velocity anomaly.

4.4 Results

We present measurements for fixed station LON in Fig. 2a. The corresponding sources and wavepaths are given in Fig. 1a. The residuals show a strong increase with distance between 84^o and approximately 89^o. The slope changes abruptly around 89^o and returns to a value close to 0 as S starts sampling a domain where SH-velocity is well predicted by PREM. *Vinnik et al.* [1997] reported several similar observations for $SH - SKS$ residuals at other stations and for different epicentral ranges for which S dives deeply into D" and diffracts along the CMB, and demonstrated that this result was very stable and that the trend was not a near source effect. The interest of station LON is twofold. First, it corresponds to a slightly smaller distance range than considered by

Vinnik et al. [1997] (approximately $84-106^0$ against $96-120^o$) where S is diffracted only for the largest distances, while at smaller distances S samples the uppermost part of D". The residuals for station LON indicate that the anomalous region is not localised at the CMB but extends throughout the whole D" layer. Second, the path considered corresponds to more northerly azimuths, which allows us to document the existence of a transition zone between very low and "normal" SH-velocities, northwest of where it has been reported so far.

We next consider a fixed event and, again, an azimuthal window of only a few degrees. This allows us to explore the lowermost mantle beneath the northwestern portion of the Fiji-Tonga to North America paths.

Data for event 06/25/92 are shown in Fig. 2b. Residuals at distances smaller than 96^o decrease regularly with distance with a slope of almost -1s/deg indicating very high SH-velocities and a strongly fast anomaly. A kink around 96^o, beyond which anomalies stop accumulating, indicates that the S-wave starts sampling a region with normal velocities in D". Another event (07/11/92, Fig. 2c) confirms the slopes observed in Fig. 2b. The abrupt kink present in the residual versus distance plots also suggests the existence of a sharp boundary between the two domains.

Residuals for event 08/25/63 (Fig. 2d) exhibit the opposite trend for slightly smaller azimuths, with a plateau followed by a rather strong increase with distance. The region of interest is northeast of the one considered in Fig. 2b and 2c.

Measurements for events 03/17/66 and 08/25/63 (Fig. 2e and 2f) allow us to extend the distance range previously considered. In Fig. 2e, there is a strong increase with distance between two plateaus which, at the shorter distances, confirms what we see on Fig. 2d. Fig. 2f does not exhibit any plateau at small distances but shows a clear flattening of the slope at large distance. Note here the increased scatter in the data, probably due to the larger interval of azimuths considered.

The exact geometries of the anomalous regions are hard to determine: there are trade-offs between depth extent and magnitude, and, in the presence of strong local anomalies, raypaths might be quite different from those predicted by PREM. If we assume that the heterogeneity of the mid mantle does not exceed 3-4%, as indicated by global tomography, the contamination by mid mantle structure is a second order effect. But the deeper

S and SKS dive, the more apart they travel. In principle, it becomes therefore possible to explain residuals by adding structure in the lower mantle above D". This is a source of uncertainty in our study, and the reason why our analysis remains only qualitative.

We have identified five distinct regions (R1..) and three transition domains (T1..) in the deep mantle underneath the Pacific and now compare those with four S-velocity tomographic models (M1..) in Fig. 3. The low SH-velocity region (R2) in the Southwest Pacific is present in all 4 tomographic models. M1, M2 and M3 saturate around -3% whereas M4 predicts a milder value. Region R1 only exists in models M1 and M4; in this region, model M2 only shows a small reduction of the magnitude of the anomaly while M3 is still saturated. M1, M2 and M3 predict high velocities in Region 3, while,for M4, velocities are still low. Proceeding east, only M1 matches the travel time results for region R4, with, however, an anomaly around -1.5% against the -4% that we report here. Finally, our estimate of the anomaly in region R5 is in agreement with models M1 and M4 but not with M2 and M3. As for the transition domains (Fig. 3), the first one (T1), in the Southwest Pacific, has already been described in Vinnik et al., (1997). It is well predicted by models M1 and M4. The second one (T2) is present in M1 where we expect it from the present data. It is further northeast in M2, but is absent in M3 and M4. T3 is only present in model M1.

Model M1 is in best agreement with our results. Transition regions and signs of anomalies are generally fairly well predicted, although the magnitude of the largest anomalies that we report are well in excess of what M1 predicts. Note however that, although the magnitude of the anomalies is underestimated, the relative scaling of the anomalies is in agreement with the local data.

4.5 Discussion

Local variations of SH-velocities in D" beneath the Pacific are on the order of 3 times larger than predicted by global mantle tomographic models, as well as tomographic models derived specifically for D" using body-wave data sensitive to that region (Wysession, 1996, Kuo and Wu, 1997).

The trends observed in Fig. 2 and 3 cannot be obtained with anomalies with mag-

nitude less than 3-4%, since 2D ray-tracing calculations for the four tomographic models considered do not produce slopes even close to the ones we observe. We illustrate this in Fig. 2g-i, where we present S, SKS and $S-SKS$ synthetic residuals for event 25/06/92 and model M1. We note the qualitative agreement between synthetics (Fig. 2i) and data (Fig. 2b), with, however, much larger amplitudes in the data. Fig. 2g and 2h confirm that the anomaly originates in SH rather than in SKS.

The success of M1 in matching the spatial variations of SH velocity predicted by the local travel time measurements can be understood as follows. This model, based upon a waveform inversion method, was obtained using tangential components exclusively: this is an "SH" velocity model, and it is therefore the most appropriate to compare with our $SH-SKS$ travel time residual plots. Other distinct features of the derivation of M1 are that (1) it was obtained using waveform data and a theoretical approach based on the Nonlinear Asymptotic Coupling Theory (NACT) [*Li and Romanowicz*, 1995] which is better suited for the modeling of broadband body waveforms compared to the Path Average Approximation (PAVA) [*Woodhouse and Dziewonski*, 1984] generally used. And (2) each body wavepacket in a seismogram is considered separately, which allows us to assign larger weights to weaker phases, such as Sdiff, which are sensitive to lowermost mantle structure.

The other 3 models (M2, M3 and M4) were derived using a combination of SH and SV sensitive data and a variety of inversion techniques (PAVA and travel times for M3 and M4, WKBJ for M2). As shown by *Vinnik et al.* [1997], anisotropy in D" can be locally very strong ($>$ 10%) and far in excess of the 1-3% generally proposed. Under such conditions, anisotropy is not a second order effect, and inverting SV and SH data simultaneously under the assumption of isotropy is likely to result in a biased picture of the average S-velocity. Separating the SH component is a first step towards a refined tomographic approach for the lowermost mantle.

4.6 Conclusions

Our analysis of differential $SH-SKS$ travel time residuals demonstrates that the D" region beneath the Pacific exhibits strong velocity contrasts. Both high and low S-velocity domains where anomalies could reach a magnitude of $\pm 10\%$ have been detected, and the

transition between these domains can be very abrupt, which implies strong lateral velocity gradients. If we add anisotropy to this already complex picture, it becomes clear that D" presents challenging conditions for global tomography. In the future, particular attention to the complexity of D" structure and anisotropy must be given in global tomographic studies.

4.7 Acknowledgements

We thank Ed Garnero for making his dataset available to us, and Michael Wyssession and an anonymous reviewer for insightful suggestions. This work was partially supported by NSF, grant EAR 9417862. It is Berkeley Seismological Laboratory contribution 97-05. Reprinted by permission from American Geophysical Union, Bréger, L. Romanowicz, B., & Vinnik, L. Test of tomographic models of D" using differential travel time data. *Geophys. Res. Lett.* **25**, 5-8 (1998).

4.8 References

Buchbinder, G. G. R., Travel times and velocities in the outer core from PmKP, *Earth Planet. Sci. Lett., 14*, 161-168, 1997.

Dziewonski, A. M., and D. L. Anderson, Preliminary Reference Earth Model, *Phys. Earth Planet., Int 25*, 297-356, 1981.

Garnero, E. J., D. V. Helmberger, and G. Engen, Lateral variations near the core-mantle boundary, *Geophys. Res. Lett., 15*, 609-612, 1988.

Garnero, E., and D. V. Helmberger, Travel times of S and SKS: implications for three-dimensional lower mantle structure beneath the central Pacific, *J. Geophys Res., 98*, 8225-8241, 1993.

Garnero, E., and D. V. Helmberger, A very slow basal layer underlying large-scale low-velocity anomalies in the lower mantle beneath the Pacific: evidence from core phases, *Phys. Earth Planet., Int 91*, 161-176, 1995.

Grand, S., R. van der Hilst, and S. Widiyantoro, Global seismic tomography: a snapshot of convection in the Earth, *G.S.A. Today, 7*, 1-7, 1997.

Kuo, B.Y., and K. Y. Wu, Global shear velocity heterogeneities in the D" layer: inversion from Sd-SKS differential travel times, *J. Geophys Res., 102*, 11775-11788, 1997.

Li, X.-D., and B. Romanowicz, Comparaison of global waveform inversion with and without considering cross-branch modal coupling, *Geophys. J. Int., 121*, 695-709, 1995.

Li, X.-D., and B. Romanowicz, Global mantle shear velocity model developed using non-linear asymptotic coupling theory, *J. Geophys Res., 101*, 22245-22272, 1996.

Liu, X.-F., W.-J. Su, and A. M. Dziewonski, Improved resolution of the lowermost mantle shear wave velocity structure obtained using SKS-S data (abstract), *Eos. Trans. AGU, 75*, 232, 1994.

Masters, G., S. Johnson, G. Laske, and H. Bolton, A shear-velocity model of the mantle, *Phil. Trans. R. Soc. London 354*, 1385-1410, 1996.

Ritsema, J., E. Garnero, and T. Lay, A strongly negative shear velocity gradient and lateral variability in the lowermost mantle beneath the Pacific, *J. Geophys Res. 102*, 20395-20411, 1997.

Vinnik, L., V. Farra, and B. Romanowicz, Observational evidence for diffracted SV in the shadow of the Earth's core, *Geophys. Res. Lett. 16*, 519-522, 1989.

Vinnik, L., B. Romanowicz, Y. Le Stunff, and L. Makeyeva, Seismic anisotropy in the D" layer, *Geophys. Res. Lett. 22*, 1657-1660, 1995.

Vinnik, L., L. Breger, and B. Romanowicz, Anisotropic structures at the base of the Earth's mantle, *Submitted to Nature*, 1997.

Woodhouse, J. H., and A. M. Dziewonski, Mapping the upper mantle: Three dimensional modeling of Earth's structure by inversion of seismic waveforms, *J. Geophys. Res. 89*, 5953-5986, 1984.

Wysession, M. E., Large-scale structure at the core-mantle boundary from diffracted waves, *Nature 382*, 244-248, 1996.

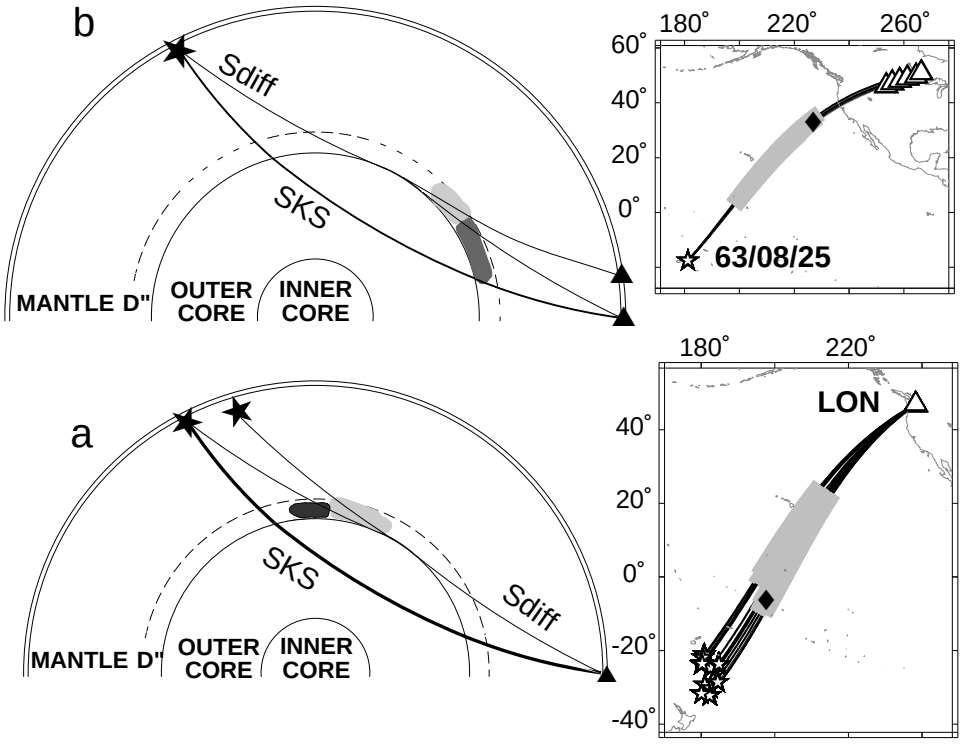
b
Sdiff
SKS
MANTLE D"
OUTER CORE
INNER CORE
180˚
220˚
260˚
60˚
40˚
20˚
0˚
63/08/25
a
SKS
Sdiff
MANTLE D"
OUTER CORE
INNER CORE
180˚
220˚
LON
40˚
20˚
0˚
-20˚
-40˚

Figure 4.1. (a) Left: schematic representation of the wavepaths of SKS and $Sdiff$ for a given azimuth and a fixed station. The wavepaths of S for two different positions of the source (stars) differ mostly on the source side. If we have two adjacent regions where SH-velocity is respectively low (light gray), and normal (dark gray), differential $SH-SKS$ travel time residuals increase with distance until S starts propagating in the normal region, where they remain constant. Right: surface projection of the wavepaths considered for fixed IRIS station LON (Fig. 3a). The light gray zone of each wavepath indicates the D" leg of S. The diamond corresponds to a D" exit point for which S starts sampling the region with normal SH-velocity. (b) Same as Fig. 1a, but for fixed event 08/25/63, and variable station.

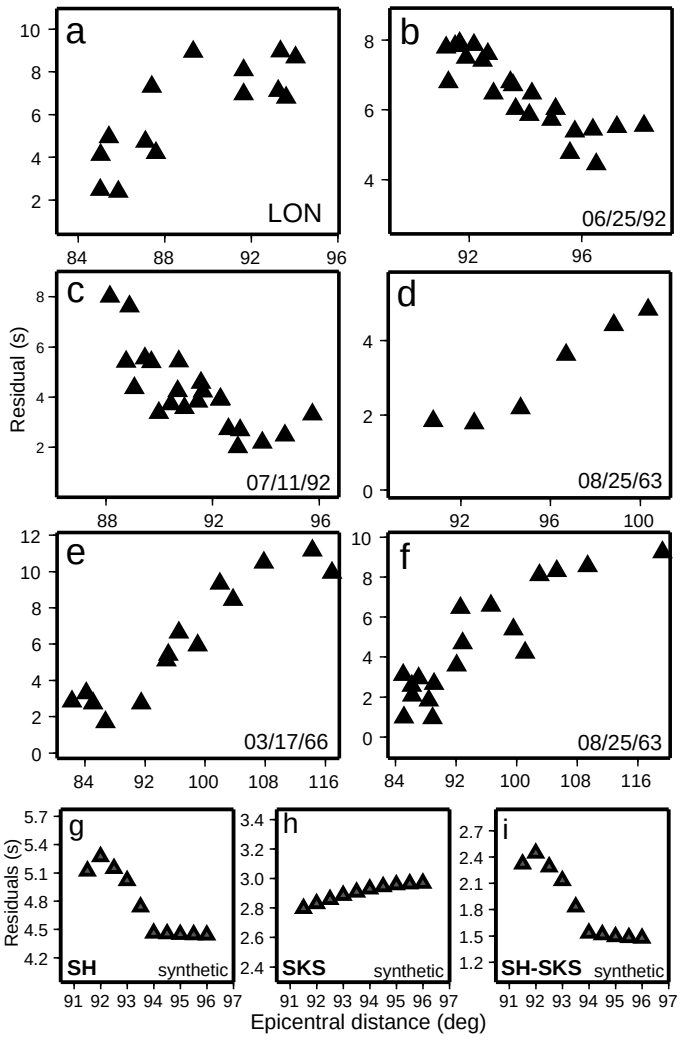
a
LON
b
06/25/92
c
07/11/92
d
08/25/63
e
03/17/66
f
08/25/63
Residual (s)
g
SH
synthetic
h
SKS
synthetic
i
SH-SKS
synthetic
Residuals (s)
Epicentral distance (deg)

Figure 4.2. (a) $SH - SKS$ differential travel time residuals with respect to those of PREM for station LON. A change in trend over a distance of a few degrees is observed with fast increasing residuals at short distances and stationary ones at larger distances. (b) $SH - SKS$ differential travel time residuals with respect to PREM for event 06/25/92. A change in trend over a distance of a few degrees is observed with fast decreasing residuals at short distance and stationary ones at larger distances. (c) Same as (b) for event 07/11/92. Note the similarity with (b). (d) Same as (b) for event 08/25/63. A change in trend over a distance of a few degrees is observed with stationary residuals at short distance and strongly increasing ones at larger distances. (e) Same as (d) for event 03/17/66 and for an extended range of azimuths and distances. The first part of (d) is confirmed, but there are also indications for a second kink at large distance. (f) Same as (e) for event 08/25/63. The trend in the residuals is consistent with the one observed in (e) despite more scatter in the data. (g) S synthetic residuals with respect model calculated for model M1, event 06/25/92 and the same azimuthal range as the one considered in (b). (h) Same as (g) for SKS. Note that the variations less than in (g) by at least a factor of 5. (i) Same as (g) for $S - SKS$. The overall shape is close to that in (b), but the slope is smaller by a factor of 3-4.

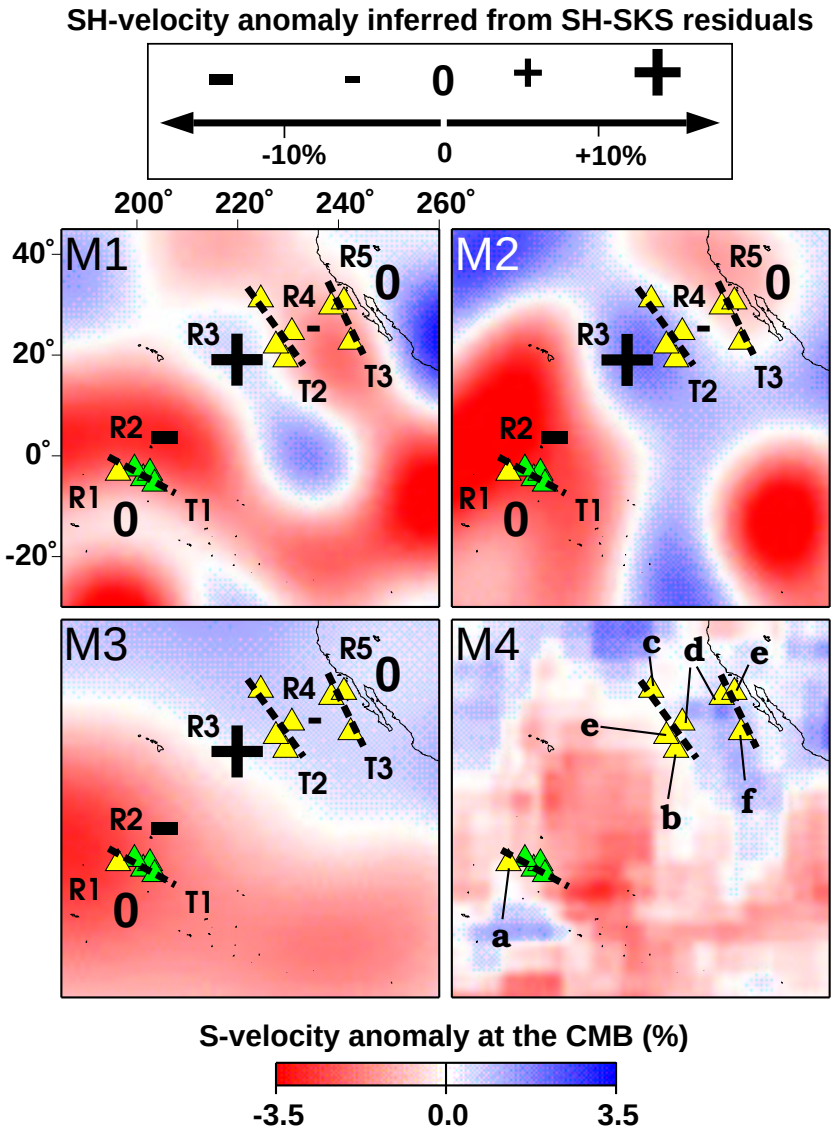
SH-velocity anomaly inferred from SH-SKS residuals
- - 0 + +
-10%
0
+10%
200°
220°
240°
260°
40°
20°
0°
-20°
M1
M2
M3
M4
R1
R2
R3
R4
R5
T1
T2
T3
a
b
c
d
e
f
S-velocity anomaly at the CMB (%)
-3.5
0.0
3.5

Figure 4.3. Comparison between the results of the analysis of $SH-SKS$ differential travel time residuals, and four recent tomographic models adopted from: M1, *Li and Romanowicz* [1996], M2, *Liu et al.* [1994], M3, *Masters et al.* [1996] and M4, *Grand et al.* [1997]. We assigned a qualitative anomaly (black symbols) to five distinct regions (R1-5), based on the slope of the residual versus distance plots: "+","0", and "-" indicate respectively faster, equal to and slower SH velocities compared to PREM. Large (or small) symbols indicate anomalies larger (or smaller) than $\pm 10\%$ in magnitude. We also underlined three transition domains (T1-3, broken lines) defined by D" exit points (triangles) associated with a kink in the residuals/distance plots. These points were obtained by picking the distance around which a kink occurs and by calculating the corresponding D" exit point on the source (respectively receiver) side when the station (respectively receiver) was fixed. Each yellow triangle is from this study and has been assigned, on the M4 frame, a letter corresponding to the plot from which it originated in Fig. 2. Green triangles are from *Vinnik et al.* [1997].

Chapter 5

Three dimensional structure at the base of the mantle beneath the Central Pacific

5.1 Summary

Forward modeling of differential travel times of phases sensitive to lowermost mantle beneath the Central Pacific, reveals lateral heterogeneity that is higher in amplitude than predicted by tomographic models. A broad zone of low S-velocity (-4% with respect to standard models), which may correspond to the base of a thermal "plume", narrows and is deflected as it extends to about 1000 km above the core-mantle boundary. To the east of this zone, a localized region of fast S-velocity (+5%) suggests strong heterogeneity or anisotropy related to the presence of high pressure and temperature assemblages, which may or may not involve core material. Its presence could also explain the observation of precursors to core reflected phases in this region [1] .

[1]Reprinted by permission from, Bréger, L. & Romanowicz, B. Three-Dimensional structure at the base of the mantle beneath the Central Pacific. *Science* **382**, 718-720 (1998). *Geophys. Res. Lett.* **25**, 679-682 (1998). Copyright 1998 American Association for the Advancement of Science.

5.2 Introduction

The D" region in the lowermost mantle (2600 to 2889 km depth) is a thermal and chemical boundary layer thought to play a critical role in the dynamics of the Earth. Seismic body wave studies reveal a complex velocity structure (*1*). To explain observations of precursors to ScS phases, one dimensional models involving a discontinuity at the top of D" have been proposed, associated with variable vertical velocity gradients (*2*). On the other hand, recent studies provide evidence for the existence of strong lateral heterogeneity and anisotropy near the CMB (*3-10*). It has also been proposed that ScS precursors might be a manifestation of complex three dimensional (3D) structure rather than layering (*11*). Global tomographic models (*12-13*) indicate a reddening of the spectrum of heterogeneity and an increase in the rms velocity fluctuations when approaching the core mantle boundary (CMB), but it has been shown that the lateral variations inferred within D" by tomographic techniques are generally underestimated (*5-6*). The characterization of 2D and 3D heterogeneity near the CMB has so far been mostly qualitative and few studies have attempted 2D (*3,10*), let alone 3D forward modeling of body wave observations to quantitatively constrain the horizontal and vertical extent of prominent structures.

5.3 Data, method, and results

We assembled a dataset of $S-SKS$ and $SKKS-SKS$ differential travel times for the Central Pacific (Fig. 1A) and, by forward modeling, developed a family of local lowermost mantle models that provide good fits to these data. Our approach is to consider the variations with epicentral distance of $S-SKS$ and $SKKS-SKS$ travel time residuals computed with respect to Preliminary Reference Earth Model (PREM) (*14*) for a fixed source or station and along narrow azimuthal corridors. This technique was used previously (*5-6*) to document that strong lateral variations in S velocity must be locally present within D". In particular, it was found that the location of velocity anomalies in the Central Pacific was relatively well constrained by recent tomographic models (*12-13*), however, these models underestimated the variations of observed residuals by a factor of 2 or 3. No modeling was attempted in these studies, and the results remained qualitative.

We have analyzed residuals for several large events in the Fiji-Tonga-Kermadec Is-

lands region recorded at 111 North American stations (Fig. 1B) and for which the SH and SV radiations were favorable, allowing the hand picking of SKS, $SKKS$, and S or $Sdiff$ with an accuracy between 1 and 2 seconds (Fig. 2). By using differential travel times between S and SKS, or SKS and $SKKS$, we minimize errors due to source mislocation, uncertainty on earthquake origin times, and heterogeneity in the crust and upper-mantle beneath sources and receivers. The 410 residuals collected were assembled into narrow azimuthal profiles. For different profiles corresponding to adjacent azimuths, residuals respectively increase (Fig. 3A-B,E) or decrease (Fig. 3C-D,F) with increasing epicentral distance. This indicates a complex 3D velocity structure at a scale of several hundred km at the base of the mantle. We ruled out contributions from the top 2000 km of the mantle, for the following reasons: (i) In the upper 1000 km, raypaths of S, SKS, and $SKKS$ are similar (Fig. 1A). To produce differential residuals varying by several seconds over less than 5^0 in epicentral distance would require unrealistically large anomalies in this depth range (larger than at least 10%), which is inconsistent with tomographic predictions. (ii) 3D tomographic models systematically indicate much lower rms amplitudes of lateral heterogeneity in the mid-mantle (1000-2000 km) than in the last 500-800 km of the lower mantle (*11-12*). Explaining our observations mainly by mid-mantle heterogeneity would imply velocity anomalies in the mid-mantle of amplitude several times larger than in D", and with shapes and signs that would be inconsistent with tomographic results. Overall, we estimate that the effect of 3D structure in the upper 2000 km can contribute at most 2 seconds to the observed differential travel times.

5.4 2D Modeling

A simple 1D model cannot account for the different trends observed in the residuals for adjacent azimuths and the same epicentral distance range. While a 2D model would be sufficient to fit the data in a single azimuthal corridor, a 3D model is necessary to explain the observations over several azimuthal corridors. A starting 3D model was chosen by computing predicted differential travel time residuals for several recent tomographic models (12-13), and selecting the model which gave the closest match to the observed trends (model SAW12D, (*13*)). Then, by forward modeling of travel time residuals (*15*), we progressively

perturbed the starting model in two ways: (i) by preserving the spatial distribution of anomalies and only modifying the amplitude of velocity fluctuations in selected high or low velocity regions of the model and (ii) by slightly shifting them laterally when necessary to fit the observations. We found that lateral shifts on the order or less than 250 km were generally sufficient to fit the observations. By trial and error, we thus obtained a family of models capable of explaining not only the trends in the travel time versus distance plots, but also the ranges of travel time fluctuations. We were able to achieve fits to all our data within 1-2 s (Fig. 3,4) which is within the accuracy of the travel time measurements.

5.5 Discussion and conclusion

Two prominent features are common to all models in the family (Fig. 1B, Fig.5). A mild to strong increase of the $S - SKS$ residuals (Fig. 3A-B) with epicentral distance is observed for a large number of events and azimuthal windows. This type of trend, which was identified in some early work (*3*) consistently requires a wide slow region at the bottom of the mantle south of Hawaii in the lowermost 1000 km of the mantle (S in Fig.1B and Fig.5). This anomalous region resembles that of the starting tomographic model in shape , but its amplitude needs to be increased to 3.5-4% throughout its domain (Fig. 1B,5). For depths greater than 2000 km, the shape of the anomaly is well constrained by the 410 $S - SKS$, and $SKKS - SKS$ residuals. While narrowing with decreasing depth, the anomaly extends up to at least 1000 km above the CMB (*16*) with constant strength. Interestingly, another well constrained feature is necessary to explain a different type of trend in the data, with rapidly decreasing residuals for distances between about 90 and 96^0 (Fig. 3C-D). To explain these trends, it is necessary to introduce a fast region (F in Fig. 1B,5C), adjacent to the large slow anomaly, where the velocity anomaly reaches +4 to 5% in a small domain that had only a mildly fast anomaly (about 1 to 2%) in the original model (Fig. 5 C,D). The exact shape and strength of those two required heterogeneous domains can vary slightly from one possible model to another, but by no more than 100-200 km in position and 1% in amplitude. Besides these two localized heterogeneous regions, no significant modification to the initial tomographic model is necessary, at least in the domain sampled by our dataset.

It has been proposed that the large slow region in the mantle beneath the Central Pacific, seen in all tomographic models, is related to a mega-plume generated by thermal boundary layer instabilities at the CMB (*17*). The large negative amplitude we infer in this region could be in part related to partial melt, as has been proposed to explain the ultra low velocities observed in some parts of this region (*18*). Some chemical heterogeneity, possibly involving core material, may be present as well (*19*). Some anisotropy produced by horizontal laminar fabrics or orientation of minerals by mantle flow could also contribute to the anomaly. Our forward modeling predicts that the base of this possible upwelling is rather wide, and that the plume narrows as it extends into the lower mantle, consistent with the spectral content of tomographic models, which shows a shift from red (large wavelengths) to white when ascending from the D" region into the bulk lower mantle (*12-13*). The plume also appears to be deflected to the southwest as it rises, indicating possible entrainement in the general circulation mantle flow (*20*).

The high velocity region documented by our modeling represents a contrast of about 7-8% with respect to adjacent "hot" mantle and cannot be explained by thermal effects alone. A portion of ancient slab lying at the CMB seems unlikely to be responsible for this velocity contrast because reconstructions of ancient subduction zones do not predict the presence of remnant lithosphere in this part of D" (*21*), and such a fossil slab might not produce a sufficient velocity contrast (*22*). This fast and localized anomaly could represent a high velocity product of the decomposition of perovskite at temperatures and pressures corresponding to the lowermost mantle (*23*), or of core-mantle reactions (*19,24*), and it may be related to the selective entrainment of chemically distinctive material into the thermal plume (*25*).

Since significant shear wave splitting has been observed for waves travelling through that region (*6,8*), the large velocity contrast that we observed could also be related to anisotropy, whether it is due to lattice preferred orientation of anisotropic minerals *24*, or laminar fabrics.

Finally, the block of fast material "sitting" on the core-mantle boundary could be responsible for the intermittent reflections observed at the top of D" in this region (*26,27*).

5.6 References and Notes

1. D. E. Loper and T. Lay, *J. Geophys. Res.* **100**, 6397 (1995).

2. T. Lay and D. V. Helmberger, *Geophys. J. R. Astron. Soc.* **75**, 799 (1983).

3. J. Schweitzer and G. Muller, *Geophys. Res. Lett.* **13**, 1529 (1986).

4. E. J. Garnero and D. V. Helmberger, *J. Geophys. Res.* **98**, 8225 (1993); M. Sylvander and A. Souriau, *Phys. Earth. Planet. Inter* **94**, 1 (1996); M. E. Wysession, *Nature* **382**, 244 (1996); J. Ritsema, E. Garnero, T. Lay, *J. Geophys Res.* **102**, 20395 (1997).

5. L. Bréger, B. Romanowicz, L. Vinnik, *Geophys. Res. Lett.* **25**, 5 (1998).

6. L. Vinnik, L. Bréger, B. Romanowicz, *Nature* **393**, 564 (1998).

7. J. M. Kendall and P. G. Silver, *Nature* **381**, 409 (1996).

8. J. Ritsema, E. J. Garnero, H. Benz, *Geophys. Res. Lett.* **25**, 1229 (1998).

9. J. E. Vidale and M. A. Hedlin, *Nature* **391**, 682 (1998).

10. L. Wen and D. V. Helmberger, *Science* **279**, 1701 (1998).

11. R. A. W. Haddon and G. G. R. Buchbinder, *Geophys. Res. Lett.* **14**, 891 (1987); V. F. Cormier, *J. Geophys.* **57**, 14 (1985); X. -F. Liu, J. Tromp, A. Dziewonski, *Earth Planet. Sci. Lett.*, in press.

12. S. Grand, R. van der Hilst, S. Widiyantoro, *G.S.A. Today* **7**, 1 (1997); X. -F. Liu, W. -J. Su, A. M. Dziewonski, *Eos (Spring Suppl.)* **75**, 232 (1994); G. Masters, S. Johnson, G. Laske, H. Bolton, *Phil. Trans. R. Soc. London* **354**, 1385 (1996).

13. X. -D. Li and B. Romanowicz, *J. Geophys Res.* **101**, 22245 (1996).

14. A. Dziewonski and D. L. Anderson, *Phys. Earth Planet. Int.* **25**, 297 (1981).

15. A finite difference (FD) modeling approach is desirable to forward model not only travel times but also waveforms in 3D. Such modeling is computationally heavy and not well suited for a trial and error approach unless the model space is restricted using independent constraints. On the other hand, travel times can be modelled using much more expedient ray approaches which can provide well constrained starting models for the more refined FD waveform modeling. We have here computed synthetic travel time residuals for available tomographic models using ray theory. The ray tracing was done in the spherically symmetric PREM model (*13*). We verified that, within the accuracy of the measurements (1 to 2 s), the results obtained for S and SKS were consistent with computations made using an acoustic 2D finite difference SH algorithm (J. E. Vidale, thesis, California Institute of Technology (1987)).

16. Large residuals (7-8s) are systematically observed at short distances ($80 - 90^0$) on some profiles implying very low velocities up to about 1000 km above the CMB. Tradeoffs between strength of anomalies and extent of the anomalous zone do not allow us to uniquely determine how much further above the CMB the anomaly extends. The model shown is, however, consistent with tomographic models, which show a significant drop in rms heterogeneity above that depth.

17. F. D. Stacey and D. E. Loper, *Phys. Earth. Planet. Inter.* **33**, 45 (1983); N. H. Sleep, *J. Geophys. Res.* **95**, 6715 (1990); P. F. Thompson and P. J. Tackley, *Geophys. Res. Lett.* **25**, 1999 (1998).

18. Q. Williams and E. J. Garnero, *Science* **273**, 1528 (1996).

19. E. Knittle and R. Jeanloz, *Science* **251**, 1438 (1991).

20. B. Steinberger and R. J. O'Connell, *Geophys. J. Int.* **132**, 412 (1998).

21. C. Lithgow-Bertelloni and M. A. Richards, *Rev. Geophys.* **36**, 27 (1998).

22. M. E. Wysession *et al.*, in The Core-Mantle boundary, M. Gurnis, B. A. Buffett, E. Knittle, M. E. Wysession, Eds (American Geophysical Union, Washington, DC, 1998), pp.

273-297.

23. L. S. Dubrovinsky *et al.*, *Nature* **388**, 362 (1998).

24. L. Stixrude, in The Core-Mantle boundary, M. Gurnis, B. A. Buffett, E. Knittle, M. E. Wysession, Eds (American Geophysical Union, Washington, DC, 1998), pp. 83-96; S. Karato, *Earth Space Sci.*, in press.

25. L. H. Kellogg and S. D. King, *Geophys. Res. Lett.* **20**, 379 (1993).

26. E. J. Garnero, D. V. Helmberger, G. Engen, *Geophys. Res. Lett.* **15**, 609 (1988).

27. J. Mori and D. V. Helmberger, *J. Geophys. Res.* **100**, 20359 (1995).

28. We thank Ed Garnero for making his data available to us and for helpful discussions. This work was funded by IGPP/LLNL grant 98-GS014. This is Seismological Laboratory contribution 98-04.

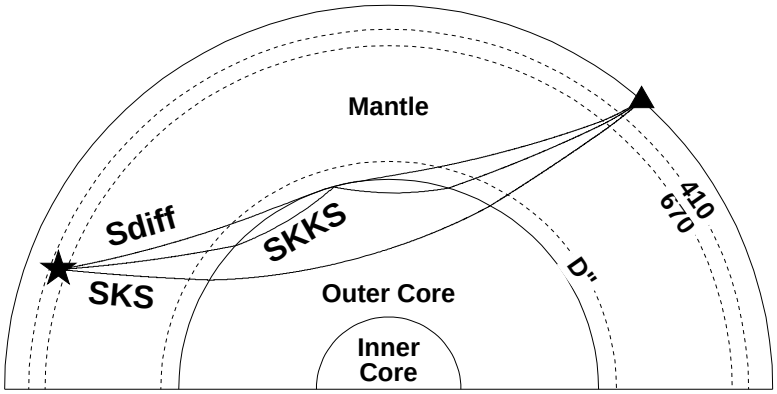

Figure 5.1. (A) Schematic representation of the wavepaths of SKS, $SKKS$, and $Sdiff$.

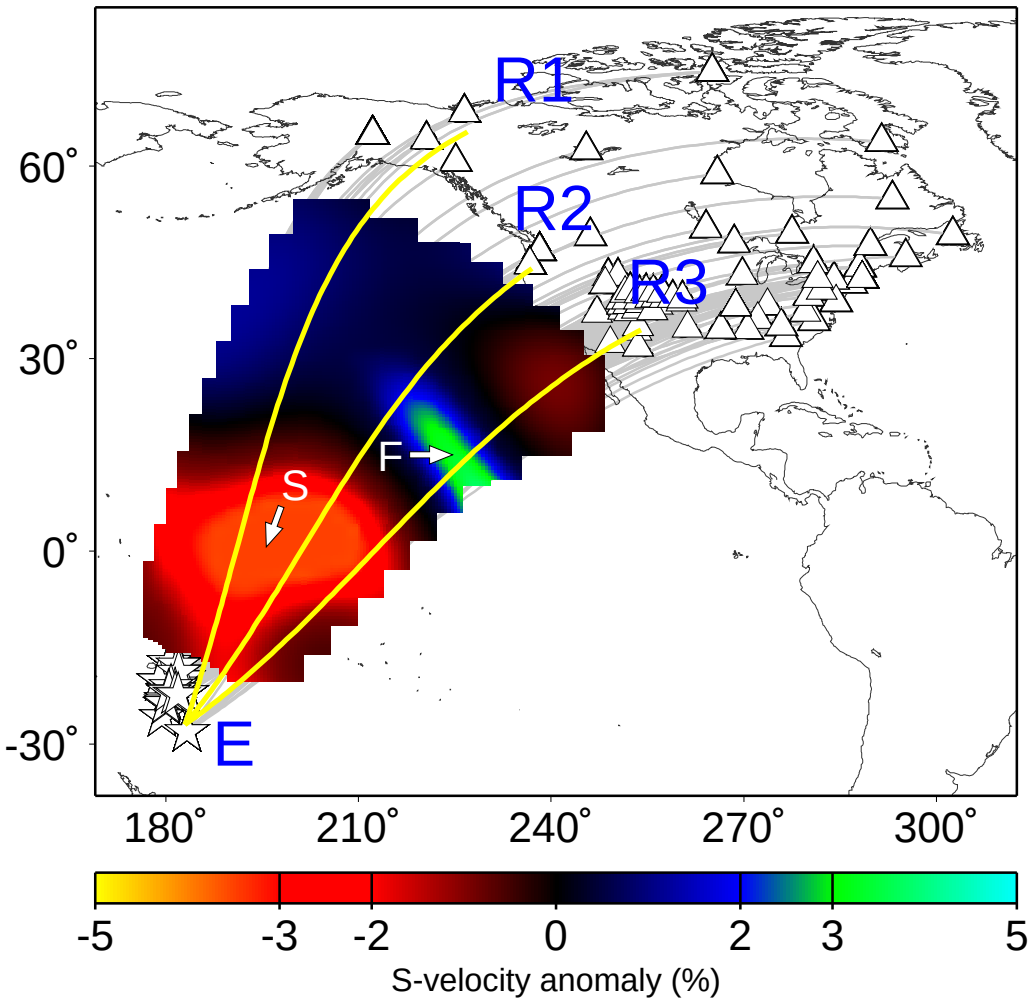
R1
R2
R3
F
S
E
60°
30°
0°
-30°
180°
210°
240°
270°
300°
-5
-3
-2
0
2
3
5
S-velocity anomaly (%)

Figure 5.1. (B) Earthquakes (stars), stations (triangles), and projections of the raypaths (gray solid lines) used in the forward modeling presented in this study. We used 31 events from 1962 to 1998. Our dataset consists of our own measurements and data from (18). Note the good coverage of the Central Pacific. Paths E1-R1, E2-R2 and E3-R3 correspond to the depth cross sections presented in Fig. 5. The color contours correspond to our preferred S-velocity model For the region covered by our dataset, at 2700 km depth. Symbols S and F point to the slow and fast domains discussed in the text and also presented in the depth cross sections of Figure 5.

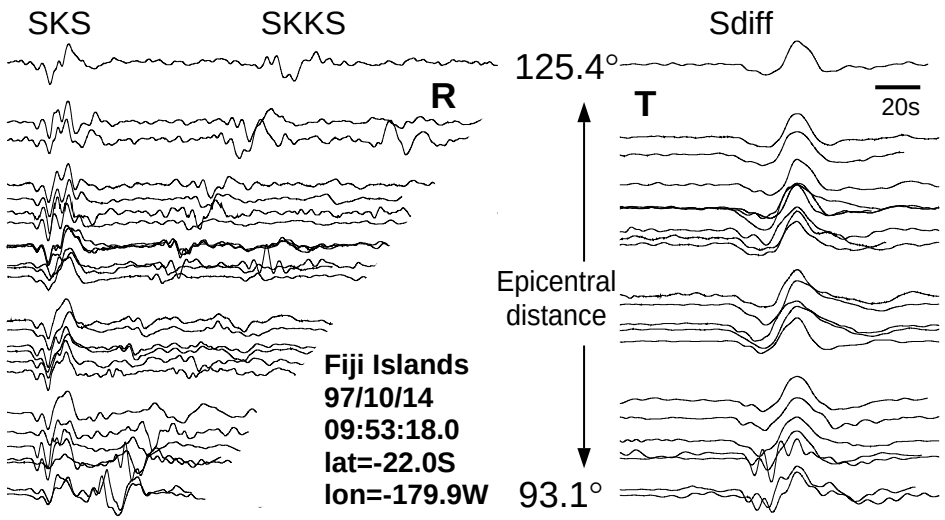

Figure 5.2. Examples of records for event 97/10/14, and stations in North America. The azimuths considered are between 0 and 60^0. R components are displayed in the left panel, and T components in the right one. The similarity of the waveforms between SKS and S, and from one station to another, yields differential measurements with low scatter (Fig. 3A). In this illustration, we have not selected data by narrow azimuthal corridors, as done in the study described in the text.

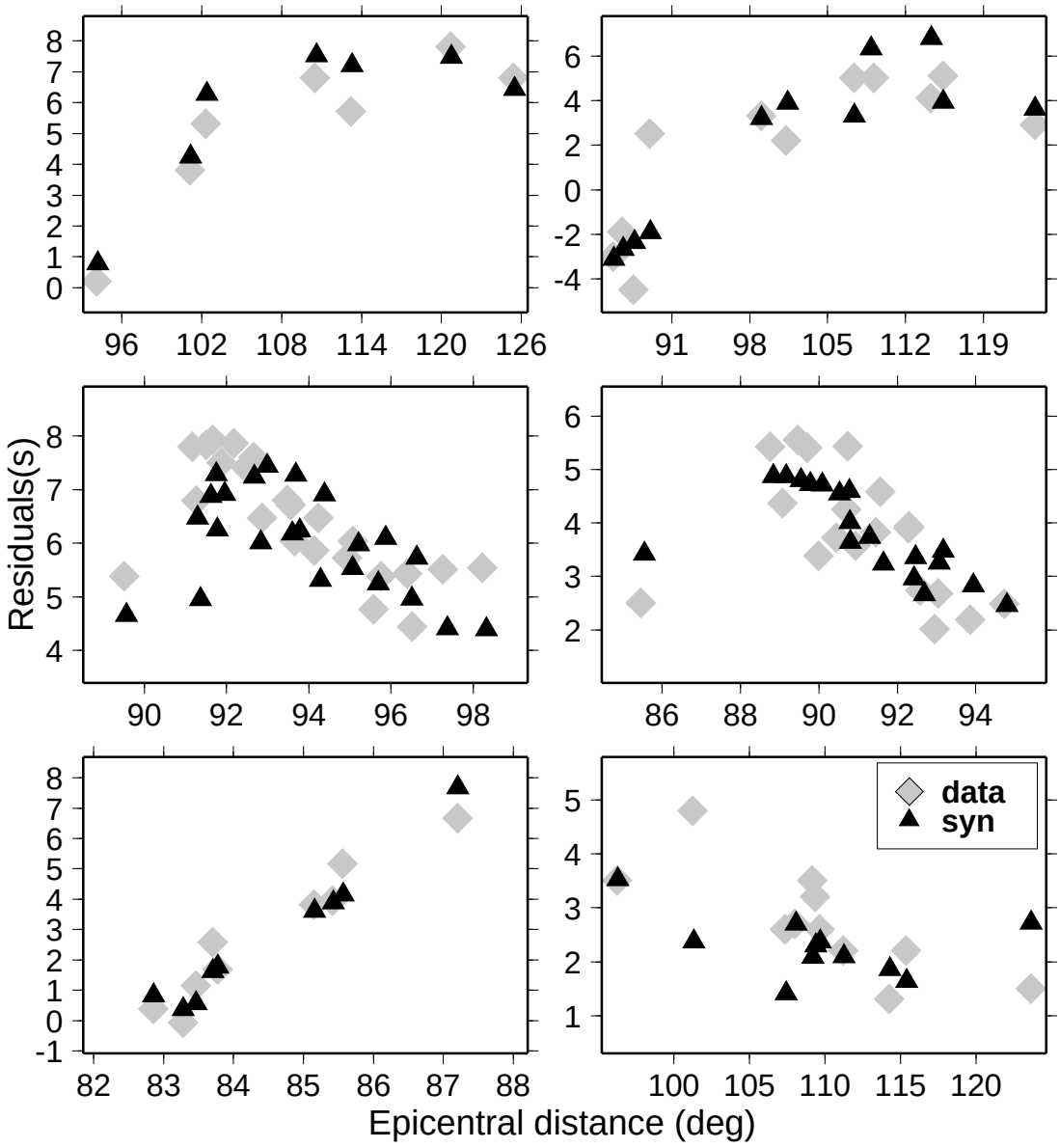
Residuals(s)
Epicentral distance (deg)
data
syn

Figure 5.3. Examples of observed variations of differential travel time residuals for $S - SKS$ as a function of epicentral distance (gray diamonds) along with synthetic predictions (black triangles) computed for our prefered 3D model. (A) and (B) Data and predicted residuals for events 97/10/14 and 98/03/29 respectively, and azimuths between 40 and 50^0. S penetrates into the slow velocity region (see Fig. 4) as distance increases, and $S - SKS$ residuals correspondingly increase. (C) and (D) Same as (A) and (B) for events 92/06/25 and 92/07/11 respectively. The trend is opposite to that observed in (A), and requires a fast region where the S-velocity anomaly reaches +5% (see Fig. 5). (E) $S - SKS$ residuals for fixed station COR and several Fiji-Toga-Kermadec Islands events, and azimuths between 35 and 37^0. (F) $SKKS - SKS$ residuals for event 98/03/29, and azimuths between 40 and 60^0.

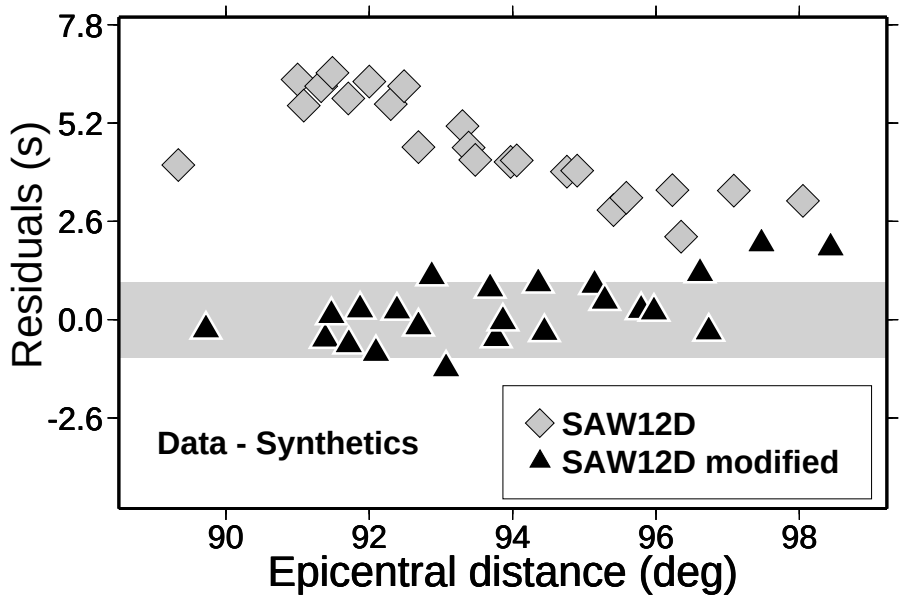

Figure 5.4. Examples of differences between observed and predicted $S - SKS$ residuals for model SAW12D and for our preferred 3D model. Residuals are for event 92/06/25 (E in Fig. 1B). By amplifying the magnitude of heterogeneity in regions S and F (see Fig. 1B and Fig. 5), it is possible to improve the fit significantly.

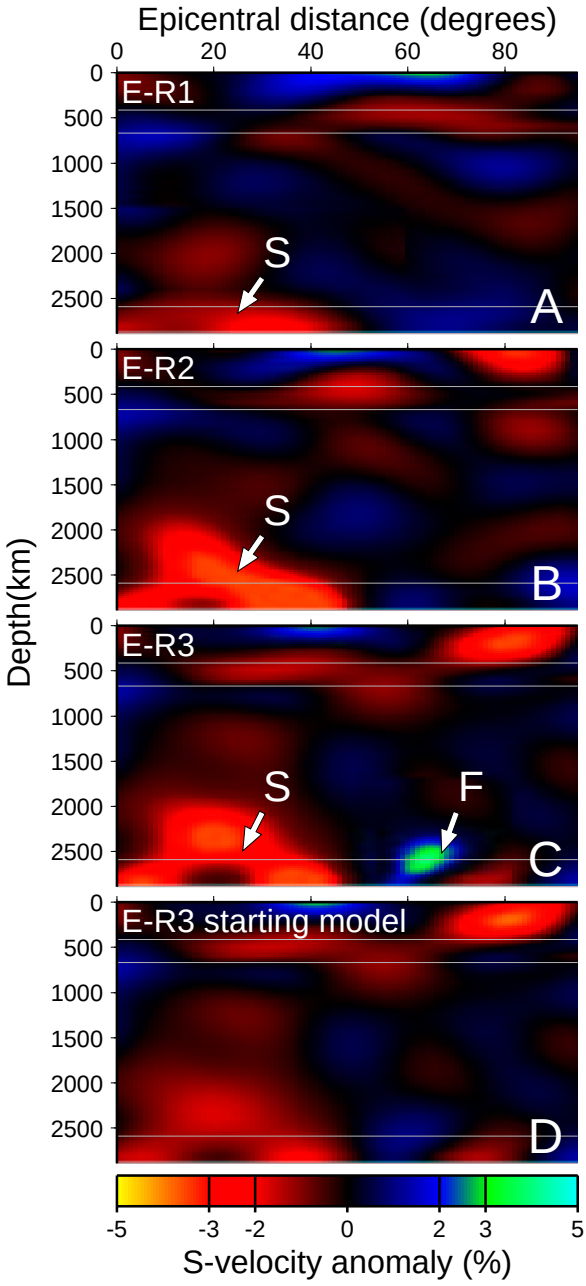
Epicentral distance (degrees)
0
20
40
60
80
Depth(km)
0
500
1000
1500
2000
2500
E-R1
S
A
E-R2
S
B
E-R3
S
F
C
E-R3 starting model
D
-5
-3
-2
0
2
3
5
S-velocity anomaly (%)

Figure 5.5. Examples of vertical cross-sections through our preferred model. (A) Vertical cross-section through our preferred model for path E1-R1 (see Fig. 1B). An horizontal lign has been added at 410, 670, and 2600 km depth. (B) Same as (A) for path E2-R2. (C) Same as (A) for path E3-R3. The cross-sections (A-C) show a velocity structure that depends strongly on the path chosen, which indicates a complex 3D structure. Note the presence of a large slow anomaly [S] where S-velocity are reduced by approximately 3.5 to 4%, and of a smaller region [F] where the heterogeneity reaches 4 to 5%. These two domains are required in all successful models, in order to fit the travel time residual data. The fast velocity region [F] does not need to extend much above D", and seems to be of smaller lateral extent than the "plume" region [S]. However, our dataset does not permit to constrain where the anomaly ends to the south-east (Fig. 1B). (D) For comparison, vertical cross-section through the starting model for path E3-R3, showing much lower amplitudes of lateral variations at the base of the mantle.

Chapter 6

PKP travel times: Inner core anisotropy or complex structure in the deep mantle?

6.1 Summary

The hypothesis that the bulk of the inner core is anisotropic is based on PKP travel time observations at large distances and relies on a small number of very anomalous measurements for paths quasi-parallel to the Earth's rotation axis. Here, we analyse a global dataset of PKP(AB-DF) travel times residuals, and discuss their significant dispersion ($\pm$ 2s), and coherent large scale patterns. We show that the trends observed are consistent with predictions from recent tomographic mantle models, when the latter are modified to account for strong heterogeneity at the base of the mantle under the Pacific Ocean and Africa, as documented in several recent studies, and that they do not necessarily require strong anisotropy ($\sim$3%) in the bulk of the inner core. The large scale trends in absolute PKP(DF) and PKP(AB) residuals appear to be strongly correlated, which suggests that DF absolute residuals may also be contaminated by structure outside of the inner core. The assumptions of the last 12 years regarding inner core anisotropy may need to be carefully revisited.

6.2 Introduction

Fifteen years ago, Poupinet et al. (1) showed that waves turning in the inner core (PKIKP, PKP(DF) or simply DF) and travelling parallel to the Earth rotation axis were on average 1 to 2s faster than those propagating along the equatorial plane. These observations were later interpreted in terms of inner core anisotropy (2), which could simultaneously explain the anomalous splitting of core sensitive free oscillations (3). This pioneer work was followed by many studies confirming and refining this interpretation (4-12). Although the existence of cylindrical anisotropy, with an average strength of about of 3 to 3.5%, in the inner core seems now widely accepted, there is no consensus on the details of its distribution. There are indications that it may be weaker near the surface than towards the center of the inner core, and that it may be laterally varying. Notably, some recent results suggest that there might be anisotropy in only one hemisphere of the inner core (13), and even that the top 250km may be isotropic (14), which is hard to reconcile with normal mode data, which require that anisotropy be present in the top third of the inner core (11,15).

In order to study inner core structure using the phase PKP(DF), outer core sensitive phases PKP(BC) and PKP(AB) (Figure 1a) are often used as reference phases. Differential travel times PKP(BC-DF) and PKP(AB-DF) have the advantage of being free of bias due to earthquake mislocation and origin time errors, near-source and near-receiver structure, and are, in principle, less sensitive than absolute times to large scale deep mantle structure. PKP(AB-DF) differential travel times obtained at large distances ($150 - 180^o$) are particularly valuable, since at those distances PKP(DF) uniquely samples the central part of the inner core. Although it has been often recognized that mantle heterogeneity contributes to the large scatter observed in the PKP(AB-DF) travel time residuals (18), so far, it has been assumed that the large scale trend observed, namely an increase of residual with decreasing angle of the path with respect to the earth's rotation axis, is best explained in terms of the effect of inner core anisotropy on the PKP(DF) phase (6,9).

6.3 Data

We have assembled a dataset of 335 PKP(AB-DF) differential travel times and 163 DF and AB absolute times, which we measured on the vertical component of Geoscope, IRIS, GRSN, and Mednet broadband records and combined them with the previously assembled collection of (6). The global coverage provided by this dataset is similar to that of other studies, with a large number of quasi-equatorial paths but considerably fewer paths quasi-parallel to the earth's rotation axis (Figure 1b).

6.4 AB-DF Differential residuals as a function of core entry point longitude

Plots of AB-DF residuals as a function of epicentral distance and angle with respect to the rotation axis (Figure 2a,b) are consistent with results from previous studies (6,9). In particular, the trend with angle (hereafter called ξ), is as expected for a simple model of constant cylindrical inner core anisotropy. The dispersion observed around that trend is on the order of $\pm$ 2.5 s, which is also consistent with earlier work (6,9,18) and is much larger than measurement uncertainty. The distribution of AB-DF data as a function of longitude of the entry point of AB into the outer core (hereafter called λ) is very non-uniform (Figure 3a). There is a small number of data points for λ between 0 and 60^o, and these data actually correspond to the quasi-polar paths, and earthquakes in the South Sandwich Islands region. Interestingly, mean AB-DF travel time anomalies present a clear dependence on λ (Figure 3b), with a maximum of 2s around $\lambda = 40^o$. In order to obtain a rough estimate of the contribution of mantle structure to AB-DF residuals, we computed synthetic anomalies (20) based on a recent tomographic model (22). Mean synthetic residuals are presented in Figure 3b. For comparison, we also plotted the predictions for a constant inner core anisotropy model (5). The two models provide similar overall fits, but they actually explain separate parts of the dataset: the tomographic model explains a large number of residuals at longitudes between -180^o and 0^{o}E and their variations with λ, although it clearly underestimates the magnitude of residuals for positive λ. As observed in earlier studies (18), it is difficult to produce synthetic residuals larger than about 1s with any existing tomographic model. The inner core anisotropy model predicts a smaller

number of large residuals for positive λ particularly well, but tends to overpredict residuals for negative λ. We tried the combination of both the mantle and the inner core model (not shown), but the fit is actually slightly degraded. A possible explanation could be, following (13), that only the western hemisphere is anisotropic, not only at shallow depths sampled by PKP(DF) but also deeper in the inner core. We here propose a different interpretation. To substantiate it, we will focus on particular source regions.

6.5 AB-DF Differential residuals for specific source regions

For events in the Fiji Islands source region, the observed AB-DF residuals as a function of azimuth (Figure 4a) and angle ξ (Figure 4b) show systematic long wavelength variations, as well as large local scatter (in excess of 2 s), which cannot be explained by either the tomographic (Figure 4a,b) or inner core model considered previously (Figure 4c,d). While we note that the tomographic model predicts more local scatter, the inner core model predicts very little long wavelength variation as a function of either azimuth or ξ. This is in agreement with the fact that for this particular source region, only angles $\xi > 45^o$ are sampled, while the effect of anisotropy only starts to be significant at $\xi < 40^o$.

Because they represent a smoothed image of heterogeneity in the mantle, tomographic models usually underpredict the trends associated with data which sample regions where strong or small scale heterogeneity may be present. This has been demonstrated, in particular, using $S - SKS$ travel time residuals sampling D" in the central Pacific and Africa (24,25,28,29). These studies showed, however, that it was possible to perturb the existing models locally, in order to obtain good fits to S-SKS, SKKS-SKS or S-ScS travel time observations (24,25). The required perturbations, although non-unique in their details, could be achieved effectively by keeping the shape of the boundaries between fast and slow anomalies fixed, and increasing the amplitudes of fluctuations, mostly in D" (the bottom 300 km of the mantle), by a factor of 2 to 3. While some trade off between the amplitude increase and the depth range affected exists, the modification of the starting tomographic model has been shown to be necessary only in the deepest mantle, where the paths of the 2 phases in the differential pair differ the most.

The geometry of the pair AB/DF is quite similar to that of S/SKS: SKS and

PKP(DF) dive at steep angles into the core, while S and PKP(AB) graze the CMB at large distances, diffract over a few degrees, and can accumulate large residuals in the strongly heterogeneous D".

As found from global tomographic studies, the lowermost mantle presents two major very slow, large scale anomalous domains: one beneath the Central Pacific, and one beneath Africa (e.g. 22,23). In an attempt to forward model our observations, we assumed, as in (24,25) that slow velocities were strongly underpredicted under the Pacific and Africa, and we increased their amplitude in the bottom 400 km of the mantle, while not changing their shape (30). In addition, in the computation of synthetic AB and DF residuals, we included the effect of Ultra Low Velocity Zones (ULVZs) in places where they have been reliably documented (31). ULVZs are particularly important to consider because they represent an average P-velocity reduction of around 10%, and may significantly slow down AB waves at the largest distances. Synthetic residuals computed using this revised model (MMM, Figure 5) now show a better agreement with the observations (Figure 4e,f), even though we did not attempt to adjust the model to fit the data on any particular path. This simple experiment demonstrates how it is possible to explain both short wavelength and long wavelength trends observed in the differential residuals by an effect of locally strong heterogeneities in the deep mantle, primarly on AB, with a distribution as documented from previous work.

After departing from the Fiji Islands region, AB and DF both travel through several hundred kilometers of slow mantle. Although heterogeneity is large there (24), because DF and AB are simultaneously affected, the resulting anomaly does not exceed about 1s. Similarly, when AB and DF later exit the outer core and propagate into the strong slow African anomaly before being recorded at African stations (Figure 5), no differential residual larger than about 2s is produced (Figure 4).

In some other regions, however, DF may propagate through a normal to fast heterogeneous region in the lowermost mantle, while AB experiences some large delays due to a consistently very slow anomaly. This, we believe, is the case for quasi-polar paths (Figure 6) from South Sandwich Islands events to northern Eurasia (25,32). This type of path happens to correspond to a geometry for which AB spends most of its time in the lower mantle within the large African slow anomaly (Figure 7), while DF misses the zone

of strongly reduced velocity. There are in addition several paths which sample the very anomalous ULVZ region recently detected beneath Iceland, on the receiver side (32). Predictions of the inner core anisotropy model (Figure 8) are unable to match either the short or the long wavelength trends and amplitudes of AB-DF travel time residuals, at the three stations considered, whereas the MMM model explains the large values of the residuals as well as their variations much better, both as a function of CMB entry point longitude of AB and angle ξ.

Returning to the complete dataset, Figure 3c shows the predictions of the modified mantle model, without adding inner core anisotropy, as a function of longitude λ. Both the amplitudes and the long wavelength trends are now well predicted by this model. Figures 2c and 2d show the remaining AB-DF residuals as a function of distance and ξ, corrected for the MMM model contribution. Although MMM has not been adjusted to provide a best fit for individual paths, and therefore some dispersion remains, the trend of increasing residuals with increasingly polar paths (Figure 2b) has disappeared (Figure 2d). Several unexplained anomalies are present at angles close to 25^o. These correspond to paths from South Sandwich Islands to stations COLA and BILL (Figure 1b). These paths have previously been identified, on the basis of PKP(BC-DF) travel time measurements, as particularly anomalous, with very strong small scale structural variations (19,33).

6.6 Discussion

Observations of PKP(AB-DF) travel time residuals exceeding 5 to 6 s are traditionally interpreted as evidence for the presence of a 3.5% average cylindrical anisotropy in the bulk of the inner core. Because of the uneven distribution of sources and receivers, these residuals happen to be mostly associated with raypaths between the South Sandwich Islands region and northern European, north American and Russian stations. AB-DF differential residuals are extremely sensitive to the P-velocity structure at the base of the mantle (18), and we have shown that it is possible to explain their variations, and even their sometimes large values, using a modified tomographic model that takes into account the complexity of the D" region, as recently documented. Our forward modeling of AB-DF travel times suggests that these large distance residuals are likely to be very strongly

affected by the strong heterogeneity present in the deep mantle beneath the Pacific and Africa, and that the anisotropy in the inner core required to explain them may have been much overestimated.

An alternative explanation would be to attribute the observed trends in differential travel times to DF, rather than AB, invoking a much more complex model of inner core anisotropy (11) or lateral heterogeneity in the inner core, as has been suggested for the very anomalous paths from the South Sandwich Islands to station COL (19). While the former deserves further investigation, the latter would require extremely strong lateral gradients of velocity within the inner core, in order to explain the local scatter in the data as discussed above. This is physically much less plausible than a D" origin, considering that the inner core is thought to have been formed by freezing of liquid core material largely homogeneized through vigorous convection. The strength of the D" interpretation lies both in its ability to explain long and short wavelength trends in the data, and in the fact that the existence of such a distribution of strong heterogeneity in D" has been documented in several independent studies (24,25,32).

Since differences in absolute travel time residuals for the phase PKP(DF) on quasi-polar versus quasi-equatorial paths were originally invoked to propose the existence of anisotropy in the inner core, it is important to discuss such data in the light of our results for PKP(AB-DF). The absolute DF residuals as a function of ξ (Fig. 9a) show the characteristic increase with ξ described in the literature, with scatter that may be attributed to source mislocation, as well as near source and near receiver structure. Absolute AB residuals show similar trends (Fig. 9b). In Figures 9c and 9d, we compare DF and AB residuals as a function of the longitude of the corresponding event. Both phases show similar trends in this representation as well, and we note that AB residuals for events in the South Sandwich Islands region (longitudes of around -30^o) are on average negative and among the fastest, as for DF. Again, because of the uneven distribution of sources and receivers, a very important subset of the polar paths corresponds to earthquakes in the South Sandwich Islands region. An analysis based exclusively on absolute DF residuals would lead to the conclusion that, on average, polar paths are faster that equatorial. We show here that the same trends can also be observed on AB absolute travel times. We infer that absolute DF travel time residuals may therefore also be strongly contaminated,

in their large scale variations, by structure outside of the inner core, which may mimic the effect of inner core anisotropy, given the non-uniform distribution of observations. The very large negative DF residuals for a small number of paths from the South-Sandwich region could be explained by a combination of near source and near receiver effects and propagation through a very fast localized zone in D" (24).

The large distance data discussed here provide insight only into the structure of the deepest two-thirds of the inner core. In order to make inferences about the shallower parts, PKP(BC) travel times and normal mode data must be considered. The case of PKP(BC-DF) needs to be analyzed with care, since BC and DF have very similar paths even in the lowermost mantle, therefore the deep mantle structure has much less effect on BC-DF than on AB-DF. Recent evidence based on PKP data in the BC range suggests however that at least one hemisphere, is isotropic (13). Interestingly, quasi-polar paths sampling this hemisphere also happen to propagate almost exclusively in a region of the deep mantle which seems less heterogeneous than Africa or the central Pacific: there is so far no evidence for ULVZ's between longitudes of 60 and 150^o E (Figure 6). Moreover, the top $\sim$250 km of the inner core may be altogether isotropic (14). While this needs to be investigated further, the lack of anisotropy near the top of the inner core requires a reconsideration of anomalous normal mode splitting, which could originate elsewhere than in the inner core (8). Evidence towards a much smaller, or even inexistent anisotropy in the inner core also calls for a new look at differential inner core rotation results (34), which rely on the hypothesis that there is a symmetry axis of anisotropy whose orientation evolves with time with respect to fixed DF paths.

There has been a lack of consensus as to the details of anisotropic structure in the inner core. We believe that the contamination of the inner core sensitive data by structure at the bottom of the mantle may have been generally underestimated, and that future efforts to derive realistic models of inner core structure will have to accurately account for such effects.

6.7 References and Notes

1. G. Poupinet, R. Pillet, A. Souriau, *Nature* **305**, 204, (1983).

2. A. Morelli and A. M. Dziewonski, *Geophys. Res. Lett.* **13**, 1545, (1986);

3. J. H. Woodhouse, D. Giardini, X. D. Li, *Geophys. Res. Lett.* **13**, 1549, (1986).

4. P. M. Shearer, K. M. Toy, J. A. Orcutt, *Nature* **333**, 228, (1988); P. M. Shearer, *J. Geophys. Res.* **99**, 19647, (1994).

5. K. C. Creager, *Nature* **356**, 309, (1992).

6. L. Vinnik, B. Romanowicz, L. Bréger, *Geophys. Res. Lett.* **21**, 1671, (1994).

7. R. Widmer, G. Masters, F. Gilbert, *Geophys. J. Int.* **111**, 559, (1992).

8. J. Tromp, *Nature* **366**, 678, (1993).

9. X. D. Song, *J. Geophys. Res.* **101**, 16,089, (1996).

10. W. Su and A. Dziewonski, *J. Geophys. Res.* **100**, 9831, (1995).

11. B. Romanowicz, X.D. Li, J. Durek, *Science* **274**, 963 (1996).

12. A. Souriau and B. Romanowicz, *Geophys. Res. Lett.* **23**, 1 (1996).

13. S. Tanaka and H. Hamaguchi, *J. Geophys. Res.* **102**, 2925, (1997).

14. X. Song and D.V. Helmberger, *Science* **282**, 924, (1998).

15. J. Durek and B. Romanowicz, *Geophys J. Int.*, in revision, (1998).

16. A. M. Dziewonski and D. L. Anderson, *Phys. Earth. Planet. Int*, **25**, 297 (1981).

17. L. R. Johnson, *Seism. Res. Lett.* **60**, 10, (1989).

18. G. Poupinet, A. Souriau, L. Jenatton, *Geophys. J. Int.* **113**, 684, (1993); X. D. Song and D. V. Helmberger, *Geophys. Res. Lett.* **20**, 285, (1993); Song and Helmberger, *Geophys. Res. Lett.* **24**, 1863, (1997).

19. K. C. Creager, *Nature* **278**, 1284, (1997).

20. A finite difference (FD) modeling approach is desirable to compute travel times in two-dimensional or three-dimensional models. Such modeling is computationally heavy and not well suited for large datasets. We have here computed synthetic travel time residuals using ray theory. The ray tracing was done in the spherically symmetric PREM model (16). The residuals obtained are within 0.5 s of those computed for a typical path from south Sandwich islands to northern Eurasia, using an acoustic 2D finite difference algorithm (21).

21. J. E. Vidale, thesis, California Institute of Technology (1987).

22. S. Grand, R. van der Hilst, S. Widiyantoro, *G.S.A. Today* **7**, 1 (1997). We used Grand's recent S-velocity model (and converted it to P, assuming dln(Vs)/dln(Vp)=2. A S-velocity model was preferred to a P-velocity velocity model for several reasons. There is, on the first hand, a reasonably good agreement between recent S-velocity tomographic models in the lowermost mantle (23). The low harmonic degrees and maximum amplitudes are in particular very similar which suggests that tomographic images now give a good description of large scale D" heterogeneity. S-velocity models were also recently shown to give a rather accurate description of the distribution of heterogeneity in the deep mantle beneath the Central Pacific (24), and Africa (25). These two regions are particularly important because they are, so far, the two most anomalous domains of D". Models of the deep mantle provided by P-velocity models, on the other hand, are still rather different (26,27), and suffer from uneven coverage in D" more than S models. We verified that the magnitude and distribution of P-velocity anomalies predicted by a model recently derived specifically for D" (28) were compatible with those predicted using our P model derived from Grand's S model, which suggests that this approach is reasonable.

23. X. -F. Liu, W. -J. Su, A. M. Dziewonski, *Eos (Spring Suppl.)* **75**, 232 (1994); X. -D.

Li and B. Romanowicz, *J. Geophys Res.* **101**, 22245 (1996); G. Masters, S. Johnson, G. Laske, H. Bolton, *Phil. Trans. R. Soc. London* **354**, 1385 (1996).

24. L. Bréger and B. Romanowicz, *Science* **382**, 244, (1998).

25. D.V. Helmberger, L. Wen, X. Ding, *Eos (Fall Suppl.)* **XX**, XXX (1997).

26. R. van der Hilst, S. Widiyantoro, E.R. Engdahl, *Nature* **386**, 578, (1997); D. Vasco and L. Johnson, *J. Geophys. Res.* **103**, 2633, (1998).

27. M. Wysession, *Nature* **382**, 244, (1996).

28. L. Bréger, B. Romanowicz, L. Vinnik *Geophys. Res. Lett.* **25**, 5 (1998).

29. L. Vinnik, L. Bréger, B. Romanowicz, *Nature* **393**, 564 (1998).

30. The following rules were applied to modify the tomographic model (20) at the base of the mantle: for depths greater than 2500 km only, all anomalies slower than 0.3% were assigned a 2% P-velocity reduction. Note that the thickness of the layer that we chose to modify trades-off with the assigned P-velocity reduction. We also took the effect of ULVZs (ultra low velocity zones) into account when computing travel time residuals. The regions where ULVZ are thought to be present were taken from (31). We assigned the values of 10% and 10km to respectively the P-velocity reduction and the thickness of the ULVZ. These values are conservative since some regions of D" have been shown to experience P-velocity reductions of more than 10% over a few tens of kilometers (e.g. 32). ULVZs can delay AB by more than one second only for paths corresponding to distances of more than about 170^o that happen to graze the CMB in a region of ULVZ. There are also trade-offs between thickness of ULVZ's and velocity reductions, which will not affect the resulting fits significantly, in terms of our conclusions.

31. E.J. Garnero, J. Revenaugh, Q. Williams, T. Lay, L.H. Kellogg, in The Core-Mantle boundary, M. Gurnis, B. A. Buffett, E. Knittle, M. E. Wysession, Eds (American Geophysical Union, Washington, DC, 1998), pp. 319-334.

32. D.V. Helmberger, L. Wen, X. Ding, *Nature* **396**, 251, (1998).

33. Comparing individual measurements at COL and neighbouring station INK, we find travel time residuals for (AB-DF) of 5 s and 2.6 s respectively, indicating that a highly complex zone is sampled somewhere along these paths, requiring strong heterogeneity. Given what we independently know about D", it is easiest to explain these strong local variations in terms of heterogeneity in D". For example DF at COL could be sampling a fast region on the border of an ULVZ, as has been documented to exist in the central Pacific (24), while both DF and AB would be travelling through the ULVZ at INK.

34. X.D. Song and P.G. Richards, *Nature* **382**, 221, (1996).

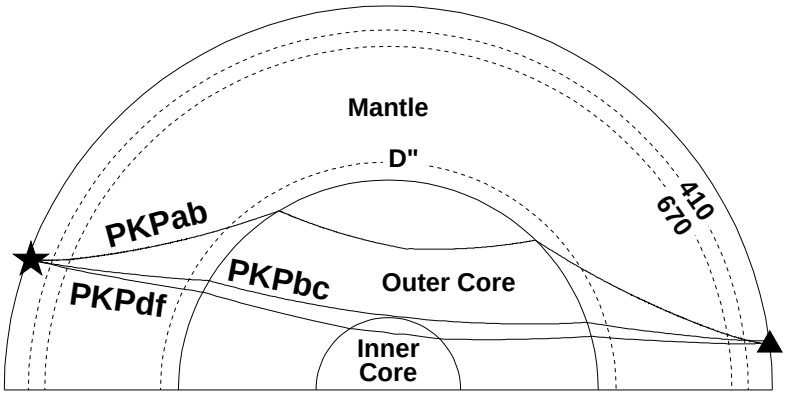

Figure 6.1. (a) Schematic representation of the wavepaths of PKP(DF), PKP(AB), and PKP(BC) discussed in this study.

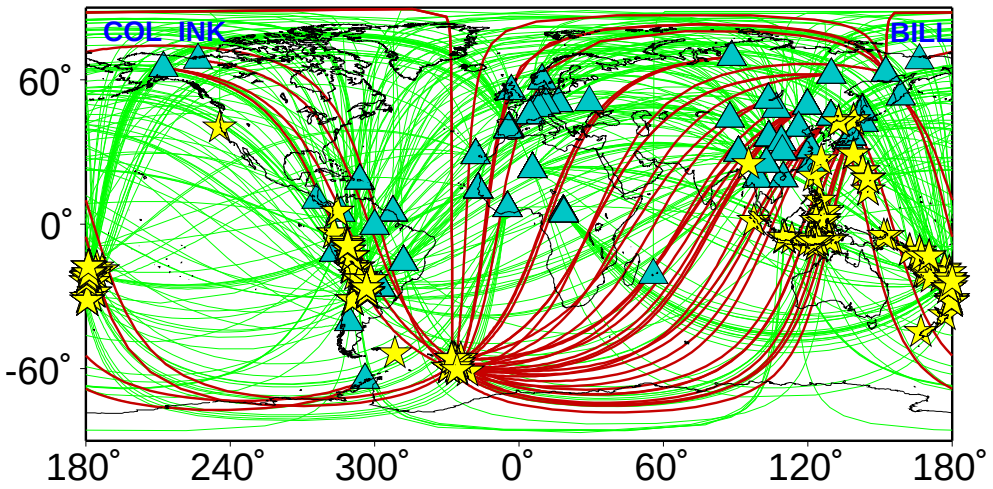

Figure 6.1. (b) Earthquakes (stars), stations (triangles), and projections of the raypaths analysed. We used 137 events from 1987 to 1998, and 57 stations. Our dataset consists of our own measurements and data from (6). The geographical distribution is representative of currently available data. Note the large number of quasi-equatorial paths ($\xi > 45^o$, gray lines), but the reduced number of quasi polar paths ($\xi < 45^o$, black lines). PKP(AB-DF) differential times were determined by overlapping PKP(AB) waveform with the Hilbert transform of PKP(DF). Residuals were computed with respect to the Preliminary Reference Earth Model (16). Standard ellipiticity corrections (17) were applied.

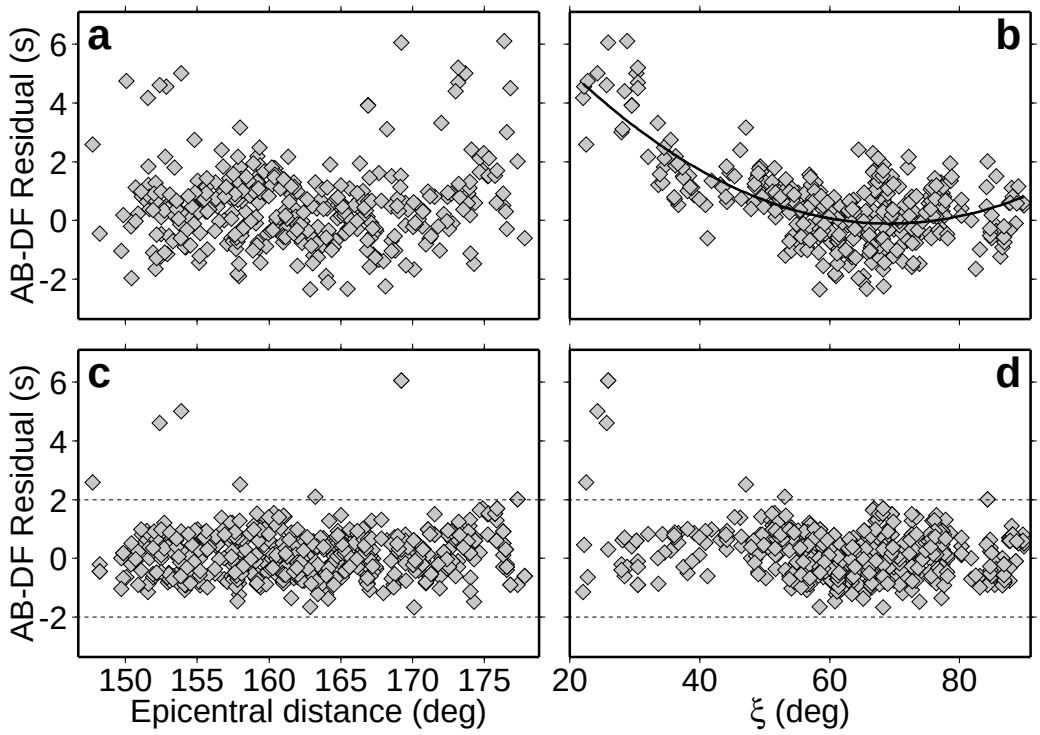

Figure 6.2. AB-DF differential travel time residuals as a function of epicentral distance (a) and angle ξ of the path in the inner core with respect to the rotation axis (b). The best fitting second degree polynomial in $cos^2\xi$ (solid line) was added in (b) to outline the observed trend. Such a trend is expected, at fixed distance, for models of constant cylindrical anisotropy in the inner core with axis parallel to the rotation axis. (c) and (d): Same as (a) and (b) after correction for the MMM model discussed in the text. Note that a few large residuals at low ξ remain unexplained. These correspond to South Sandwich Islands paths to stations COL and BILL. The complexity of these particular paths has been noted previously, for instance, BC-DF residuals differing by more than 2s for neighbouring stations (13).

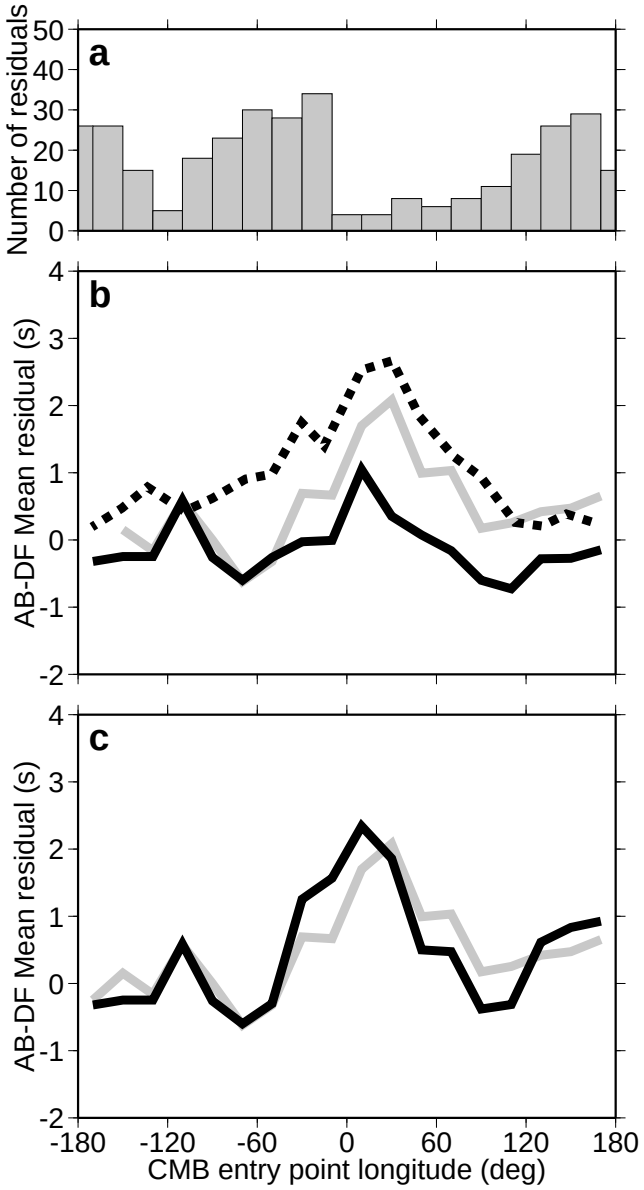
a
b
c
Number of residuals
AB-DF Mean residual (s)
AB-DF Mean residual (s)
CMB entry point longitude (deg)
50
40
30
20
10
0
4
3
2
1
0
-1
-2
-180
-120
-60
0
60
120
180

Figure 6.3. (a) Number of AB-DF residuals as a function of the longitude λ of the point where AB penetrates the outer core. (b) Plotted as a function of λ, mean AB-DF residuals observed (solid gray line), and predicted by Creager's (5) inner core constant (3.5%) anisotropy model (dashed line), and by the tomographic model (22) (solid black line). (c) Same as (b) with observed residuals (gray line) compared to predictions by our MMM model (30). Mean residuals were obtained by averaging observed anomalies over 20^o in λ. The Root Mean Square differences between observations and predictions are 0.15s for the tomographic model, 0.21s for the inner core model, 0.24s for a model combining the tomographic and inner core models, and 0.06s for our modified mantle model.

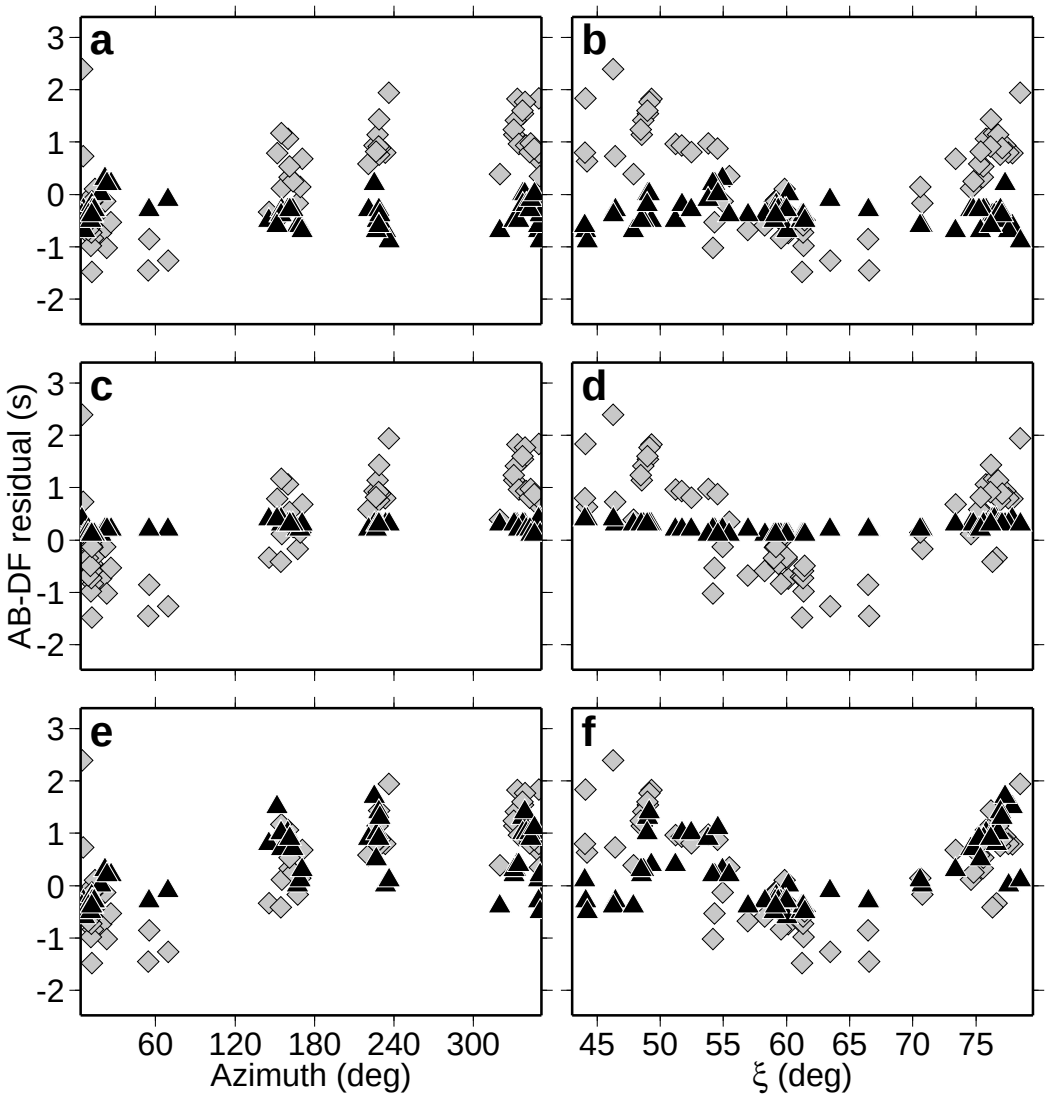
a
b
c
d
e
f
AB-DF residual (s)
3
2
1
0
-1
-2
60
120
180
240
300
Azimuth (deg)
45
50
55
60
65
70
75
ξ (deg)

Figure 6.4. Observed AB-DF travel time residuals (gray diamonds) for events located in the Fiji Islands region as a function of azimuth from the source (left) and angle ξ with respect to the earth's rotation axis. Predicted anomalies (black triangles) are (a)(b) for the tomographic model described in (20), (c)(d) for Creager's (5) inner core anisotropy model, and (e)(f) for the MMM model (30). Observed residuals show characteristic patterns that only the modified tomographic model can reproduce. Note that the fit of the MMM model is not perfect, and in particular, additional forward modeling of paths at azimuth of less 60^o (and mostly $\xi < 50^o$) could improve the fit significantly. This could be achieved by adjusting the lateral extent of ULVZ's near the source or the receiver. It is not the purpose of this study, however, to provide a best-fitting model, which would involve resolving many trade-offs which are beyond the scope of this paper. There is actually direct evidence of an average mantle contamination of about 4s on PKP(AB): for South Sandwich Islands events, station SEY (62.93^oN 152.37^oE) reports an average AB-DF residual of 5.0s, but an average DF residual of -1s.

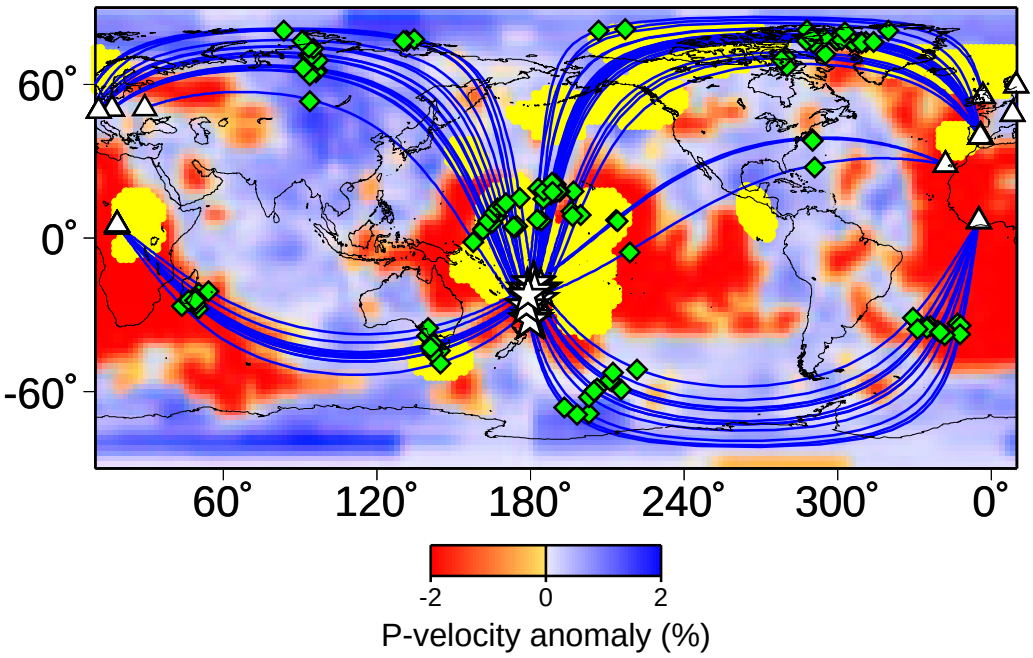

Figure 6.5. Projections of the raypaths (blue lines) for the Fiji Islands events (white stars) used in this study, along with the corresponding stations (white triangles). Also indicated are the regions where ULVZs have been documented (yellow), and the points were the AB ray enters and exits the outer core (diamonds). The background MMM P-velocity model has been modified from Grand's S-velocity model (30).

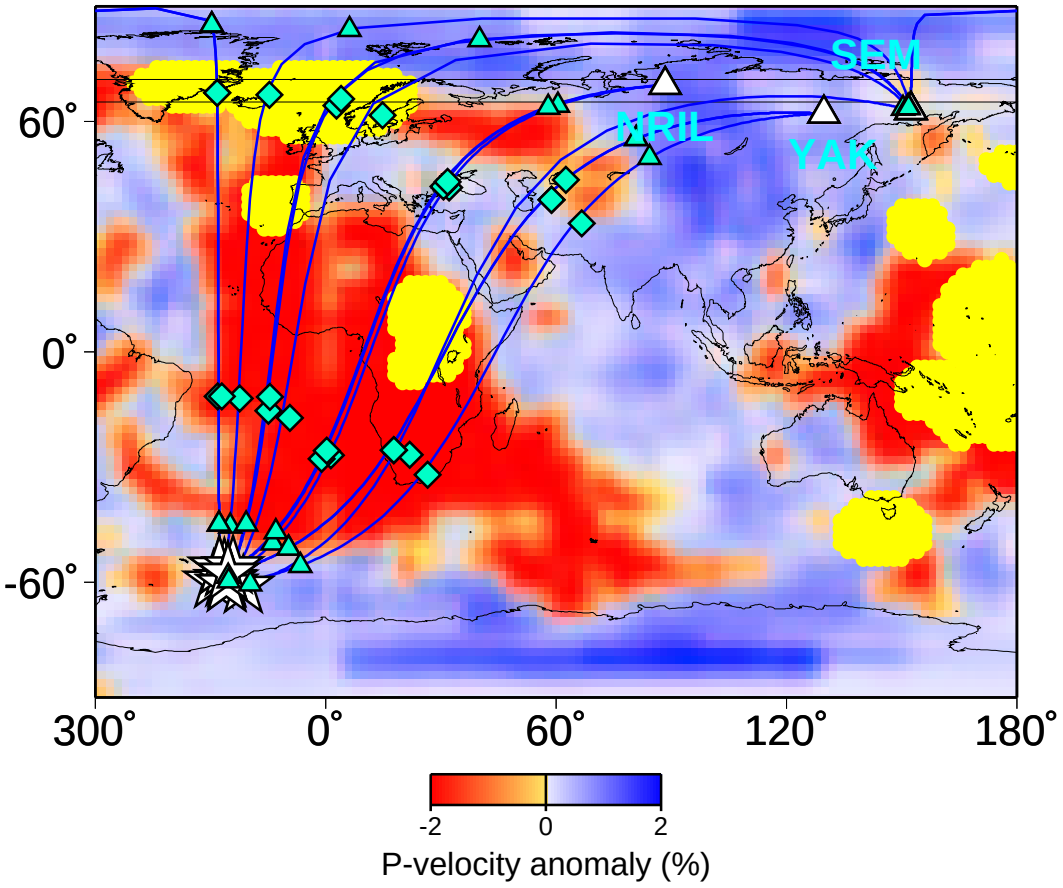

Figure 6.6. Projections of the raypaths (blue lines) associated with stations SEY (Seymchan, Russia, 62.93^{o}N 152.37^{o}E), NRIL (Norilsk, Russia, 69.50^{o}N 88.44^{o}E), and YAK (Yakutsk, Russia, 62.017^{o}N 129.72^{o}E) (white triangles), along with the corresponding events (white stars) in the South Sandwich Islands source region. Also indicated are the regions where ULVZs were detected (yellow regions), and the points were the AB and DF rays enter and exit the outer core (diamonds and triangles, respectively). The background P-velocity model is the same as in Figure 5.

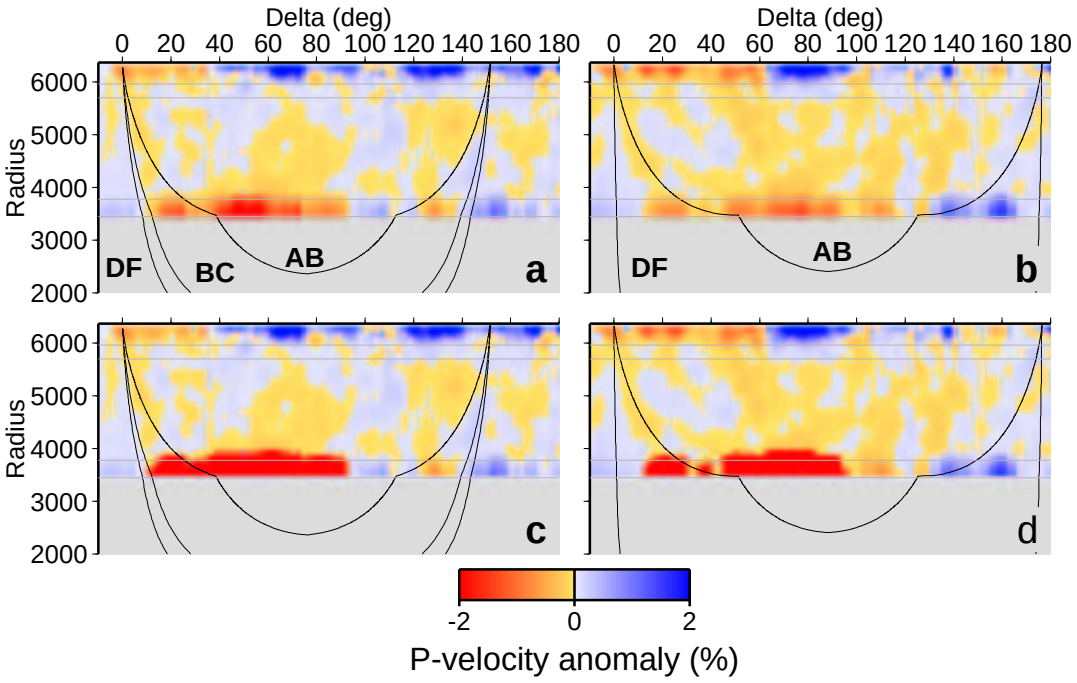

Figure 6.7. (a) Cross section through the original tomographic model for a path between South-Sandwich Island event 93/01/10 (-59.42^oN -25.78^{o}E 33km) and station NRIL (distance 151.50^o). Also plotted are AB, BC, and DF raypaths. (b) Same as (a) for a path to station SEY (distance 176.37^o). Also plotted are the AB and DF raypaths (BC does not exist at this distance). (c) and (d) Same as (a) and (b) for the modified velocity model.

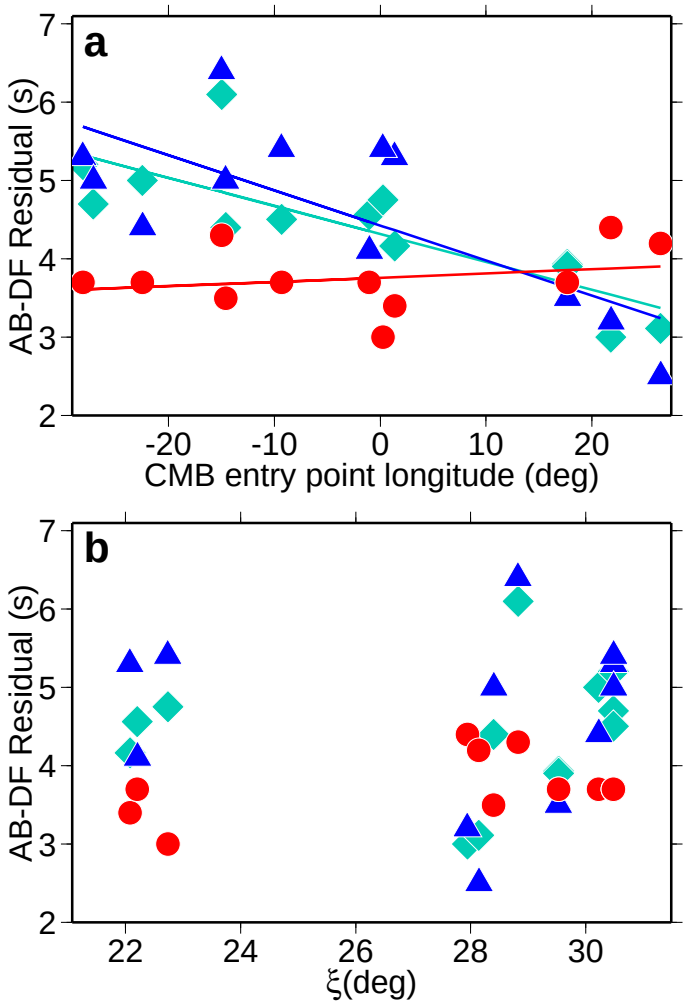

Figure 6.8. AB-DF residuals for stations SEY, NRIL, and YAK, and South Sandwich Islands earthquakes, plotted as a function of the longitude of the point where AB enters the outer core (a) and as a function of ξ (b). We compare observations (gray diamonds),to predictions for Creager's (5) inner core anisotropy model (white circles), and our modified tomographic model (black triangles). The rms residual is 0.32 s for Creager's model, and 0.16 s for the MMM model.

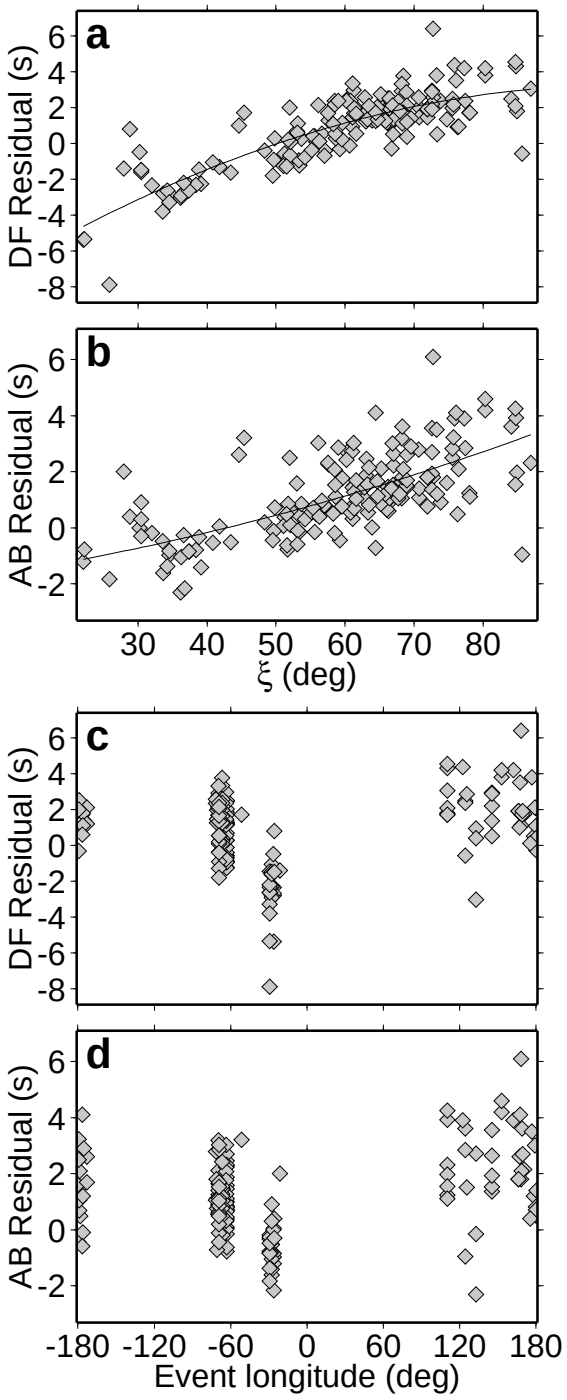
a
DF Residual (s)
6
4
2
0
-2
-4
-6
-8
b
AB Residual (s)
6
4
2
0
-2
30
40
50
60
70
80
ξ (deg)
c
DF Residual (s)
6
4
2
0
-2
-4
-6
-8
d
AB Residual (s)
6
4
2
0
-2
-180
-120
-60
0
60
120
180
Event longitude (deg)

Figure 6.9. (a) Absolute DF residuals as a function of ξ. Residuals show a clear increase with ξ. (b) Same as (a) for absolute AB residuals. Only data from records for which both DF and AB measurements were available are shown. A second degree polynomial fitting line (solid line) was added (c) Absolute DF residuals as a function of the longitude of the point where DF penetrates the outer core. (d) Same as (c) for absolute AB. Absolute DF arrival times were hand picked, with an accuracy of a few tenths of a second; absolute AB residuals were then computed by subtracting the absolute DF residuals from the (AB-DF) ones. DF and AB residuals present a similar pattern of variations with similar amplitudes (except for a small number of very negative residuals for South Sandwich Island events), which implies that the two phases are sensitive to similar structures outside of the inner core.

Chapter 7

PKP(BC-DF) travel times residuals: New constraints on short scale heterogeneity in the deep earth

7.1 Summary

Differential PKP(BC)-PKP(DF) travel time residuals for quasi-polar paths in the earth present large excursions from the trends predicted by simple models of inner core anisotropy. We analyze a set of such paths classified according to specific source and station regions, and show that a constant cylindrical anisotropy model of the inner core compatible with observations cannot exceed a strength on the order of 1.5%. To explain local departures of up to 3 sec from the predictions of such a model, strong lateral variations on scale lengths shorter than 500 km need to be invoked, either in the core or at the base of the mantle. Independent results of D" modelling argue in favor of an important contribution from the latter.

7.2 Introduction

Proposed thirteen years ago and based on the analysis of travel time anomalies (1-2) as well as normal mode splitting (3), the anisotropy of the earth's inner core seems today firmly established, the fast axis of iron crystals being roughly aligned with the earth's axis of rotation. Yet, there is still no consensus as to what the exact distribution and strength of this anisotropy are, and very different models have been proposed. Some authors have favored constant anisotropy ranging from 1 to 3.5% (e.g. 4-8), while others have argued that the top 90-250 km of the inner core is isotropic (9), or that anisotropy increases in strength at the center of the inner core (10,11). Two recent studies have shown that anisotropy is not evenly distributed with longitude, and that less that two thirds of the inner core might be anisotropic (12-13), while normal mode studies call for a predominantly axisymmetric pattern of anisotropy (3,11,14). Clearly there are still many contradictions in our view of inner core structure, which however needs to be well resolved in order to understand the physics, chemistry, dynamics, and history of the deepest regions of the earth.

Unfortunately, our knowledge of inner core structure relies mostly on waves which are sensitive to deep mantle heterogeneity, such as PKP-AB, PKP-BC, and PKP-DF (Figure 1a) (hereafter called AB,BC, and DF). To reduce the contamination due to mislocation effects and mantle structure, differential travel times, such as BC-DF and AB-DF have been frequently used (4-8,12-13). It is generally assumed that mantle heterogeneity, in particular at the base of the mantle, is responsible for the scatter observed in differential residuals, but that large scale trends can only be explained by an effect of inner core structure on DF.

On the other hand, strong lateral variations in the D" region have been recently quantified (15-16), with, in particular the existence of patches of ultralow P velocity, with velocity reductions in excess of 10% over thicknesses of up to 50km and lateral extents of a few hundred km (17). PKP(AB) is particularly sensitive to D" structure and Bréger et al. (18) showed recently that AB-DF differential travel times could largely be explained by deep mantle structure, including the trend with angle of the path with respect to the earth's rotation axis, usually attributed to inner core anisotropy. Because BC and DF propagate very close to each other in the mantle (Figure 1a), BC-DF travel times are in principle

much less sensitive to mantle structure than AB-DF. In view of recent findings regarding AB-DF, understanding and quantifying the effect of the mantle on BC-DF differential times is important since it will help to better resolve the fine structure of the inner core.

7.3 Data and Method

We have compiled the measurements of Tanaka and Hamaguchi (11), Souriau et al. (19), Li and Richards (20), and Wysession (21), complemented by some of our own picks in order to obtain a representative dataset of 608 BC-DF differential travel time residuals. Residuals were computed with respect to reference model AK135 (22), and are plotted in Figure 1b-c as a function of the angle between the ray at its turning point and the earth's axis of rotation (hereafter called ξ), and also as a function of the longitude of the corresponding event. Polar paths lead to the largest values, but their distribution is very non uniform. A small number of points are responsible for creating the large scale trend that shows an increase of the residuals when ξ decreases. Most of these points correspond to events in the South Sandwich Islands region (longitude around -25^o on Figure 1c) while many other polar paths lead to small residuals. Although the average variations can be explained by cylindrical inner core anisotropy with an axis of symmetry aligned with the earth's spin axis, data binned by angle ξ present highly variable values ranging from -1 to 4s, and cannot be explained by a simple axisymmetric model alone (Figure 1b).

By fixing a station and comparing residuals in a given source region, it is possible to gain insight into small scale spatial variations in different parts of the world. Station COL, in Alaska, is unfortunately the only one for which a relatively large dataset of broadband PKP(BC)-PKP(DF) travel times on quasi-polar paths is available, and the complexity of this dataset has been noted previously (23).

On the other hand, International Seismological Center (ISC) bulletins provide a large dataset spanning several decades which has been used extensively in previous studies (2,4,10). One drawback of this dataset is that, by its nature, it is very noisy. However, it has recently been improved by systematic elimination of misidentified phases and earthquake relocation (24). From this improved catalog, we have extracted BC and DF absolute travel time residuals with respect to the AK135 model (22) for a number of key stations

corresponding to polar paths (Figure 2) and classified them by source region. For a given region, the scatter of the residuals gives a direct estimate of the data quality, and poor subsets can be rejected. A second drawback of the ISC dataset is that measurements of both BC and DF travel times for the same event/station pair are infrequent, so that PKP(BC)-PKP(DF) residuals cannot be computed path by path. However, when absolute residuals show systematic trends as a function of a parameter such as epicentral distance or angle ξ, it is possible to estimate the corresponding variations of PKP(BC)-PKP(DF) and their standard deviations in a "composite" fashion, as illustrated in Figure 3 for station COL. In this particular case, the comparison with broadband data is possible and shows a generally good agreement (Figure 3e-f). In what follows, we present and discuss trends observed for a number of polar paths for which a sufficient number of ISC data are available to robustly estimate trends with epicentral distance Δ and angle ξ.

7.4 South Sandwich Islands Earthquakes recorded in North America

The path between events in the South Sandwich Islands and North America is well documented. A large number of BC-DF differential residuals have been measured for several stations, yielding generally large values. COL is probably the most notorious station, its long recording history having lead to the discovery of the super-rotation (26). Composite BC-DF residuals range from about 3.5s for southermost events (Δ=154^o), to roughly 2s for events at the northernmost tip of the South Sandwich Islands region (Δ=149^o). Canadian station INK is located 660km northeast of COL. Absolute DF and BC residuals from the ISC dataset also show systematic trends, and composite BC-DF residuals are in agreement with the few broadband data available (Figure 4). They are 1 to 1.5s smaller than for station COL. The data at station COL are, on average, compatible with a model of 3.5% constant anisotropy in the inner core, but such a model overestimates the anomalies at INK (Figures 3-4). The geographical relations for the trends observed at these 2 stations are summarized in Figure 6a,c.

7.5 South Sandwich Islands Earthquakes recorded in Eurasia

Similar systematic trends in the absolute ISC travel times are also observed for South Sandwich Island events observed at a group of stations in Eurasia (KHE, NRIL, IRK), so that composite BC-DF residuals can be robustly estimated for these paths (Figure 5). For these 3 neighboring stations, trends with angle ξ (and also epicentral distance, not shown) are very different. At station KHE, there is practically no variation with ξ, whereas NRIL shows a strong increase with increasing ξ and latitude (ranging from 0 to 3 sec) opposite to what is expected from a simple model of inner core anisotropy. At station IRK, BC-DF residuals increase midly with ξ and latitude. At all three stations, estimated residuals from an inner core model with constant 3.5% anisotropy largely overpredict the observations, whereas a 1.5% model underpredicts residuals at NRIL and still overpredicts those at KHE and IRK, even though KHE happens to correspond to particularly small values of angle ξ, where the effect of inner core anisotropy should be most pronounced.

On the other hand, we note that paths to these three stations are such that, on the source side, entry points of BC and DF into the core plot at the southwestern edge of the large low velocity zone present in tomographic models in D" under Africa ("African Plume" (16), Figure 2) where strong lateral gradients of structure have been proposed to explain observed variations of AB-DF residuals (18). In the case of AB-DF, the geometry was such that AB travelled through the low velocity of the plume whereas DF missed it, resulting in large AB-DF delays. In the right column of figure 6, we have plotted the relation of BC and DF entry points into the core, on the South Sandwich source side, to the African plume as described in Grand's tomographic model (25). The particularly large residuals observed at NRIL seem to correlate with a more pronounced interaction with the anomalous region than for the two other stations. Thus a significant contribution of D" heterogeneity to the observed anomalies along these paths is likely.

7.6 High latitude earthquakes recorded in Antartica

The trends observed at Antarctica stations SNA, MIR, SYO MAW, and SPA show a wide range of behaviours as summarized in Figure 6. Residuals recorded at SYO and SNA

correspond to relatively small and stable BC-DF residuals between -0.5 and 0.5 sec (Figure 6). Neighboring stations MIR and MAW, on the contrary, lead to differential residuals that vary with the position of the earthquake. And interestingly, although the two stations correspond to similar paths (Figure 2), they show some very different trends and values, yielding lateral variations of 2.5s sec on a scale of just a few degrees in epicentral distance. ISC bulletins for events in the Aleutians reported at SPA suggest, on the other hand, some strong lateral variability and large values, with BC-DF residuals changing rapidly from 0.5 to 3s (Figure 6).

7.7 Discussion

In order to summarize the observed trends for quasi-polar paths, we have plotted the composite BC-DF travel time anomalies as a function of angle ξ obtained at a specific distance of 148^o (Figure 7) for all 10 stations discussed above, compared to predictions from different simple models of inner core anisotropy. Figure 7 shows a large scatter with large excursions, both locally and over the range of ξ considered, from a trend that is compatible with the predictions of a model of anisotropy with strength on the order of 1.5%.

In order to explain the excursions from the simple inner core anisotropy model on the paths described here, a very complex model of inner core anisotropy needs to be invoked. The average anisotropy would change on a hemispherical scale (12,13),but also over distances of a few hundreds of kilometers, from one station to another, and on even shorter scales, when the station is fixed (Figure 6). Some very large residuals are sometimes observed: hand-picked residuals at station COL vary from 2s to exceptionnal values of some 5s. An anisotropy of more than 5% would be required in order to speed up DF by 5s at 154^o. This is extremely high since the intrinsic anisotropy of hcp iron at inner core pressures is expected to be around 3 to 4% (27), but could be compatible with the results of recent high-pressure experiments (28) and the existence of a complex convective pattern (29,30).

A complex D" lowermost mantle structure could indeed be a complementary, or even alternative, explanation to the complex behaviour of BC-DF differential travel time residuals, both for equatorial and for polar paths. The very strong heterogeneity of the last few hundreds kilometers of the mantle is now well documented, with the presence of

strong lateral variations (e.g. 15), of ULVZs (e.g. 17) and possibly partial melt (31), of anisotropy (e.g. 32), and possibly remnant slab material (33).

Such an explanation has so far not been considered for three main reasons. The first one is that DF and BC absolute residuals and BC-DF differential travel time residuals show a large scale trend when plotted with respect to ξ (Figure 1b). Due to the imperfect coverage of the globe by polar paths, approximately 95% of BC-DF residuals exceeding 2s correspond to paths between the South Sandwich Islands region and North America or Eurasia on the one hand, and Alaska and Antartica, on the other. Our analysis shows that BC-DF and DF residuals vary strongly with the position of the source and receiver. For these three types of paths, there are some source/receiver geometries for which BC-DF residuals are close to zero, but they correspond to a small minority of earthquakes at the tip of the Alaska and South Sandwich source regions. If earthquakes at the extremeties of these source regions dominated the dataset, the trend observed in Figure 1b would largely disappear. The very large number of positive residuals corresponding to paths between the South Sandwich Islands and stations in northwestern North America happen to dominate the dataset, but the lateral coverage of the inner core by DF waves remains very poor.

BC-DF travel times are not anomalous for polar paths for roughly one third of the globe, over Asia and Russia (12-13). Interestingly, the deep mantle beneath these regions seems weakly anomalous: they do not encompass the two large plumes (Africa and Pacific), tomographic models predict comparatively very little heterogeneity, no ULVZs have so far been detected (17), there are no hotspots at the surface, and little fossil lithosphere is expected at the CMB (33). On the other hand some of the largest residuals are obtained at station NRIL (Figure 5), for which we have seen an interaction of the path with the African plume at the base of the mantle (Figure 6). The paths between Alaska and SPA, MAW and MIR also sample a complex deep mantle structure (Figure 2). DF and BC enter and exit the outer core in a region closely surrounding the Pacific anomaly, with again the possible presence of subducted slabs and ULVZs. The paths between the South Sandwich Islands and station COL and INK may interact with heterogeneous domains of D" below North America as well, which could explain the average difference of about 1 to 1.5s observed between the two stations. Additional complexity at the CMB northwest of the South Sandwich Islands can be invoked to explain the fast variations observed for

each of the stations: these paths sample a region of D" where a large volume of subducted material may be lying at the CMB (33).

The second argument against a strong mantle contribution is based on the fact that BC and DF travel close to one another in the mantle, and that raytracing through tomographic models suggests that the effect of the mantle on BC-DF cannot exceed a few tenths of a second. However, in order to give a reasonable estimate of the potential effect of deep mantle structure, a model that includes an accurate mapping of short scale heterogeneity needs to be used, since tomographic models filter out the short scale anomalies of the deep mantle and considerably underestimate the amplitudes of heterogeneity as well as lateral gradients. BC and DF are actually also quite well separated at the CMB: AK135 (22) predicts a separation of BC and DF at the CMB of 650km and 400km at epicentral distances of 145 and 155^o respectively. D" can affect the source and receiver legs of BC and DF, with represents a total path length of at least 4 x 400km = 1600 km. A combination of lateral variations in D" with contrasts on the order of 5% (15,16), ultralow velocity zones, and additional heterogeneity in the deep mantle above D" could add up to differential residuals in excess of 3 s for exceptional geometries in which both source and station legs are affected. Explaining the very exceptional and rare observations of up to 5 sec at station COL remains nevertheless a challenge for this lower mantle interpretation, although it is important to note that this unusually large residual could be reduced to about 3.9s if it was computed with respect to PREM reference model (34).

Anisotropy in the inner core is also the favorite explanation for large BC-DF residuals because it simultaneously provides an explanation for the splitting of inner core sensitive modes (3,11,14). Several recent findings indicate some important contradictions that need yet to be resolved: 1- modes are primarily sensitive to the top of the inner core, however, the first 200km or so may not be anisotropic (e.g. 9); 2- recent studies of BC-DF travel times imply a strongly non axisymmetric component to inner core anisotropy (12-13), contrary to the modal observations (3,11,14). An alternative, and controversial, explanation for anomalous core mode splitting has previously been proposed in terms of outer core structure (35) and may deserve to be reexamined (36).

7.8 Conclusions

The rapid variations of BC-DF residuals on scales of a few hundreds kilometers can be understood as an effect of very complex inner core anisotropic structure or deep mantle heterogeneity. There is no independent evidence corroborating the former hypothesis. Lowermost mantle structure, on the contrary, happens to geographically correlate with the complex behaviour of BC-DF residuals, in locations where it is well documented. Whatever their origin, the existence of such strong variations shed a new light on the complexity of the deep earth (37).

References and Notes

1. Poupinet, G., Pillet, R. & Souriau, A. Possible heterogeneity of the Earth's core deduced from PKIKP travel times. *Nature* **305**, 204-206 (1983).

2. Morelli, A., & Dziewonski, A.M. Anisotropy of the core inferred from PKIKP travel times. *Geophys. Res. Lett.* **13**, 1545-1548 (1986).

3. Woodhouse, J.H., Giardini, D. & Li, X.-D. Evidence for inner core anisotropy frpm splitting in free oscillation data. *Geophys. Res. Lett.* **13**, 1549-1552 (1986).

4. Shearer, P.M., Toy, K.M. & Orcutt, J.A. Axi-symmetric Earth models and inner-core anisotropy. *Nature* **333**, 228-232 (1988).

5. Shearer, P.M. PKP(BC) versus PKP(DF) differential travel times and aspherical structure in the Earth's inner core. *J. Geophys. Res.* **96**, 2233-2247 (1991).

6. Creager, K.C. Anisotropy of the inner core from differential travel times of the phases PKP and PKIKP. *Nature* **356**, 309-314 (1992).

7. Vinnik, L., Romanowicz, B. & Bréger, L. Anisotropy in the central part of the inner core. *Geophys. Res. Lett.* **21**, 1671, (1994).

8. Song, X.-D. Anisotropy in central part of inner core. *J. Geophys. Res.* **101**, 16,089-16,097 (1996).

9. Song, X.-D. & Helmberger, D.V. Seismic evidence for an inner core transition zone. *Science* **282**, 924-927 (1998).

10. Su, W. & Dziewonski, A.M. Inner core anisotropy in three dimensions. *J. Geophys. Res.* **100**, 9831-9852 (1995).

11. Romanowicz, B., Li, X.-D. & Durek, J. Anisotropy in the inner core; could it be due to low-order convection? *Science* **274**, 963-966 (1996).

12. Tanaka, S. & Hamaguchi, H. Degree one heterogeneity and hemispherical variation of anisotropy in the inner core from PKP(BC)-PKP(DF) times. *J. Geophys. Res.* **102**, 2925-2938 (1997).

13. Creager, K.C. Large-scale variations in inner core anisotropy. Submitted to *J. Geophys. Res.*, (1998).

14. Tromp, J. Support for anisotropy of the Earth's inner core from splitting in free oscillation data. *Nature* **366**, 678-681 (1993).

15. Bréger, L. & Romanowicz, B. Three-Dimensional structure at the base of the mantle beneath the Central Pacific. *Science* **382**, 718-720 (1998);

16. Ritsema, J., Ni, S., Helmberger D.V & Crotwell, H.P. Evidence for strong shear velocity reductions and velocity gradients in the lower mantle beneath Africa. *Geophys. Res. Lett.* **25**, 4245-4247 (1998).

17. Garnero, E.J., Revenaugh, J., Williams, Q., Lay, T., Kellogg, L.H. in *The Core-Mantle boundary* (eds Gurnis, M., Buffett, B.A., Knittle, E. & M. E. Wysession) 319-334 (American Geophysical Union, Washington, DC, 1998).

18. Bréger, L., Romanowicz, B. & Tkalcic, H. PKP travel times: Inner core anisotropy or complex structure in the deep mantle? Revised for *Science*, (1999).

19. Souriau, A. & Romanowicz, B. Anisotropy in the inner core; relation between P-velocity and attenuation. *Phys. Earth Planet. Inter.* **101**, 33-47 (1997).

20. Li, A. & Richards, P.G. Study of inner core travel times using nuclear explosion data. *Eos (Spring Suppl.)* **75**, 232 (1998).

21. Wysession, M. Unpublished data.

22. Kennett, B.L.N., Engdahl, E.R, & Buland, R. Constraints on seismic velocities in the Earth from travel times. *Geophys. J. Int.* **122**, 108-124 (1995).

23. Creager, K.C. Inner core rotation rate from small-scale heterogeneity and time-varying travel times. *Science* **278**, 1284-1288 (1997).

24. Engdahl, E.R., van der Hilst, R. & Buland, R. Global teleseismic earthquake relocation with improved travel times and procedures for depth determination. *Bull. Seismol. Soc. Am.* **88**, 722-743 (1998).

25. Grand, S., van der Hilst, R. & Widiyantoro, S. Global seismic tomography; a snapshot of convection in the Earth. *G.S.A. Today* **7**, 1-7 (1997).

26. Song, X.-D. & Richards, P.G. Seismological evidence for differential rotation of the Earth's inner core. *Nature* **382**, 221-224 (1996).

27. Stixrude, L. & Cohen, R. High-pressure elasticity of iron and anisotropy of Earth's inner core. *Science* **275**, 1972-1975 (1995).

28. Mao H., Shu, J., Shen, G., Hemley, R.J., Li, B. & Singh, A.K. Elasticity and rheology of iron above 220 GPa and the nature of the Earth's inner core. *Nature* **396**, 741-743 (1998).

29. Jeanloz, R. & Wenk, H.R., Convection and anisotropy of the inner core, *Geophys. Res. Lett.* **15**, 72-75 (1988).

30. Wenk, H.-R., Baumgardner, J., Lebenson, R., & Tomé, C. A deformation model to explain anisotropy of the inner core. Submitted to *J. Geophys. Res.* (1998).

31. Williams, Q. & and Garnero, E.J. Seismic evidence for partial melt at the base of the Earth's mantle. *Science* **273**, 1528-1530 (1996).

32. Vinnik, L., Farra, V. & Romanowicz, B. Observational evidence for diffracted SV in the shadow of the Earth's core. *Geophys. Res. Lett.* **16**, 519-522 (1989).

33. Lithgow-Bertelloni, C. & Richards, M.A. The dynamics of Cenozoic and Mesozoic plate motions. *Rev. Geophys.* **36**, 27-78 (1998).

34. Dziewonski, A. M., & Anderson, D.L. Preliminary Reference Earth Model. *Phys. Earth Planet. Int* **25**, 297-356 (1981).

35. Widmer, R., Masters, G., & Gilbert, F. Observably split multiplets-data analysis and interpretation in terms of large-scale aspherical structure. *Geophys. J. Int.* **111**, 559-576 (1992).

36. Romanowicz, B. & Bréger, L., *In preparation.*

37. We are particularly grateful to A. Souriau and G. Poupinet, M. Wysession, P. Richards, and S. Tanaka and H. Hamaguchi for providing us with their data, and E. R. Engdahl, R. van der Hilst, and R. Buland for making their ISC dataset available. We benefited from discussions with H.R. Wenk and R. Jeanloz. We also thank the IRIS, CNSN, Geoscope, GRSN, Mednet, BDSN, SCSN, and GRSN teams. Figures were made with the General Mapping Tools (P. Wessel and W. H. F. Smith, *EOS Trans. AGU* **76**, 329, (1995)).

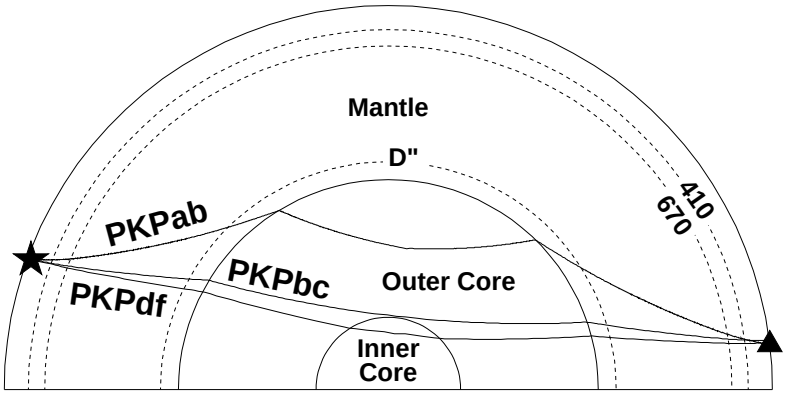

Figure 7.1. (a) Schematic representation of the wavepaths of $PKPdf$, $PKPab$, and $PKPbc$ discussed in this study.

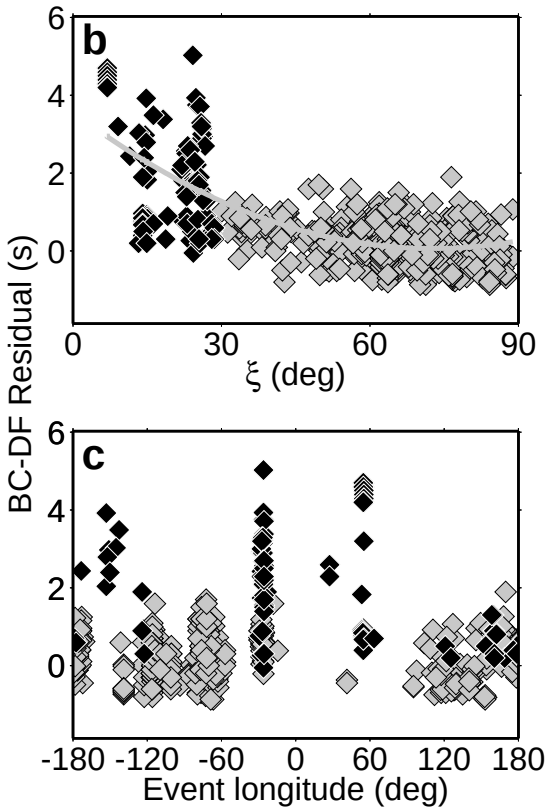

Figure 7.2. BC-DF differential travel time residuals computed with respect to AK135 (22) plotted as a function of (b) angle between the ray at its turning point and the earth's spin axis, ξ , and (c) the longitude of the earthquake. Darker symbols correspond to quasi-polar paths ($\xi < 30^o$). AK135 was chosen as the reference model for consistency with the ISC residuals used later in this study.

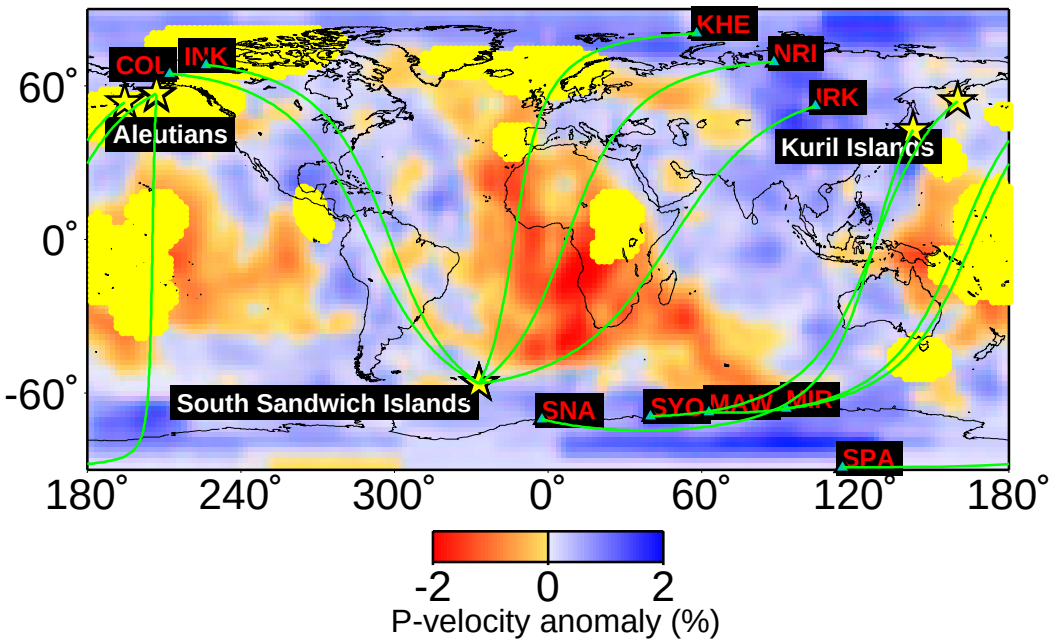

Figure 7.3. Near polar source-receiver paths analysed in this study. Stations, source regions, and great circle paths are indicated by blue triangles, yellow stars, and green lines respectively. Plotted as background is Grand's (25) tomographic model for which we have converted S velocity to P velocity using the scaling dlnVs/dlnVp=2. This model was found to be a good starting point to describe the large scale distribution of P-velocity in D" on the global scale, including low velocity regions in the Pacific and under Africa (18). Yellow patches indicate the regions where Ultra Low Velocity Zones (17) have been detected.

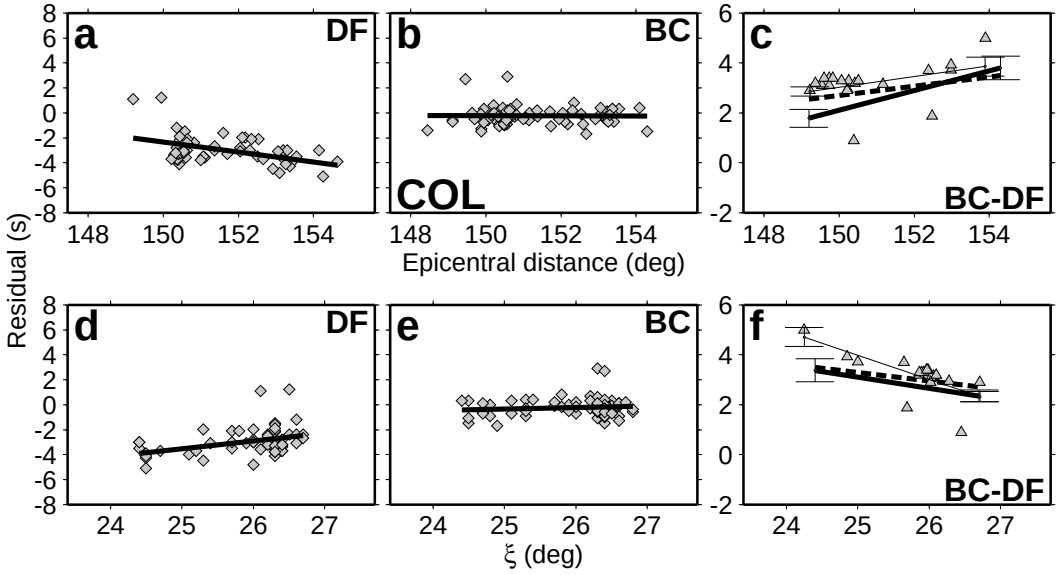

Figure 7.4. Reprocessed ISC residuals (24) with respect to reference model AK135 (22) for station COL, plotted as a function of epicentral distance (a,b,c), and ξ (d,e,f). Left to right: DF,BC, BC-DF. Composite BC-DF variations (thick line in panels c and f) were obtained from BC and DF ISC residuals by substracting the linear regression obtained for DF from that obtained for BC (thick lines in panels a,b and d,e respectively). Also plotted in panels c and f are the predicted variations for Creager's (6) 3.5% inner core anisotropy model (thick dashed line), and observed hand picked residuals (black triangles and thin line). The computed slopes for BC, DF and BC-DF residuals plotted as a function of epicentral distance (respectively ξ) are $0.0 \pm 0.06 s/^o$, $-0.4 \pm 0.1 s/^o$, and $0.4 \pm 0.16 s/^o$ (respectively $-0.2 \pm 0.1 s/^o$, $-0.6 \pm 0.2 s/^o$, and $-0.4 \pm 0.3 s/^o$). The computed regression slopes for hand-picked BC-DF residuals plotted as function of epicentral distance (respectively ξ) are $0.4 \pm 0.1 s/^o$ (respectively $-1.2 \pm 0.3 s/^o$). Hand-picked differential residuals show somewhat larger variations and values, but correspond to relatively few measurements. ISC data provide broader coverage of the source region that leads to smaller average variations. The regressions obtained from them thus represent a conservative estimate of actual variations.

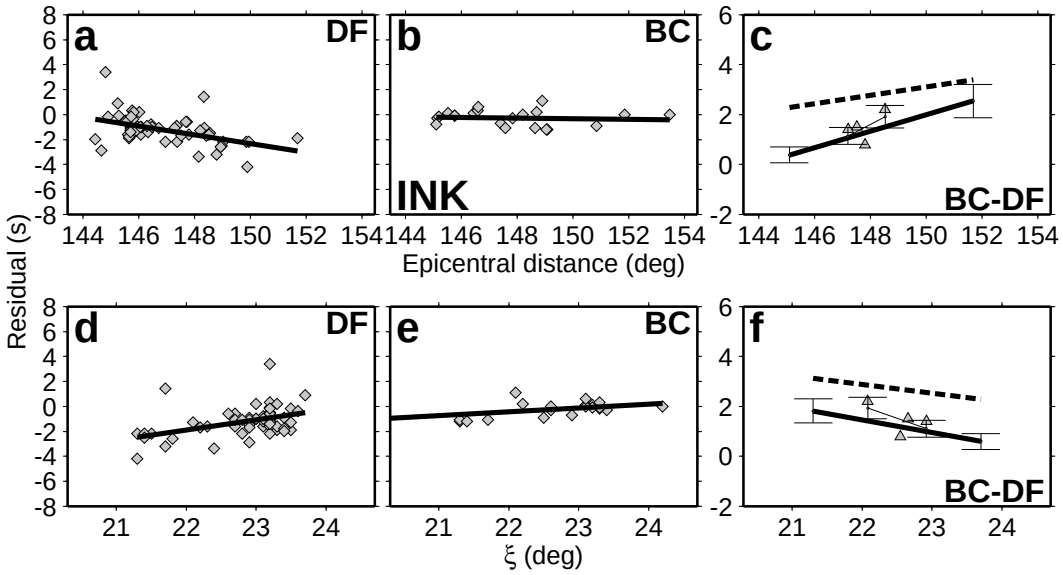

Figure 7.5. Same as Figure 3 for station INK. The computed regression slopes for BC, DF and BC-DF residuals plotted as a function of epicentral distance (respectively ξ) are $0.0 \pm 0.1 s/^o$, $-0.4 \pm 0.1 s/^o$, and $0.4 \pm 0.2 s/^o$ (respectively $0.3 \pm 0.1 s/^o$, $0.8 \pm 0.2 s/^o$, and $-0.5 \pm 0.3 s/^o$). The computed regression slopes for hand-picked BC-DF residuals plotted as function of epicentral distance (respectively ξ) are $0.6 \pm 0.1 s/^o$ (respectively $-1.0 \pm 0.9 s/^o$). Note the good agreement between the ISC estimates and the hand picked residuals.

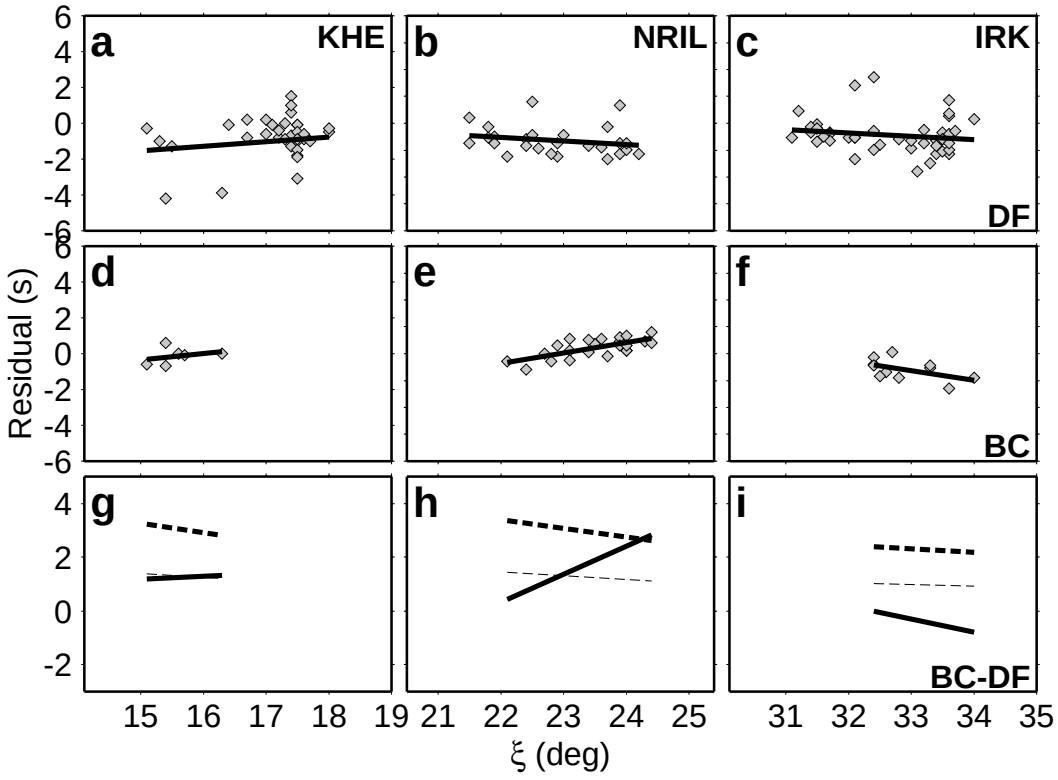

Figure 7.6. Observed DF (abc) and BC (def) ISC residuals (diamonds) for, left to right, KHE, NRIL and IRK respectively, as well as corresponding composite BC-DF residuals (g,h,i, continuous line) and predictions (dashed lines for Creager's (6) 3.5% inner core anisotropy model. Regression lines have been added to outline the trends in the residuals.

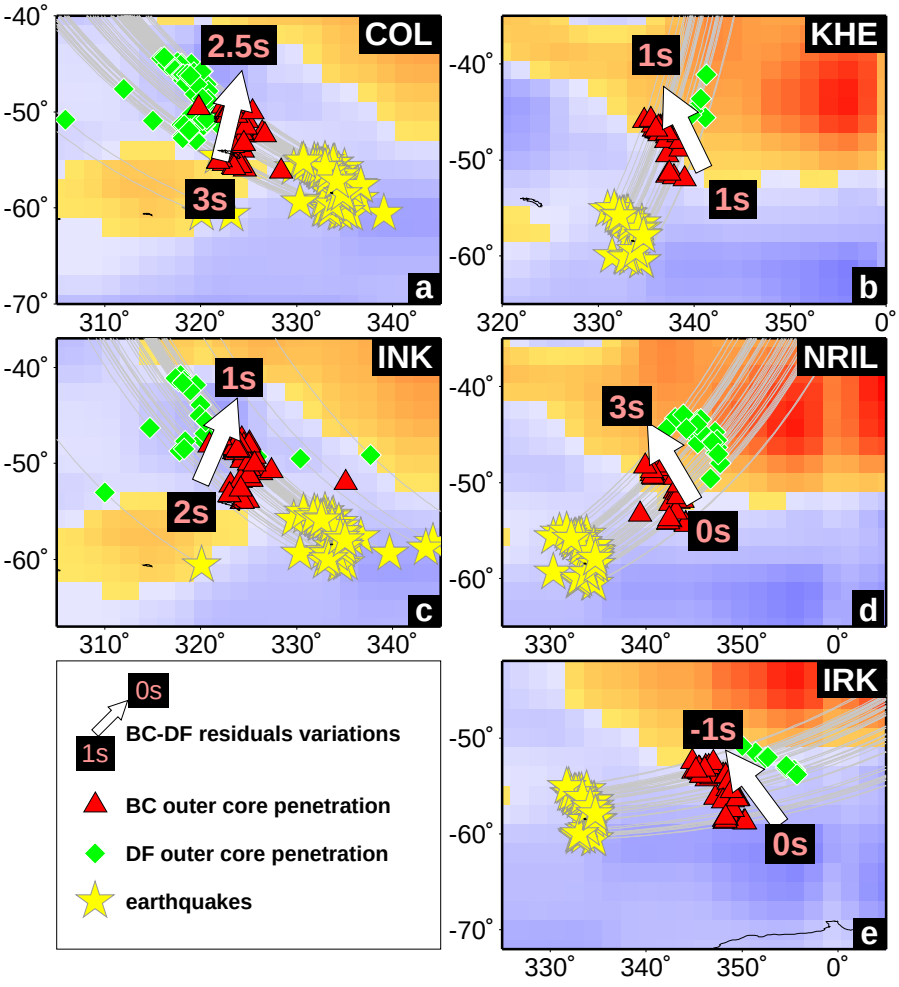
COL
2.5s
3s
a
KHE
1s
1s
b
INK
1s
2s
c
NRIL
3s
0s
d
IRK
-1s
0s
e
-40°
-50°
-60°
-70°
310°
320°
330°
340°
350°
0°
0s
1s
BC-DF residuals variations
BC outer core penetration
DF outer core penetration
earthquakes

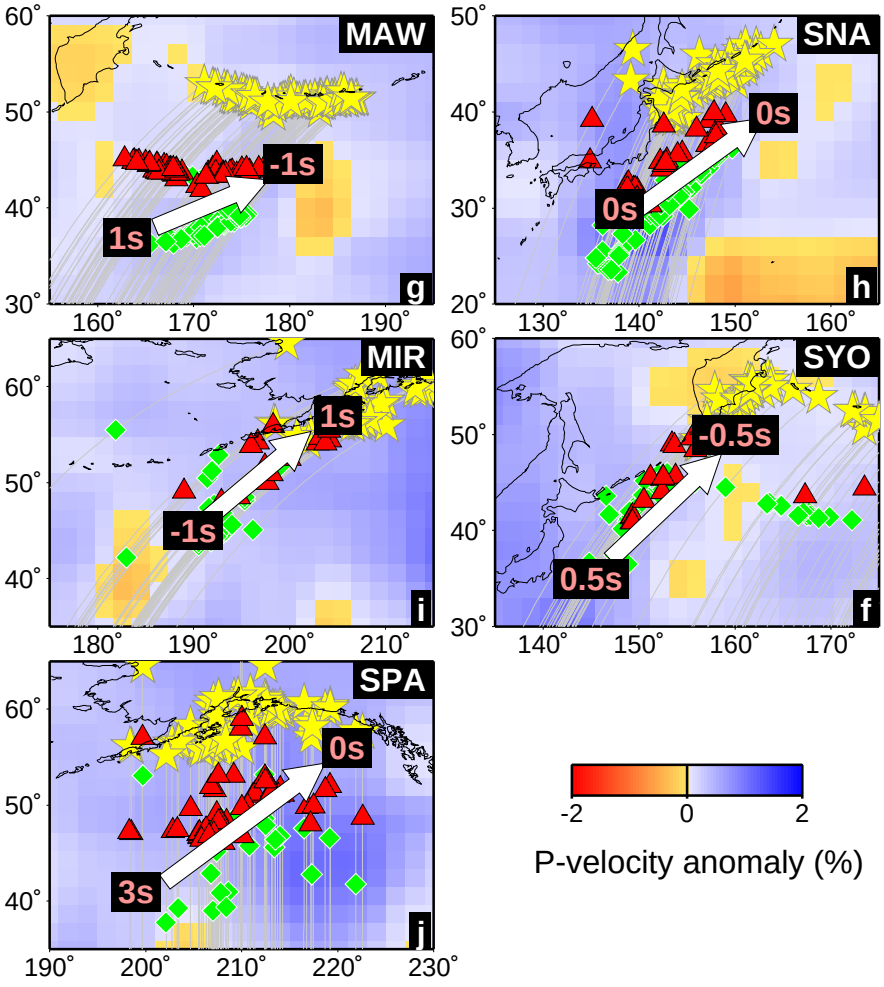
MAW
-1s
1s
g
SNA
0s
0s
h
MIR
1s
-1s
i
SYO
-0.5s
0.5s
f
SPA
0s
3s
j
-2
0
2
P-velocity anomaly (%)

Figure 7.7. Summary of the estimated variations of BC-DF travel time residuals, showing the geometrical relation of earthquake epicenters (yellow stars), great circle paths (gray lines), DF and BC penetration points into the core (red triangles and green diamonds respectively). Plotted in the background is Grand's tomographic model (25) converted to P velocity as in figure 2. Arrows and values indicate trends in the residuals across the swath of great circle paths sampled. The case of neighboring stations KHE,NRIL,IRK deserves particular attention. For station IRK, and for the southernmost paths, both BC and DF "miss" the plume, resulting in dt(BC-DF) $\pm 0s$, whereas for northernmost paths BC samples the edge of the plume resulting in dt(BC-DF) $\pm 1s$ (Figure 6). For station NRIL, the situation is similar, except that , for more northern sources, BC samples more of the "core" of the plume, resulting in larger BC-DF residuals (up to 3 s). Finally, for station KHE, the collection of DF core entry points follows the outside edge of the plume, whereas BC samples the plume, resulting in mild BC-DF (1s) residuals and no significant variation with source position.

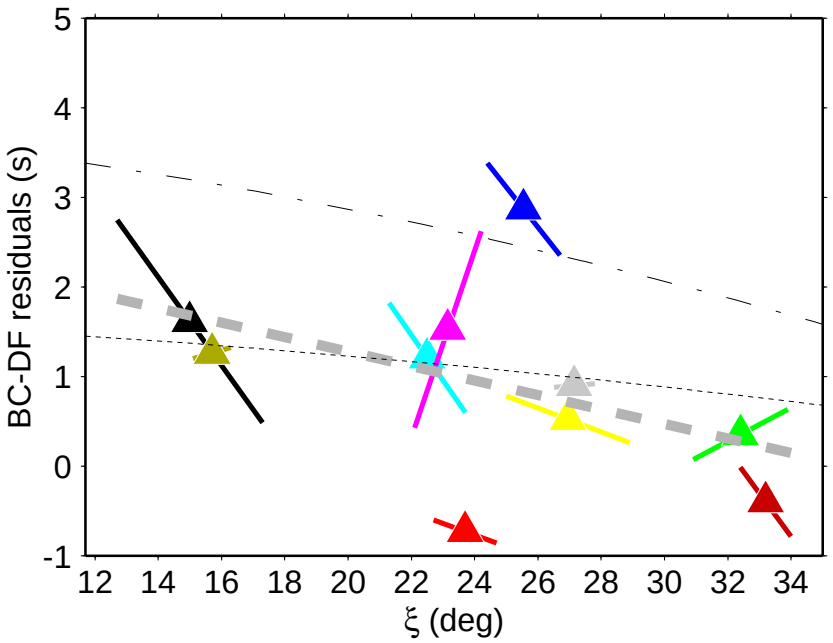

Figure 7.8. Summary of the estimated variations of BC-DF travel time residuals for polar paths. Triangles represent values of composite residuals at an epicentral distance of 148^o. A constant distance is required to obtain a smooth trend as a function of angle ξ for a constant anisotropic model of the inner core. Thick solid lines are the trends of composite residuals, as a function of angle ξ at individual stations. The thick dashed line represents the average observed linear trend at 148^o, and is compared with the predictions for 3.5% (thin dashed line) and 1.5% anisotropy (dotted line) at the same distance. We here give the estimates of the slopes of the observed trends at individual stations: COL, dark blue, $-0.4 \pm 0.3 s/^o$; INK, light blue, $-0.5 \pm 0.3 s/^o$; KHE, dark yellow, $-0.1 \pm 0.9 s/^o$; NRIL, pink, $1.0 \pm 0.4 s/^o$; IRK, dark red, $-0.5 \pm 0.6 s/^o$; SPA, black, $-0.5 \pm 0.3 s/^o$; MAW, gray, $0.0 \pm 0.8 s/^o$; MIR, light red, $-0.1 \pm 1.2 s/^o$; SYO, yellow, $-0.1 \pm 0.4 s/^o$; SNA, green, $0.2 \pm 0.6 s/^o$).

Chapter 8

General Conclusion

The research work presented in this dissertation answers a few questions. We have shown that the degree of heterogeneity of D" was much higher than predicted by tomographic models, and that the lower mantle was associated with sharp lateral gradients, and strong heterogeneity (up to ±4-5%) and anisotropy on scales of a few hundred kilometers, which suggests a chemical origin. This strong heterogeneity can have a significant effect on wave used for the study of the inner core and may have biased analysis of its anisotropic structure. We have finally documented the short-scale variations of BC-DF travel time residuals, which can be interpreted as an effect of strong small scale heterogeneity in either the lowermost mantle or the inner core. We have presented the former explanation as the most natural, in the light of the abundant litterature devoted to D" heterogeneity, and of our modeling of PKP(AB-DF) residuals. This does not necessarely imply that the inner core has not structure, and that the alignment of the iron crystal that form it is random. It just suggests that its structure is hard to resolve, given the pattern of orientation of iron crystals in the deepest shell of the earth and their intrinsic anisotropy. It could still be convecting. If the complex variations of BC-DF residuals are indeed an effect of inner core anisotropy, we have shown that the inner core is formed of a strongly anisotropic mineral in state of complex convection.

In the next decade, seismology will have to address several important questions. The most urgent problem is probably to discriminate between the two interpretations proposed above. Core sensitive modes have to be relooked at. We have made an extensive

use of travel time residuals, but waveform data need to be carefully examine. The rapid development of powerful computing tools will allow seismologists to investigate the effect of any complex three-dimensional structure on seismic waves and to refine the analysis of deep earth structure through, for instance, forward modeling.

The potential new problems related to the core are particularly exciting. If the inner core is weakly anisotropic or even not anisotropic at all, how can we explain the splitting of core sensitive modes? Could the origin of this splitting be in the outer core? And if yes, how? If the rapid variations of BC-DF residuals are indeed due to the inner core, what mechanism and chemistry are responsible for such a tormented structure? Whatever the answers to those questions, I hope that the work presented in this dissertation will have contributed to add a new dimension to the question of deep earth processes.